FIRENWOOD

Improved fire design of engineered wood systems in buildings

Design model for timber-to-timber connections with glued-in steel rods

Editors/Authors:

Patrick Dumler

Norman Werther

Stefan Winter

Deliverable Number: D2.4

Date of delivery: 31/08/2022

Month of delivery: M41

Gefördert durch:

Bundesministerium für Ernährung und Landwirtschaft

aufgrund eines Beschlusses des Deutschen Bundestages

The FIRENWOOD project is supported under the umbrella of ERA-NET Cofund ForestValue by Germany (Federal Ministry of Food and Agriculture (BMEL); Agency for Renewable Resources (FNR) project number FKZ 2219NR120), Sweden (The Swedish Research Council for Environment, Agricultural Sciences and Spatial Planning (FORMAS); Swedish Energy Agency (SWEA); Swedish Governmental Agency for Innovation Systems (Vinnova) project number 2018-04989) and Norway (Research Council of Norway (RCN) project number 298587). ForestValue has received funding from the European Union's Horizon 2020 research and innovation programme under grant agreement No 773324.

Coordinator: Tian Li at RISE Fire Research AS

Table of Contents

Appendix A – Sensitivity Analysis
Appendix B – Test series 2
Appendix C – Test series 4

Symbols

c	Material heat capacity (c_p)
$\dot{h}_{net,r}$	Net heat flow from radiation [W/m²]
t	Time
T	Temperature
x, y, z	Length
λ	Material thermal conductivity in the respective direction
ρ	Density
Φ	Configuration factor (also form factor)
ε_m	Emissivity of the component surface
ε_f	Emissivity of fire
σ	Stephan-Boltzmann constant (=5.67 · 10-8 W/m²K⁴)
Θ_r	Effective radiation temperature of the fire [°C]
Θ_m	Specimen surface temperature [°C]

1 General

1.1 Basics in Ansys

The heating of components exposed to fire is a transient process. In order to be able to simulate this numerically using the finite element method, the solution of the Fourier equation is required. The thermal material parameters required for this are thermal conductivity, the specific heat capacity and the density. Because the materials are subject to physical and/or chemical changes when exposed to temperatures of up to several hundred degrees - as is the case in the event of fire - the thermal material parameters must generally be formulated at least as a function of the temperature.

In order to simulate the test specimen temperatures of the individual test series 2 of the Firenwood tests, a finite element method (FEM) was performed using ANSYS Workbench Version 21 R2. Based on these results, the test specimens of test series 4 were planned and the design model was validated.

The aim of the thermal FEM was to determine the temperature distribution in the connection and especially in the area of the glued in rod after a thermal load is applied. The tests have shown that the mechanical properties of glued in rods depend to a large extent on the temperature of the adhesive. Therefore, the temperature distribution in the cross-section and especially the critical temperature limit is decisive for the load-bearing capacity. In all series of tests, a thermal load that changed over time was present. Furthermore, the effective material properties of the individual materials change at different temperatures, which is why a thermal-transient (non-stationary), non-linear temperature field calculation was carried out as a model approach.

1.2 Method

The same pattern was used in all examined test series with glued in rods to create the models. First, a simplified model of the test specimen was created. An attempt was made to achieve the shortest calculation time using symmetry. A sensitivity analysis was then carried out in order to minimize the influence of errors in the mesh or in the model on the results.

The thermal load was defined on the basis of the load applied in the different test setups. Characteristic values for these are already known from the literature, which relate to tests with the Standard Fire Curve. Therefore, the values had to be adjusted for the tests with the heating box in test series 3 with a convective heat input of 110 °C.

The effective material parameters were determined and the results compared with the measured results from the tests. Based on the data, the effective material parameters were adjusted to reflect the test results as accurately as possible. By simulating the various test series and test specimens, the selected material parameters could be further checked and validated.

2 Heat Transmission

Heat is a form of energy transport across a thermodynamic system boundary. Besides physical work, heat is the only way energy can enter or leave a closed system. Heat as a form of energy transport is the result of a temperature gradient and is accompanied by a change in the entropy of the system. [1]

Two types of heat transmission occur:

- Heat transmission by conduction with free or forced convection
- Heat transmission through thermal radiation by electromagnetic waves without a material carrier.

Heat transmission often occurs as a combination of conduction, with or without convection, and radiation. [2]

2.1 Transient and steady heat transmission

By dividing heat transmission problems into stationary and transient heat transmission, the time dependency of these issues is considered.

In stationary heat transmission, the temperatures in systems do not change at all or only very little, so these changes can be neglected. The internal energy in the components remains the same because the temperatures do not change. If energy is added to the system from outside the system boundaries, energy must also be removed from the system.

Transient thermal processes consider temperature distributions in systems that change over time. The temperature changes can also be caused without external influences by the energy stored in the system. An energy balance for non-stationary heat transmission must consider the external energy supply or the energy removal as well as the internal energies. Typical applications include heating and cooling processes. [3]

In this work, temperature-dependent material properties of materials are optimized. These materials are subjected to a thermal load. The load temperatures and the internal temperatures of the components change over time. Hence, these are transient heat transmission problems.

2.2 Heat conduction

Heat conduction takes place in resting, liquid and gaseous substances when there is a temperature gradient. A heat flow occurs in the direction of decreasing temperatures. It is therefore a matter of transporting energy in the form of heat. Atoms, molecules, electrons or photons serve as transport media. There are two types of heat conduction. If there is stationary heat conduction, the heat transport takes place while maintaining a constant heat flow. It follows that, viewed over time, all temperatures are constant at each location.

In the case of heating and cooling processes, one speaks of transient heat conduction. The heat flow varies with time, causing local temperatures to change over time. [2] For the present transient question, the heat conduction can be described with Fourier's parabolic differential equation.

$$\frac{\partial}{\partial x}\lambda_1\frac{\partial T}{\partial x}+\frac{\partial}{\partial y}\lambda_2\frac{\partial T}{\partial y}+\frac{\partial}{\partial z}\lambda_3\frac{\partial T}{\partial z}=\frac{\partial T}{\partial t}\cdot c\cdot\rho \tag{1}$$

With:

λ	material thermal conductivity in the respective direction
c	material heat capacity (c_p)
T	temperature
x, y, z	length
t	time
ρ	density [4]

2.3 Thermal Radiation

In the case of thermal radiation, heat is transferred by electromagnetic radiation. This radiation is not an interaction between neighboring molecules and is therefore not dependent on a carrier fluid. [1] All bodies emit energy into their environment in the form of electromagnetic waves. By emitting rays, the internal energy of a body can be converted into energy that is passed on through electromagnetic waves. When electromagnetic waves collide with a solid, part of the transported energy is absorbed by the body, while another part is either reflected or transmitted. The absorbed energy is converted into internal energy of the solid.

In solid bodies, radiation is already completely absorbed after penetrating thin layers. Rays are not emitted from inside a body, but from layers close to the surface. Therefore emission and absorption are surface effects and one can speak of radiating and absorbing surfaces instead of radiating bodies. [5] The ability to emit rays depends on the constitution of the body. The black body is an idealized body that radiates the maximum possible energy at any temperature. The entire specific radiation is absorbed by it, so neither transmission nor reflection is possible. A black body has an emission coefficient of $\varepsilon = 1$.

The ability of other bodies to emit radiation at the same temperature can be specified by the emission ratio ε. The ratio of the radiant intensity of a body at a given temperature compared to the radiant intensity of a black body at the same temperature is the emissivity ratio. [2] The tested specimens are so-called gray bodies. In contrast to the black body, thermal radiation that hits the component surfaces is not completely absorbed. Part of the radiation is reflected while another part passes through the materials. They have an emission ratio of $\varepsilon < 1$.

The net heat flow is calculated using the following formula:

$$\dot{h}_{net,r} = \Phi \cdot \varepsilon_m \cdot \varepsilon_f \cdot \sigma \cdot [(\Theta_r + 273)^4 - (\Theta_m + 273)^4] \quad (2)$$

With:

$\dot{h}_{net,r}$	net heat flow from radiation [W/m²]
Φ	the configuration factor (also form factor)
ε_m	the emissivity of the component surface
ε_f	the emissivity of fire
σ	the Stephan-Boltzmann constant ($=5.67 \cdot 10^{-8}$ W/m²K⁴)
Θ_r	the effective radiation temperature of the fire [°C]
Θ_m	the component surface temperature [°C] [6]

The net heat flow caused by radiation corresponds to the heat energy that is transferred to the component via radiation per area and time. The configuration factor gives the part of the total thermal radiation that is radiated from one surface and received from another surface. It depends on the size of the radiating surface, the distance between the radiating and receiving surface and the orientation of the surfaces to each other. In this project, a configuration factor of $\Phi = 1$ is assumed for the radiation from the fire area to the specimen surface. The emissivity of the specimen surface was set to be $\varepsilon_m = 0.8$.

3 Thermal material properties

The thermal simulation in ANSYS is carried out on the basis of the Fourier series with the transient temperature field calculation. For this calculation method, the program needs the temperature properties of the materials used in the simulation. These are the thermal con-

ductivity λ [W/mK], the specific heat capacity c [J/kg] and the density ρ [kg/m³] of the materials, which can change depending on the temperature. It is possible to model material-specific behavior with changing temperature using these properties. These are effective material parameters that do not represent the real values, but have been developed and simplified for the simulation. The effective material parameters used in the simulations are shown and described in the next chapters.

3.1 Timber

The material wood essentially consists of approx. 45% cellulose, 20% hemicellulose and 35% lignin. These components consist of carbon, oxygen and hydrogen. Due to this structure, the material wood contains bound water, which is evenly distributed throughout its structure. [7]

Due to the temperature change during fire exposure, wood undergoes different processes. The changes in the wood can be directly linked to temperature-dependent material properties. However, due to their complexity, these processes cannot always be clearly assigned to a specific temperature level.

For the effective material parameters for the fire tests under Standard Fire Curve, the values according to Schleifer were used, as good agreements could be achieved here. For comparison, the material parameters from EN 1995-1-2 were used, which, however, led to more conservative results and are therefore not listed further. [8, 9]

For test series 3, the effective parameters had to be adjusted, as no fire load in the form of the Standard Fire Curve was applied here. The results of the simulation far exceeded the real temperature curves. For this reason, an attempt was made to calibrate the material and thermal parameters to the test results.

3.1.1 Thermal conductivity λ

The thermal conductivity λ is specified in [W/mK] and describes the thermal energy that is transported through the material in the form of heat by means of thermal conduction. For the three-dimensional simulations in test series 2.2, the values of thermal conductivity were adjusted depending on the fiber direction of the wood. For heat conduction parallel to the fiber, the characteristic values were quadrupled in accordance with the proposal from the 3rd draft of EN 1995-1-2.

Figure 1 shows the curves of the effective values for the thermal conductivity λ as a function of the temperature of a solid wood panel based on the values from Schleifer. [9] In the diagram shown, the first peak can be seen at around 100 °C. This is due to the moisture in the wood, which produces a significantly higher thermal conductivity value λ during evaporation. After that, the thermal conductivity falls to the value of 0.15 W/mK of a dry wood cross-section. The second peak at around 200 °C can be explained by the process of pyrolysis in the wood. In this area, the wood begins to break down lignin. When the transformation from wood to charcoal is complete and this insulating layer has fully formed, the value of the thermal conductivity λ falls to its lowest point of 0 .09 W/mK at approx. 350 °C. A further increase can be seen at temperatures above approx. 500 °C. The cracking in the wood that begins here leads to an increase in thermal conductivity. From approx. 800 °C the layer of charcoal that formed at 350°C begins to fall off. This leads to a last rise up to the temperature of 1,200 °C. At 1,200 °C the value for λ is fixed at 2.0 W/mK. [9]

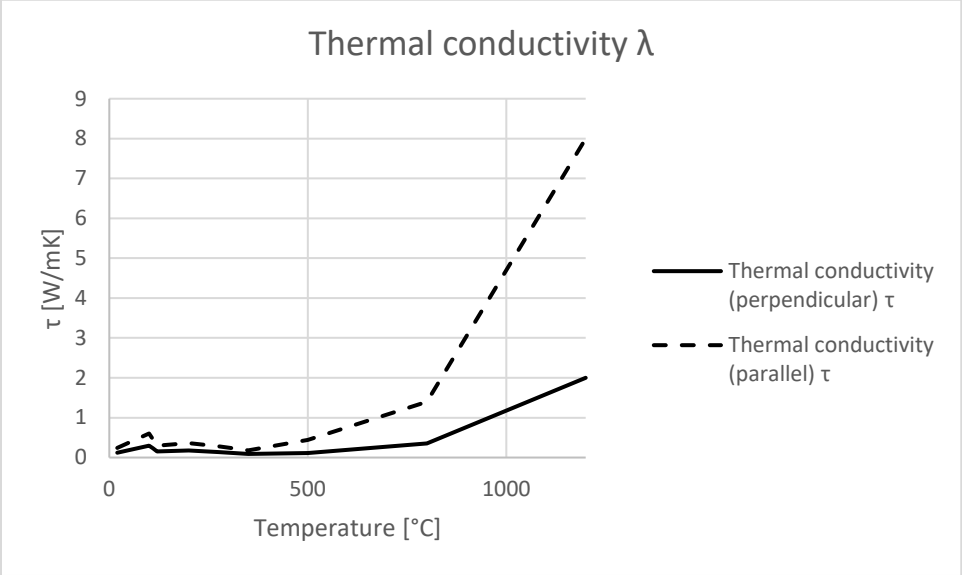

Figure 1: The effective values of thermal conductivity for timber used in the numerical simulation

3.1.2 Specific heat capacity c

The specific heat capacity c is given in [J/kgK] and describes how much energy or amount of heat must be supplied to a mass of 1 kg in order to heat it up by 1 Kelvin. [10]

The specific heat capacity of wood depends on the moisture content and the change in the components of the wood as the temperature rises. Figure 2 shows the course of the used effective specific heat capacity. The first peak at 100 °C to 120 °C is due to the evaporation of the water in the wood. If the wood reaches a temperature of 100 °C, the temperature in the wood remains constant until all the water has evaporated from the cross-section. The next phase at 200 °C to 350 °C is related to the pyrolysis of wood. The energy required for the pyrolysis was according to the experiments of [11] and [9] set to 6173 J/kgK.

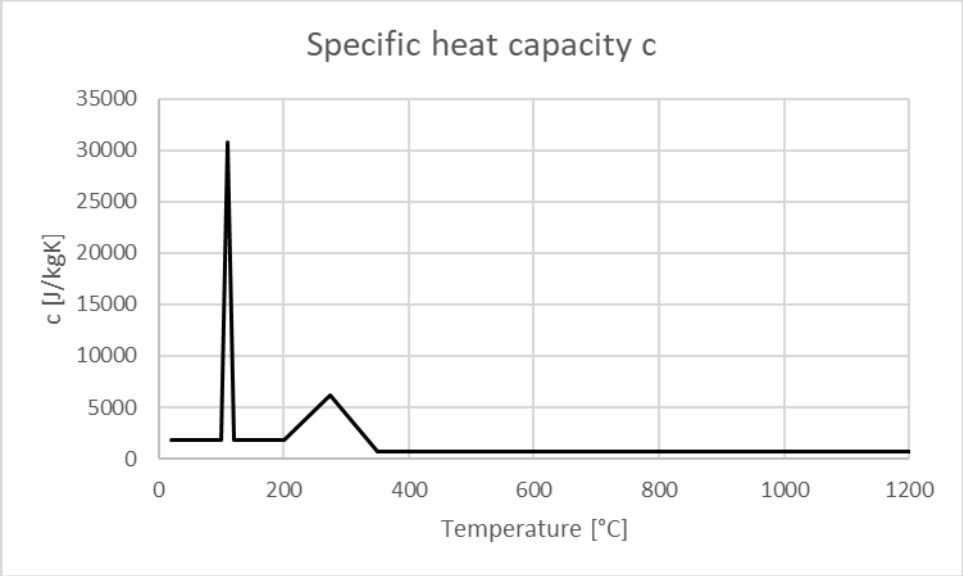

Figure 2: The effective values of specific heat capacity for timber used in the numerical simulation

3.1.3 Density ρ

The density ρ is measured in [kg/m³] and indicates the mass per volume of a substance.

As soon as the cross-section has completely dried, one speaks of the dry density for wood. To calculate this, the dry mass m and the volume V of the dry specimen must be used.

In this work, the ratios for the density of [9] were used according to the experimental data from [12]. The values are shown in relation to the density at 20 °C and the dry density. The corresponding mean densities of the individual test series were used in the numerical simulations to adjust the material parameters. For the simulation of the design method and the design of test series 4, however, a standard density of 450 kg/m³ was assumed. The most important phases of the density properties can be seen in Figure 3. The first change in density between 100 °C and 120 °C is due to the evaporation of the bound water. The specified raw density falls there to its dry density. Charcoal is formed in the range up to 350 °C. In this area pyrolysis takes place and the cellulose is decomposed in the cross-section. Therefore, the largest mass or density decrease is recorded.

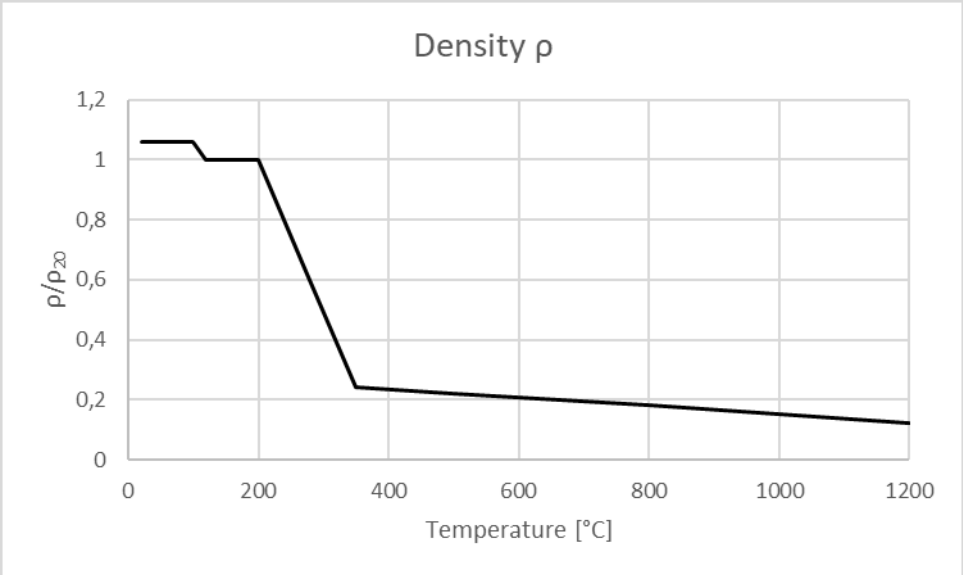

Figure 3: The effective values of the density in the ratio ρ/ρ20 used in the numerical simulation for timber

Table 1 shows an overview of all effective material properties for timber used in this work for the simulation in test series 2.

Table 1: The effective values used in the numerical simulation for timber in test series 2

Temperature	**ρ/ρ20**	**T2.1**	**T2.2**	**T2.3**	**Thermal conductivity (perpendicular) λ⊥**	**Thermal conductivity (parallel) λ∥**	**Specific heat capacity c**
		Density ρ					
[°C]			[kg/m³]		[W/mK]	[W/mK]	[J/kgK]
20	1,06	435,1	430,9	452,2	0,12	0,24	1790
100	1,06	435,1	430,9	452,2	0,3	0,6	1790

110	1,03	422,8	418,7	439,4	0,23	0,46	30796
120	1	410,4	406,5	426,6	0,15	0,3	1790
200	1	410,4	406,5	426,6	0,18	0,36	1790
275	0,62	254,5	252,0	264,5	0,14	0,28	6173
350	0,24	98,5	97,6	102,4	0,09	0,18	690
500	0,22	90,3	89,4	93,8	0,11	0,44	690
800	0,18	73,9	73,2	76,8	0,35	1,4	690
1200	0,12	49,3	48,8	51,2	2	8	690

3.2 Gypsum plasterboard

3.2.1 Thermal conductivity λ

A Gypsum plasterboard consists of a gypsum core and a covering of solid cardboard. Manufacturers such as Rigips and Knauf specify the raw densities of these board types as approx. 680 kg/m³.

Figure 4 shows the effective thermal conductivity values for gypsum plasterboard proposed by [9] and used for the test series 2.2. A thermal conductivity of 0.4 W/mK is assumed between 20 °C and 70 °C. The thermal conductivity then drops as the water evaporates. By raising the thermal conductivity between 600°C and 1000°C, cracking of the gypsum boards is considered.

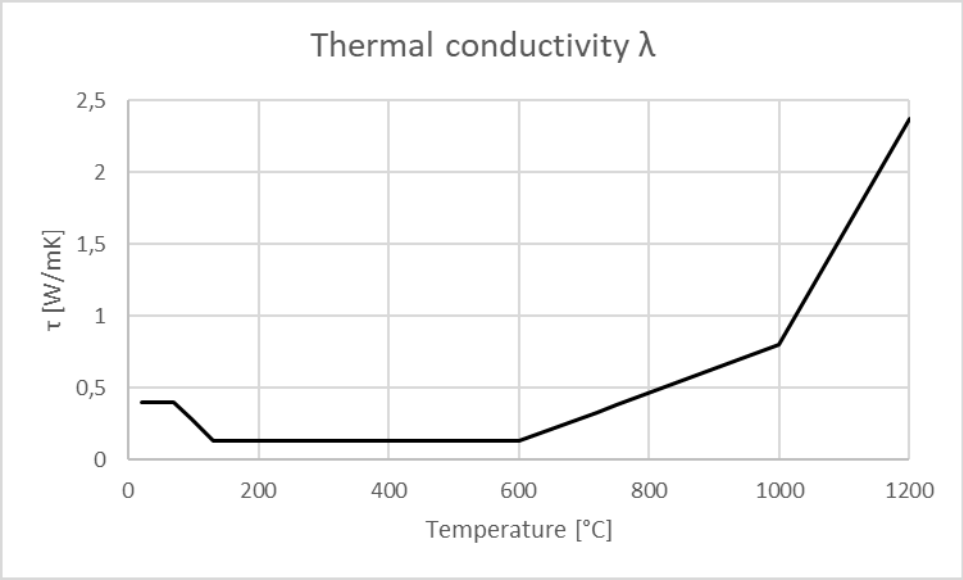

Figure 4: The effective values of thermal conductivity used in the numerical simulation for gypsum plasterboards

3.2.2 Specific heat capacity c

Figure 5 shows the effective specific heat capacity c of the plasterboard. The initial value of 960 J/kgK was taken from the manufacturer's information from Knauf and Rigips in the dissertation by [9]. The two peaks are due to the increased energy requirement for the evaporation of crystal water and the energy requirement for the chemical processes taking place.

During exposure to fire (temperature increase), gypsum undergoes various chemical conversion reactions that require energy. As the temperature increases, gypsum (calcium sulfate dihydrate) goes through five different chemical states. During the first phase at 20°C, gypsum has bound water and some free water. In phase two, calcium sulfate dihydrate converts to calcium sulfate hemihydrate. The free water and part of the crystal water are released (100 °C - 170 °C). Phase three is characterized by the release of the remaining bound water, which is confirmed by a measured loss of mass of the gypsum board. This second increase from 600°C to 720°C is also due to a chemical reaction of gypsum, the conversion of calcium sulfate hemihydrate to anhydrite III and the associated energy consumption. At phase four, the gypsum has almost no water left. Since only a small amount of thermal energy is required in this phase, it is not considered when determining the specific heat capacity. Phase five is also not taken into account when determining the specific heat capacity, as it only begins at a temperature greater than 1180°C. The Standard Fire Curve only reaches this temperature range after about five hours. [9]

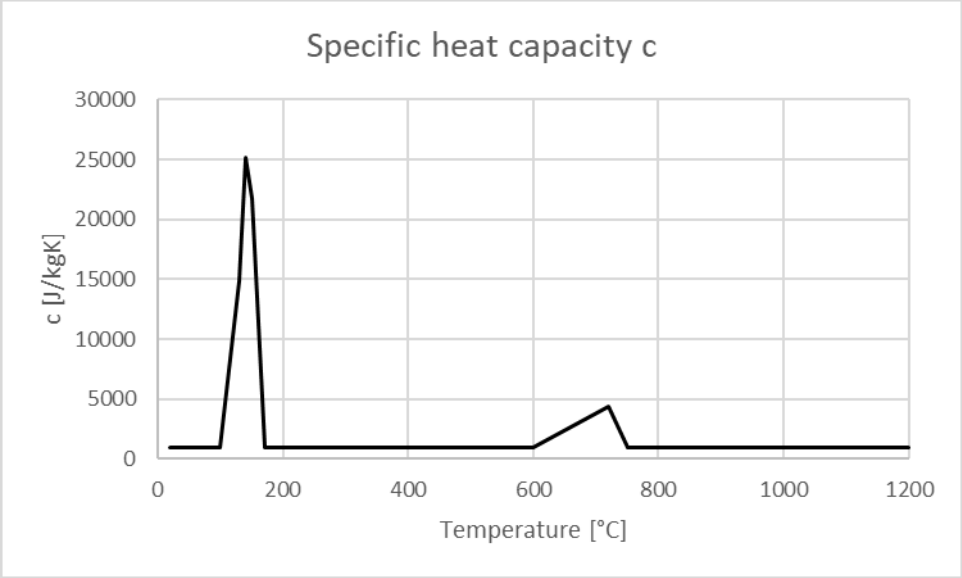

Figure 5: The effective values of specific heat capacity for gypsum plasterboards used in the numerical simulation

3.2.3 Density ρ

[9] specifies densities at 20°C for gypsum boards as 720 to 900 kg/m³. The ratio of the raw density ρ to the raw density at 20°C ρ_{20} was taken from the test reports. The decrease in the density shown in Figure 6 as a function of the temperature is mainly due to the evaporation of the water. The second drop in density from 600 °C is due to the escape of the remaining bound crystalline water.

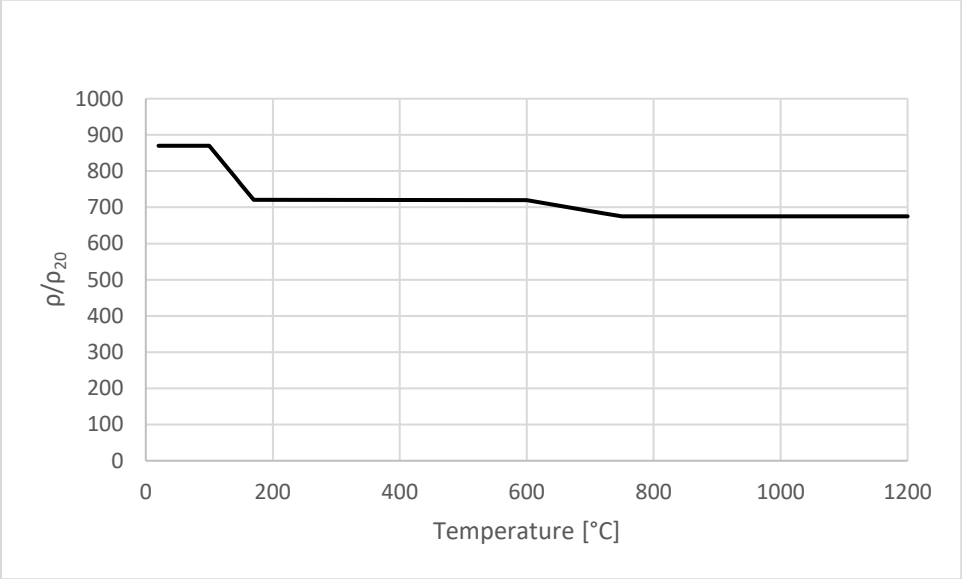

Figure 6: The effective values of the density in the ratio ρ/ρ20 used in the numerical simulation for gypsum plasterboards

The effective material parameters used in the simulation are shown in the Table 2.

Table 2: The effective values used in the numerical simulation for gypsum plasterboards in test series 2 [9]

Temperature	Density ρ		Thermal conductivity λ	Specific heat capacity c
[°C]	ρ/ρ_{20}	[kg/m³]	[W/mK]	[J/kgK]
20	100	870	0,4	960
70	100	870	0,4	960
100	100	870	0,27	960
130	92,6	805,6	0,13	14915
140	90,2	784,7	0,13	25207
150	87,7	763,0	0,13	21764
170	82,8	720,4	0,13	960
600	82,7	719,5	0,13	960
720	78,6	683,8	0,33	4359
750	77,6	675,1	0,38	960
1000	77,6	675,1	0,8	960
1200	77,6	675,1	2,37	960

3.3 Steel

3.3.1 Thermal conductivity λ

The thermal properties of steel from the specifications in EN 1993-1-2 were used for the rods (see Figure 7). [13] In contrast to wood, the thermal conductivity is significantly higher with a value of over 50 W/mK and gradually decreases to a value of approx. 29 W/mK up to 800 °C.

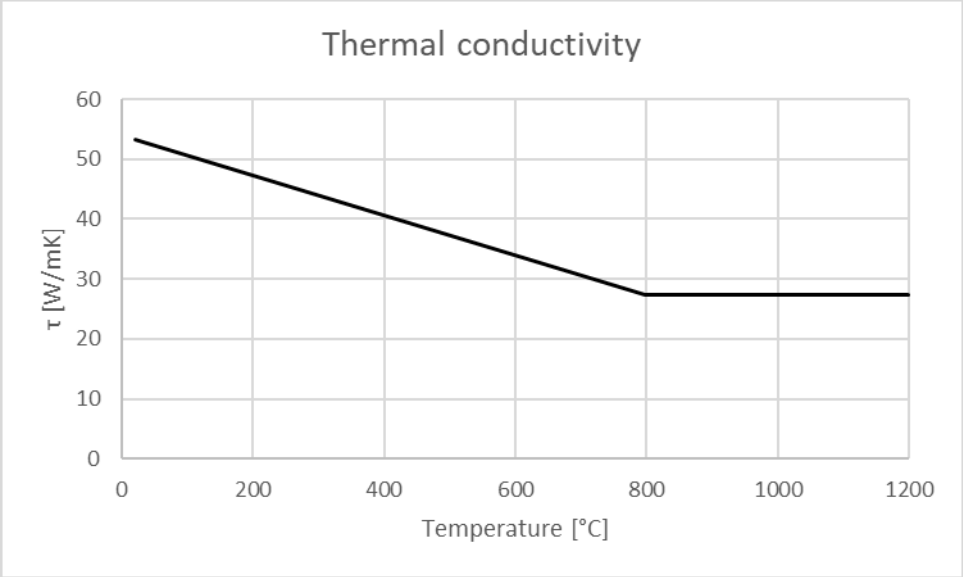

Figure 7: The effective values of thermal conductivity for steel used in the numerical simulation

3.3.2 Specific heat capacity c

The values of EN 1993-1-2 provide a peak at 735 °C for the specific heat capacity of steel. The temperature of 735°C is called "Curie-temperature" and corresponds to the magnetic phase transition (see Figure 8). [14]

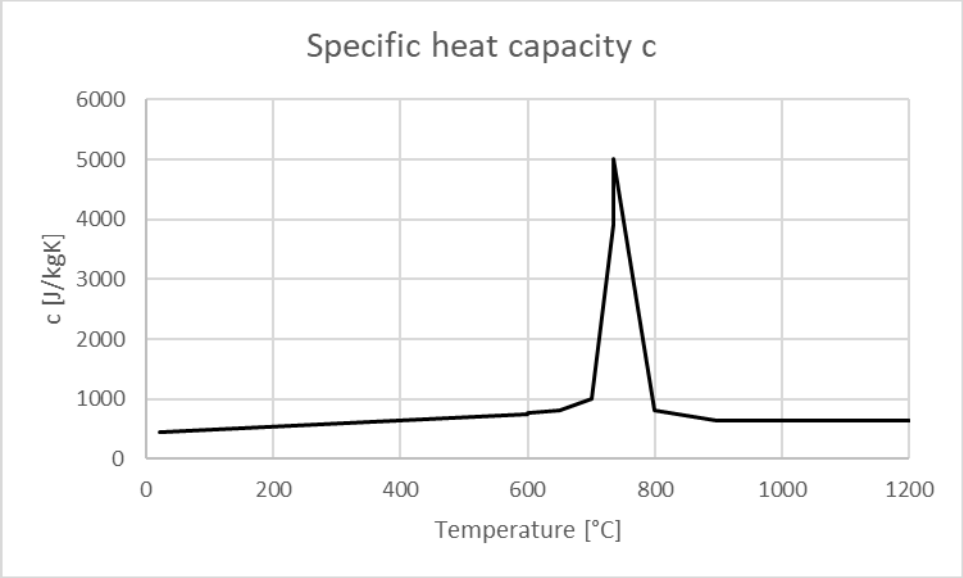

Figure 8: The effective values of specific heat capacity for steel used in the numerical simulation

3.3.3 Density ρ

The density is assumed to be constant over the entire temperature range and has a value of 7850 kg/m³. Table 3 shows the temperature-dependent material parameters used for the simulation.

Table 3: The effective values used in the numerical simulation for steel

Temperature	Specific heat capacity c	Temperature	Thermal conductivity λ
[°C]	[J/kgK]	[°C]	[W/mK]
20	439,8	20	53,3
599	758,8	799	27,4
600	760,2	800	27,3
650	813,8	1200	27,3
700	1008,2		
734	3916,5		
735	5000		
800	803,3		
899	651,1		
900	650		
1200	650		

3.4 Adhesive

Hardly no values for the thermal conductivity and the specific heat capacity are available for adhesives in the literature. The various manufacturers have stated that the parameters are generally not required. This can be due to the fact that adhesive joints are usually so thin that their influence on the heat development in components is only insignificantly small. Therefore, also no information is available on the high-temperature behavior of adhesives. For the sake of simplicity, the assumption was made that the adhesive retains its properties over the entire temperature spectrum.

In order to determine the adhesive parameters, simulations were carried out with three adhesives from the literature. Here, the adhesives with the highest (Adhesive A) and lowest thermal conductivity (Adhesive B) were selected, as well as an adhesive that was similar in the values of density to the two adhesives used in the test (Adhesive C). Then, for a fire load of 30 minutes with Standard Fire Curve, a test specimen with a glued- in rod in the middle of the cross-section was simulated with all three adhesives and three joint thicknesses of 1 mm – 3 mm. The temperature at the edge of the borehole and on the edge of the rod were used as outputs. The wood coverage was the same for all joint thicknesses with 39 mm. A diameter of 12 mm and 20 mm was used for the rod. The heat transmission took place from the wood surface via the glue line into the steel. The results for the M20 rod are shown in the following Figure 9.

It shows that the material parameters have a greater influence on the temperature development in the glue line with increasing joint thickness.

Overall, the deviation of the temperature as a function of the glue line thickness per adhesive is approx. 2 %. For the adhesive types, deviations of max. 3 % in the final temperature are measured for small joint thicknesses of 1 mm. For larger joint thicknesses of 3 mm, this increases to up to 6 %. Similar results are calculated for the rod of 12 mm diameter. The results of Adhesive C are in a similar range as the values for Adhesive B and only deviate by less than 2 % for all three glue line thicknesses.

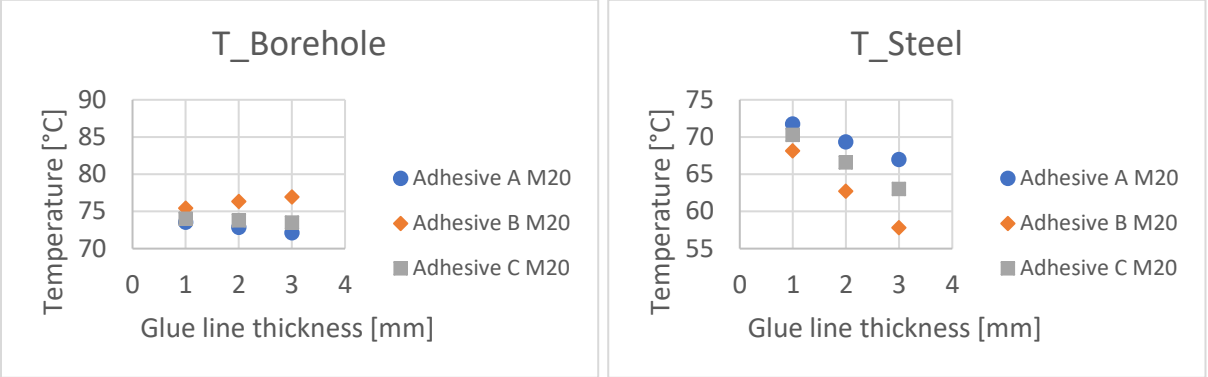

Figure 9: Influence of adhesive type (left) and glue line thickness (right) on temperature inside the connection

The thermal values of Adhesive C were chosen for the simulations because its density is close to that of the adhesives actually used. However, the specific densities of the individual adhesives were used to reduce the errors from the simplifications.

Table 4 shows the material characteristics for the individual adhesives used and compared during the simulations.

Table 4: Effective values used for the different adhesives in the numerical simulation

	Density ρ	**Thermal conductivity (perpendicular) λ**	**Specific heat capacity c**
	[kg/m³]	[W/mK]	[J/kgK]
Adhesive A	1600	0,6	897
Adhesive B	1070	0,14	1531
Adhesive C	1300	0,283	1268
Adhesive 1	1111	0,283	1268
Adhesive 2	1350	0,283	1268

4 Sensitivity analysis

The sensitivity of the model was analyzed with the test specimens of test series 2.3. The test series 2 was loaded with the Standard Fire Curve. In the simulation model a thermic transient approach was used in order to involve the time dependent temperature in the specimens. To simulate the specimen with glued in rods a quarter section was used to reduce the calculation time since the test specimens had a symmetrical cross-section in two axes (see Figure 10).

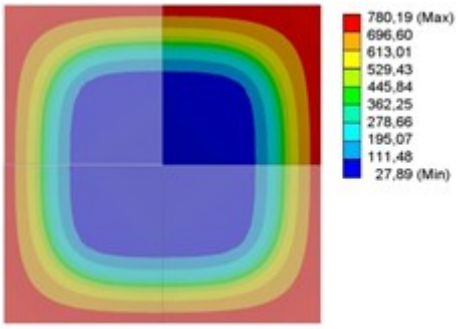

Figure 10: Symmetry effects to get a shorter computing time

At the beginning, the influence of the mesh density was checked. Changing the size of the individual nodes changes their total number, which can lead to improvements in computing time. The two-dimensional models were checked first.

In the beginning just, the entire cross-section was made from one material without areas representing the adhesive or the rod. After the thermal load was applied the meshing size of the square shaped elements was changed between 0.25 mm and 4 mm. Measurement point was at the planned borehole edge at the transition of wood and adhesive. The results are shown in Figure 11. The time step was set to 30 minutes. However, only a detail of 10 minutes is shown for a better overview. The diagrams for the whole time slot are given in Appendix A. It can be seen that a big element size of 4 mm shows smaller values for the temperature.

The finer the meshing the lower were the deviations. The deviations for 1 mm sized elements was below 1 % from the elements with 0.25 mm at the end temperature. Therefore 1 mm sized meshes were used for 2-dimensional models as a compromise between accuracy and calculation time.

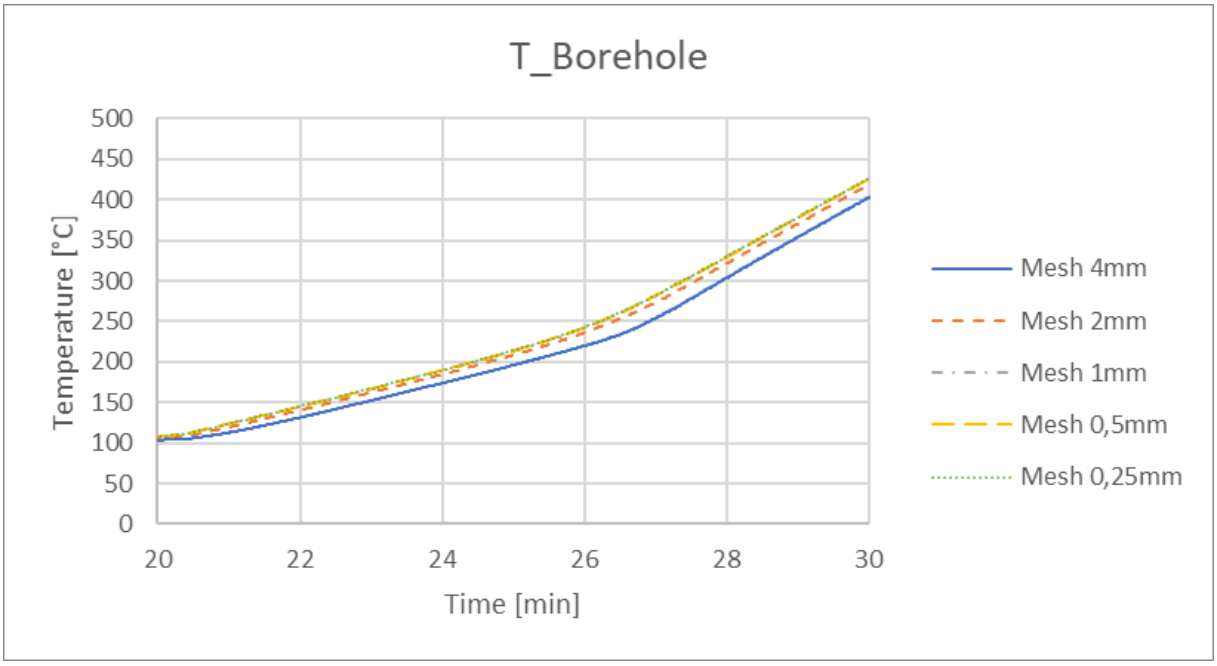

Figure 11: Influence of the mesh density on the temperature curve for a wooden cross-section

In Figure 12 the modeled meshes with the calculated temperature distribution in the cross-section with changed mesh width for the two-dimensional models are shown as an example. On the left side the element size was 4 mm whereas on the right side 1 mm sized elements were used. Red color shows the highest temperatures in the model.

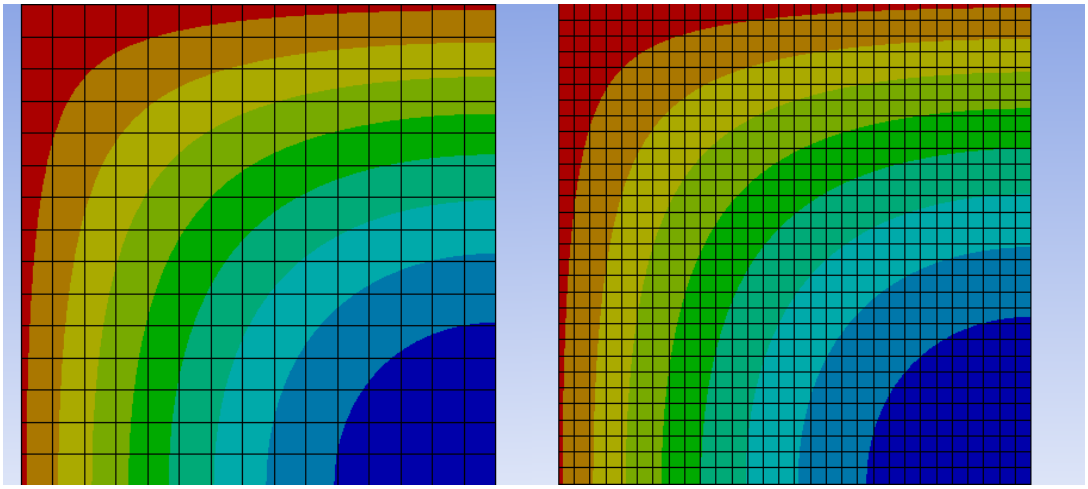

Figure 12: Sketch of simulation model with different mesh sizes and temperature profile of the wooden cross-section

Table 5 shows the number of nodes and elements as well as the necessary calculation time for a simulation under the specified parameters.

Table 5: Computing time for different meshing densities

T_borehole			**T_borehole**			**T_borehole**			**T_borehole**			**T_borehole**		
Mesh [mm]	Load steps	Time step [s]	Mesh [mm]	Load steps	Time step [s]	Mesh [mm]	Load steps	Time step [s]	Mesh [mm]	Load steps	Time step [s]	Mesh [mm]	Load steps	Time step [s]
4	1	3600	2	1	3600	1	1	3600	0,5	1	3600	0,25	1	3600
Knots	Ele-ments	Time [s]	Knots	Ele-ments	Time [s]	Knots	Ele-ments	Time [s]	Knots	Ele-ments	Time [s]	Knots	Ele-ments	Time [s]
246	67	228	782	233	139	2894	913	408	11392	3695	852	44509	14628	3253

A three - dimensional system with the same edge dimensions was then created and compared with the results from the two - dimensional calculations (see Figure 13). A duration of 30 minutes was simulated. However, only a 10 - minute excerpt is shown for illustration purposes. The complete graph can be found in the Appendix A. Again, the measuring point represents the position of the edge of the borehole. The length of the test specimen in the model was 150 mm. As expected, there were no changes in the temperature curves when the thermal conductivity was increased for the fibers in grain direction, since the body is symmetrical and the heat is only introduced perpendicular to the direction of the fibers. It can be seen that in the 3-dimensional model, a mesh width of just 4 mm leads to similar results. Since a further reduction in the mesh size in the three - dimensional model leads to a significant increase in computing time of more than 100 %, a mesh size of 4 mm was used for calculation.

In the next step, the materials of adhesive and steel were implemented in the model and recalculated. The model was created for the two cross-sections of 60 mm x 60 mm and 100 mm x 100 mm used in test series 2.3. The rod diameters were 12 mm and 20 mm respectively. In Figure 13 the result of the smaller cross-section is shown as an example. The curves for the model with a larger cross-section can be found in the Appendix A. The curves with glued in rods (Wood_rod) show a slower heat development than for a solid wood cross-section. However, it also becomes apparent that the two mesh widths of 1 mm in the two-dimensional model and 4 mm in the three-dimensional model continue to lead to almost the same temperatures.

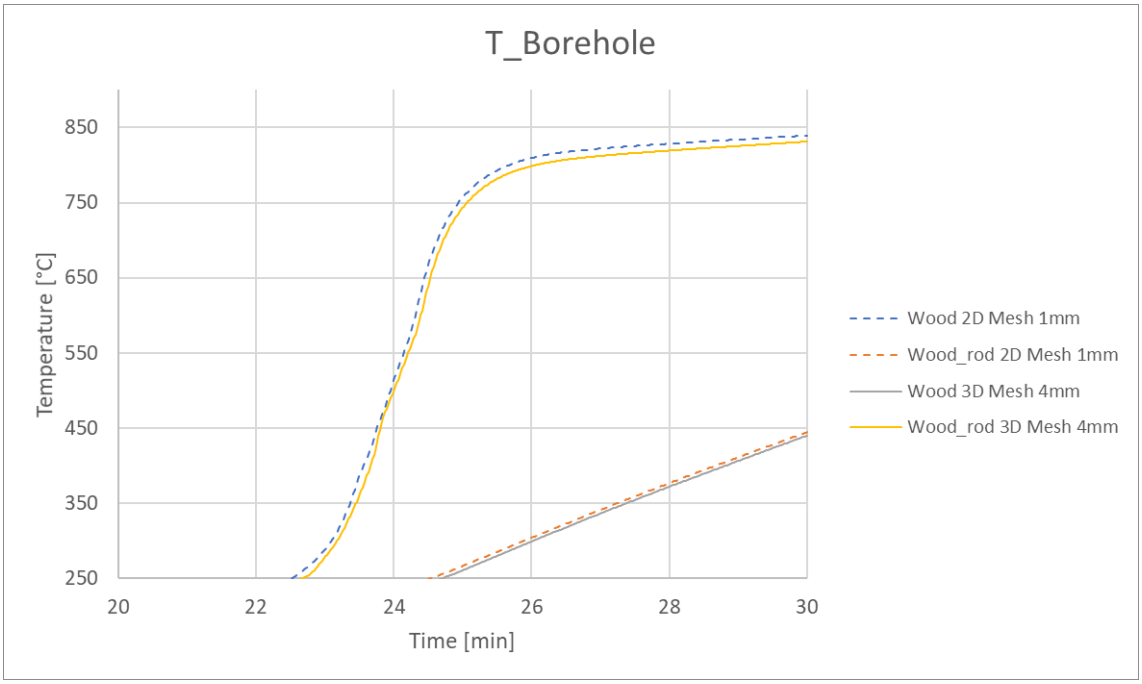

Figure 13: Influence of the mesh density on the temperature curve for a two-dimensional and a three-dimensional model with cross-sections of only timber and cross-sections with a glued in rod

Due to the visible cooling effect of the rod, the temperature curves were also evaluated along the axis of the rod. The models had a length of 150 mm. The rod itself was 50 mm long (greenish in Figure 14). The adhesive is colored yellow whereas the wood is colored either brown or grey. The individual components were thermally coupled. The evaluated temperature paths run in the direction of the rod from position 1 to position 2 at different measuring depths y. The figure shows the temperature distribution in the three-dimensional model as an example (blue → coldest point, red → warmest point). This makes it clear that the lowest temperatures occur at the position of the rod and that there is a cooling effect during simulation. A thermal load duration of 30 minutes was simulated.

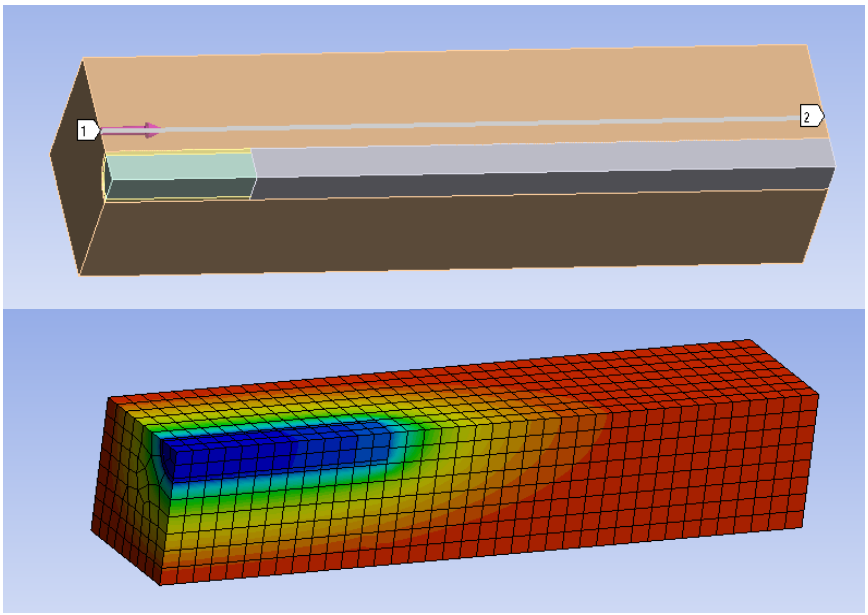

Figure 14: Temperature profile of a 3-dimensional model with a glued in rod M12 (blue colder than red)

Figure 15 shows the curve of the temperatures for the test specimen with a cross-section of 60 mm x 60 mm. The length of the test specimen of 150 mm is plotted on the x-axis. The rod in the model lies within the length from 0 mm to 50 mm. The measuring depths range from 0 mm to 12 mm. 0 mm represents the origin in the rod. 6 mm is the edge of the rod and 7 mm is the edge of the borehole. The curves show a drop in temperature in the area of the rod. The cooling effect decreases drastically with increasing distance from the borehole (y=9.5 mm and y=12 mm). An influence can also be seen from the side. Only 50 mm behind the bar with the test specimen length of 100 mm almost constant temperatures can be seen again for the wooden cross-section. A similar result was shown for the 20mm rod with a cross-section of 100mm x 100mm. The illustrations are in the Appendix A.

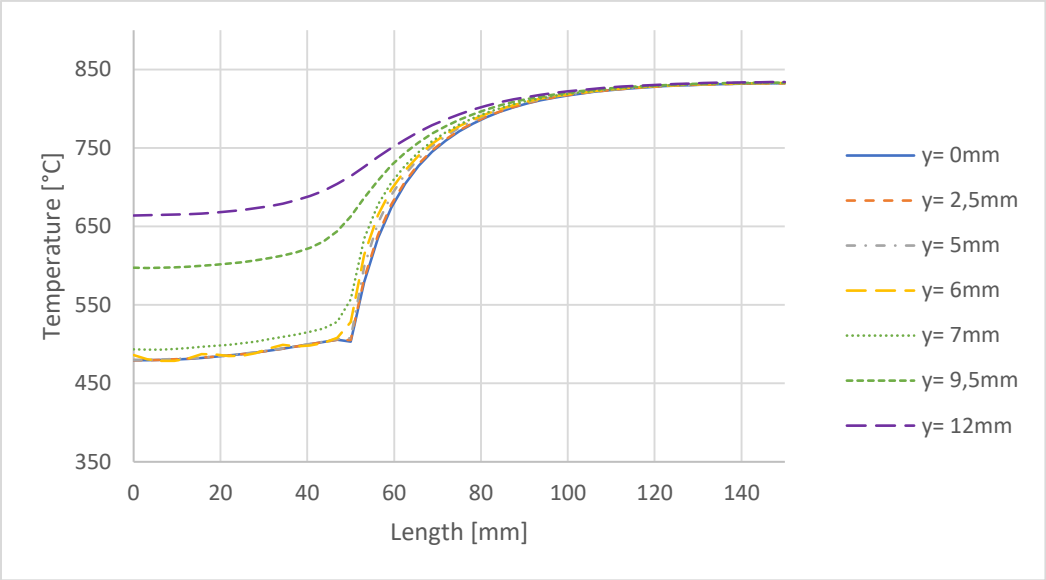

Figure 15: Temperature profile for different depths of a three-dimensional model with a glued in rod after 30 minutes of fire load with Standard Fire Curve with a cross-section of 60 mm x 60 mm and a rod diameter of 12 mm

The influence of the glue line thickness on the temperature curves was examined afterwards (see Figure 16). The same cross-sections were used for the M12 and M20 rods and only the glue line thickness was changed. The wood cover remained the same for all models to ensure comparability. The results show that a thicker glue line leads to a faster heating at the edge of the borehole. Since a lower thermal conductivity was used than for wood, this seems plausible. In the tests, no major differences could be determined for the glue line thickness, which can be due to the uneven combustion of the wood.

Under the selected boundary conditions, the simulations also show that at lower temperatures in the critical temperature range of the adhesives between 60 °C and 80 °C, the differences between the individual glue line thicknesses are insignificantly small. For this reason, it is assumed that the glue line thickness has only a marginally small influence on the temperature development. Further temperature curves along the side edges of the specimens and in the diagonal direction are shown in the Appendix A. However, these show similar trends.

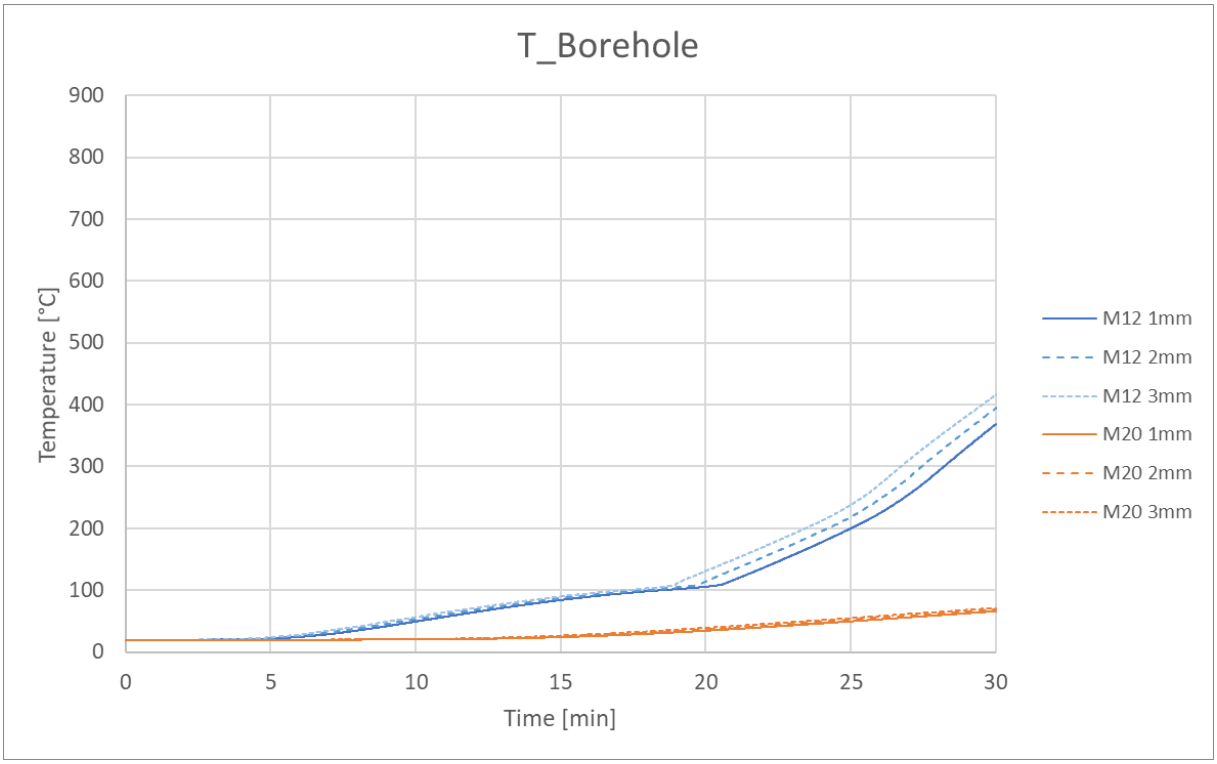

Figure 16: Influence of the glue line thickness on the temperature of the borehole edge for two rod diameters

In the next step of the sensitivity analysis the influence of the meshing quality was investigated. Since round shapes due to the rod and the borehole are present the automatically designed mesh isn`t evenly distributed (see Figure 17).

An automatically generated mesh and an adaptation for a more evenly distributed mesh using sweep method in ANSYS Workbench are shown below as an example. The thermal load was applied to the two sides where only wood is present on the surface.

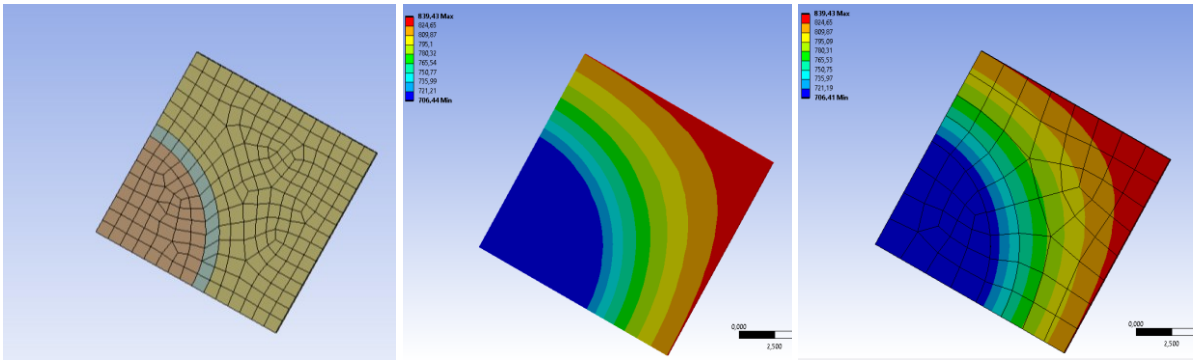

Figure 17: Sketches of the mesh generation with glued in rods

The results for a 30-minute simulation time are shown below as an example in Figure 18. The maximum time step size was one second. The Standard Fire Curve was used as the thermal load. It can be seen that the two graphs show hardly any deviations and the influence of the irregularities from the automatic meshing can be classified as very low. Further investigations were also carried out on a three-dimensional model. During a 60-minute simulation, there were differences of a maximum of 2 °C in the end temperature, which is why the automatic meshing for the thermal models was found to be sufficient.

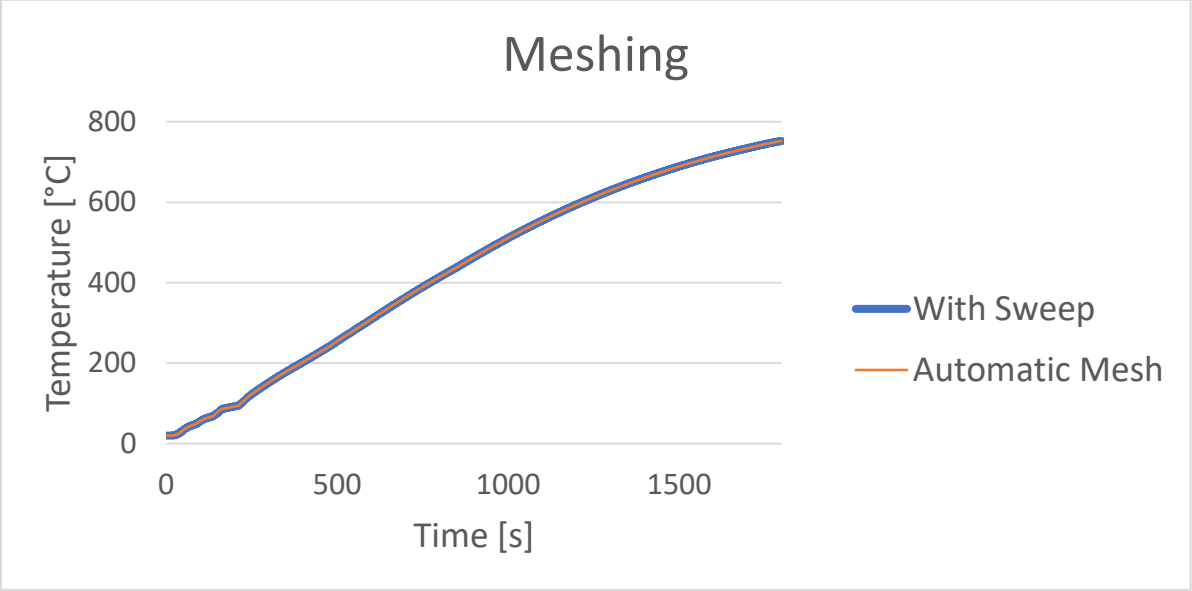

Figure 18: Temperature curve for a two-dimensional model with sweeped and automatic mesh configuration

5 Test Series 2

5.1 Thermal influences

The fire load is applied to the system according to the Standard Fire Curve (SFC). The heat transmission from the SFC to the simulated test specimen takes place via radiation and convection on the specimen surface facing the fire (exposed). The formula for the applied temperature is shown below.

$$T_g = 20 + 345 \cdot log_{10}(8 \cdot t + 1) \quad (3)$$

The test specimens from test series 2.1 and 2.2 are only exposed to fire from one side. Therefore, a different radiation and convection coefficient is applied for the heat transmission from the test specimen on the side facing away from the fire (unexposed). The temperature there is set to 25 °C according to the ambient temperature.

Heat transfer by radiation or convection depends on the ambient temperature and the emissivity (radiation) or the heat transmission coefficient (convection). The loads defined in the model and the boundary conditions used are listed in Table 6.

Table 6: Values for heat transmission in numerical simulation

Heat Transfer	Exposed	Unexposed
Convection α [W/m²K]	25,0	4,0
Radiation ε	0,8	0,8

5.2 Test series 2.1

In test series 2.1 there were five specimens tested. The different structures are briefly shown in Figure 19 for a better overview. For more detailed information, please refer to the sub reports of D3.4.

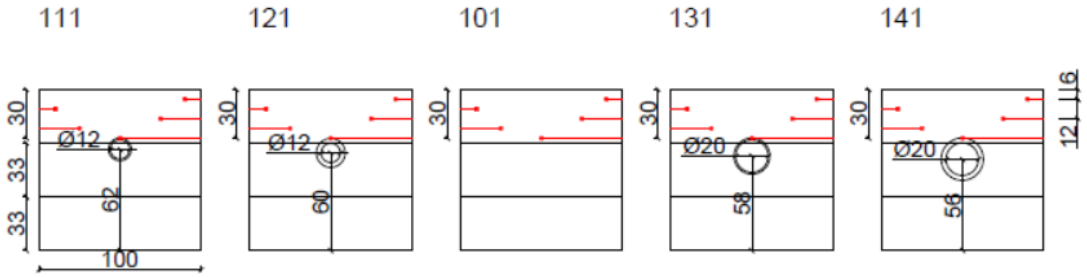

Figure 19: Sketches of the five different specimens in test series 2.1 (red markings are the spots for temperature measurements inside the specimen)

Due to the same cross-sectional structure and the one-sided fire load, a 2-dimensional model is created in the thermal FE analysis. At the same time, the symmetry axes are used to shorten the computing time and only half a cross-section is modeled.

The values defined in Chapter 3 are used as material parameters. The simulation time is 60 minutes with a maximum time step of one second.

The program gives the temperatures at the real measuring points over time. Figure 20 shows an example of the model with the temperature distribution after a simulation time of 60 minutes. It can be seen that the rod has an influence on the heat development within the test specimen. On the one hand, it has a cooling effect on the side facing the fire, while the rod leads to a faster heating to the unexposed side of the rod.

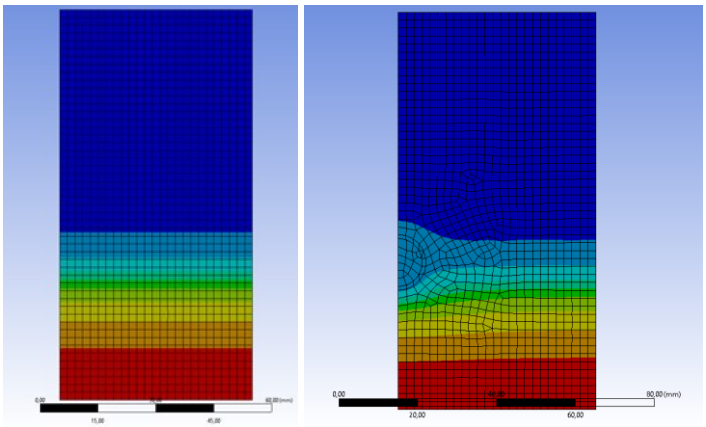

Figure 20: Comparison of temperature profile between specimens with timber (left) and a glued in rod (right)

The cooling effect is also shown by the temperature curves. Figure 21 shows the temperatures of all 5 test specimens for a measuring depth of 6 mm and 30 mm (at the edge of the bore-hole) from the side facing the fire. Here you can see that with the small measuring depth of 6 mm, there are hardly any deviations. With a higher depth of 30 mm (position of the bore-hole edge) the specimens with glued in rods show lower temperatures than with the reference test specimen (PK 101). You can also see that the test specimens with the thicker rod diameter of 20 mm (131 and 141) have even cooler temperatures. In this case, the glue line thickness of 1 mm also delivers smaller values, since there is a larger wood cover due to the same cross-sections of the test specimens, which shields the rod for a correspondingly longer time. The full graphs for the other measurement depths can be found in the Appendix B.1.

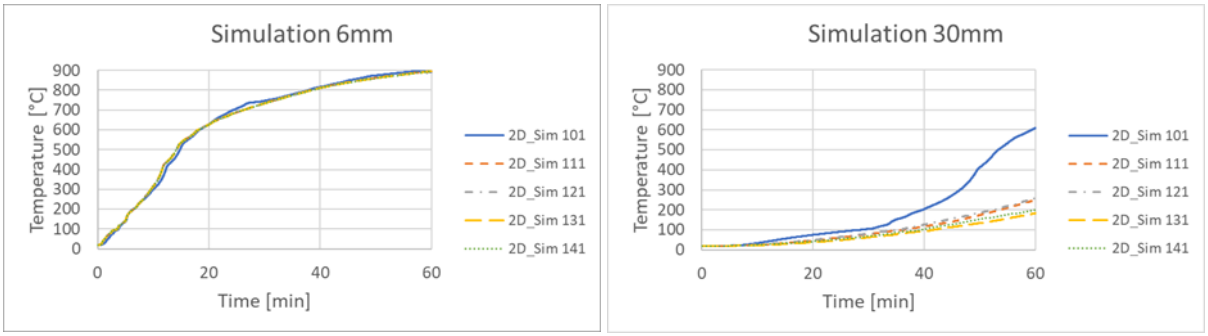

Figure 21: Temperature curves for a depth of 6 mm (left) and 30 mm (right) for the five specimens in test series 2.1

The simulation results were then compared with the mean measurement results (see Figure 22). For test specimen 101 without rods, the measured values agree well with the simulation results. The simulation delivers values that are usually a little lower, especially for measurements at a depth of 6 mm and 18 mm. Here, higher charring rates were determined in the test.

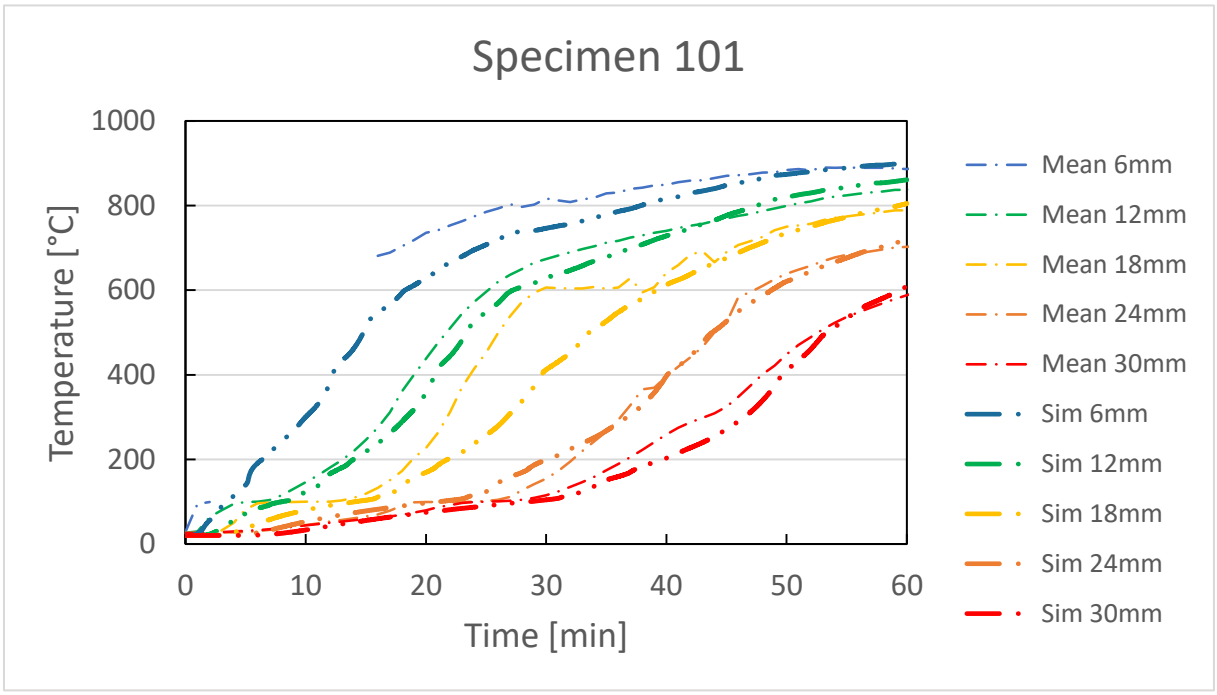

Figure 22: Comparison of test results (mean values) and simulation results for specimen 101 for the five measurement depths

Test specimen 111 had an M12 rod with a glue line thickness of 1.0 mm (see Figure 23). The simulation again shows similar progressions as the measured values. Here, however, the difference is higher than in the case of test specimen 101. That seems plausible, since the highest charring rates were measured with this test specimen in the test. The biggest difference is at the measuring point in the area of the borehole. Here, the simulation predicts a significant reduction in temperature, which was not observed in the test.

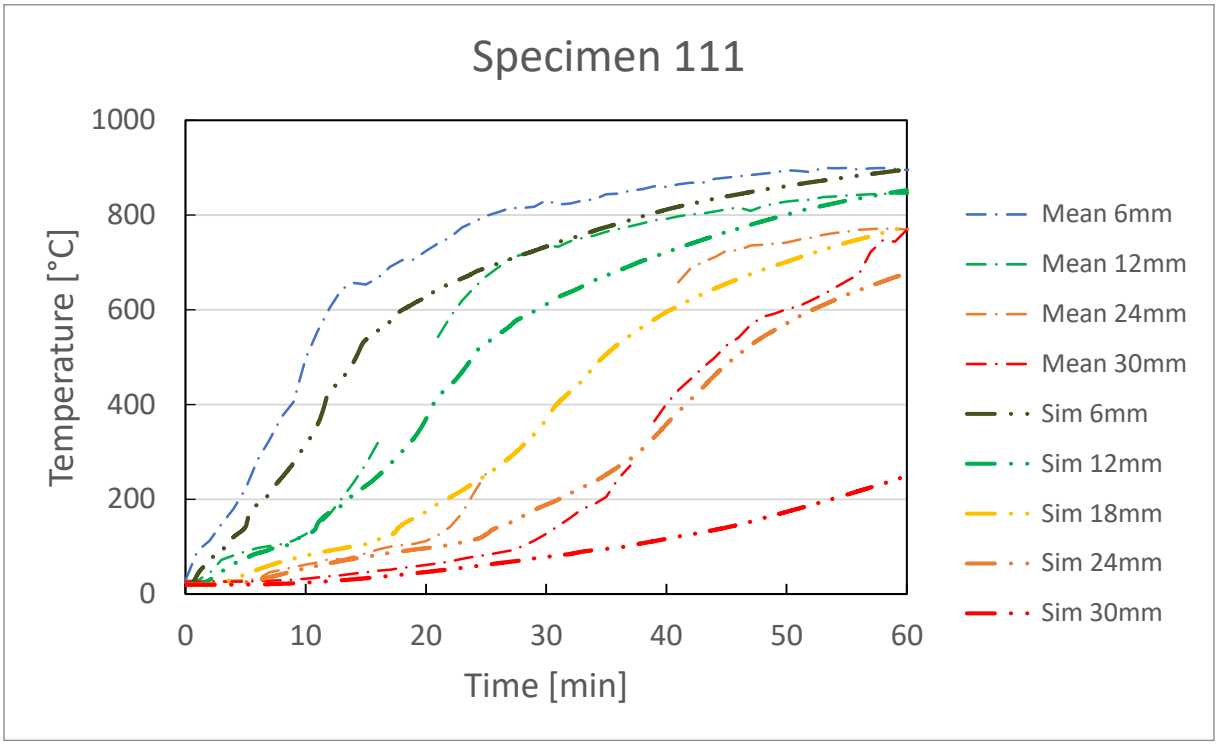

Figure 23: Comparison of test results (mean values) and simulation results for specimen 111 for the five measurement depths

Test specimen 121 also had an M12 rod with a glue line thickness of 3 mm (see Figure 24). Here the simulation results are close to the measured values. A significantly higher temperature is only achieved at the edge of the borehole at a measuring depth of 30 mm. The values for the simulation again show the lower results, which may be due to the increased charring in the test.

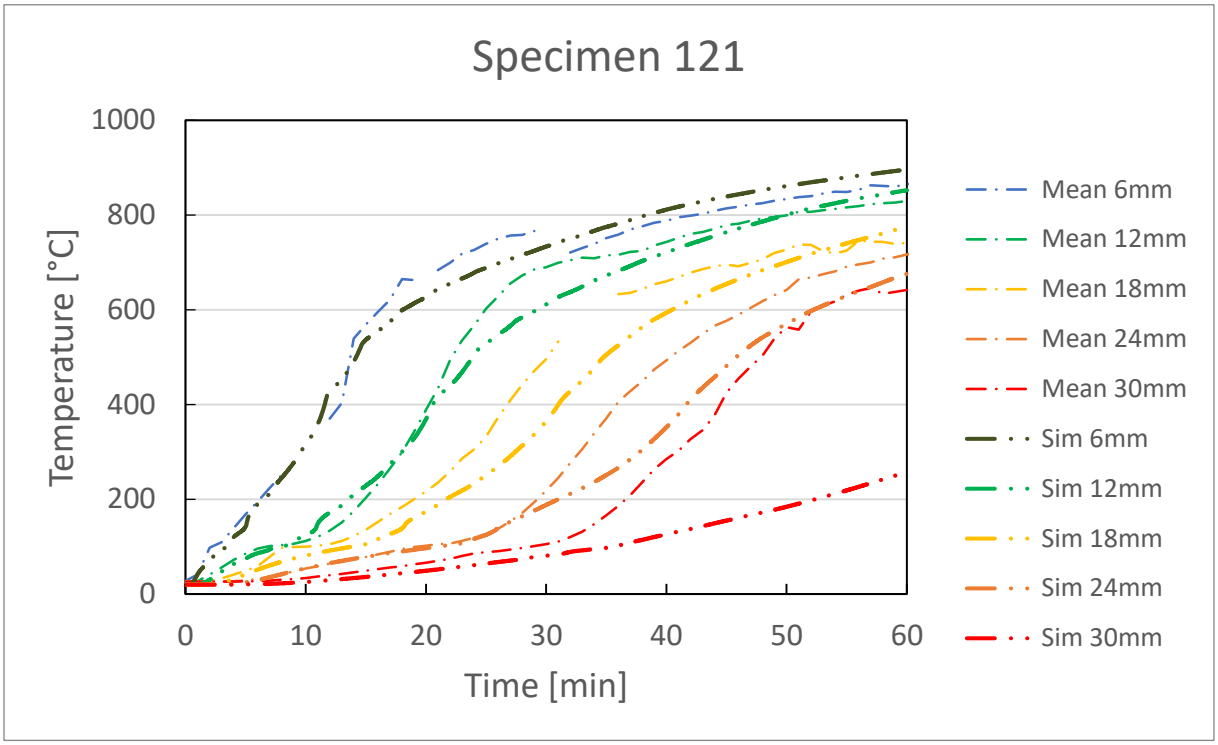

Figure 24: Comparison of test results (mean values) and simulation results for specimen 121 for the five measurement depths

With a rod thickness of 20 mm and a glue line thickness of 1 mm in test specimen 131, the simulation again shows similar curves to the measurement results (see Figure 25). However, a significantly greater temperature rise for the measurements is already established for the depths of 12 mm. This increases again for the depths of 18 mm and 24 mm. There could have been a larger joint gap in the area of the thermocouples, which leaded to higher temperatures. No measurements were available for the edge of the borehole. However, based on the previous temperature curves and the other specimen results, a significant increase above the simulation values is assumed.

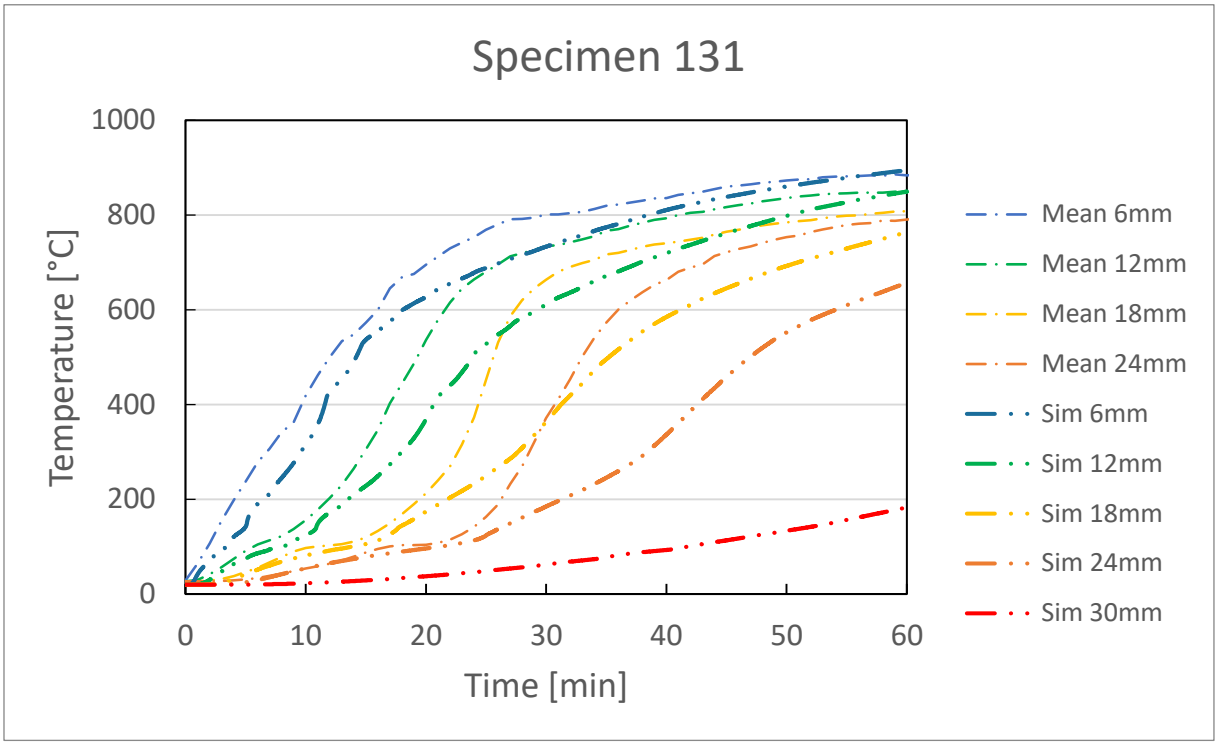

Figure 25: Comparison of test results (mean values) and simulation results for specimen 131 for the five measurement depths

Specimen 141 had an M20 rod with 3mm glue line thickness (see Figure 26). For the measuring depths of 6 mm and 12 mm, the simulation results are close to the measured values. Larger deviations are found for the greater depths, which may be related to increased combustion at the level of the measuring points. In this case, smaller deviations are shown for the edge of the borehole than with the previous test specimens. However, the simulation is still greatly exceeded by the measurement results after 60 minutes.

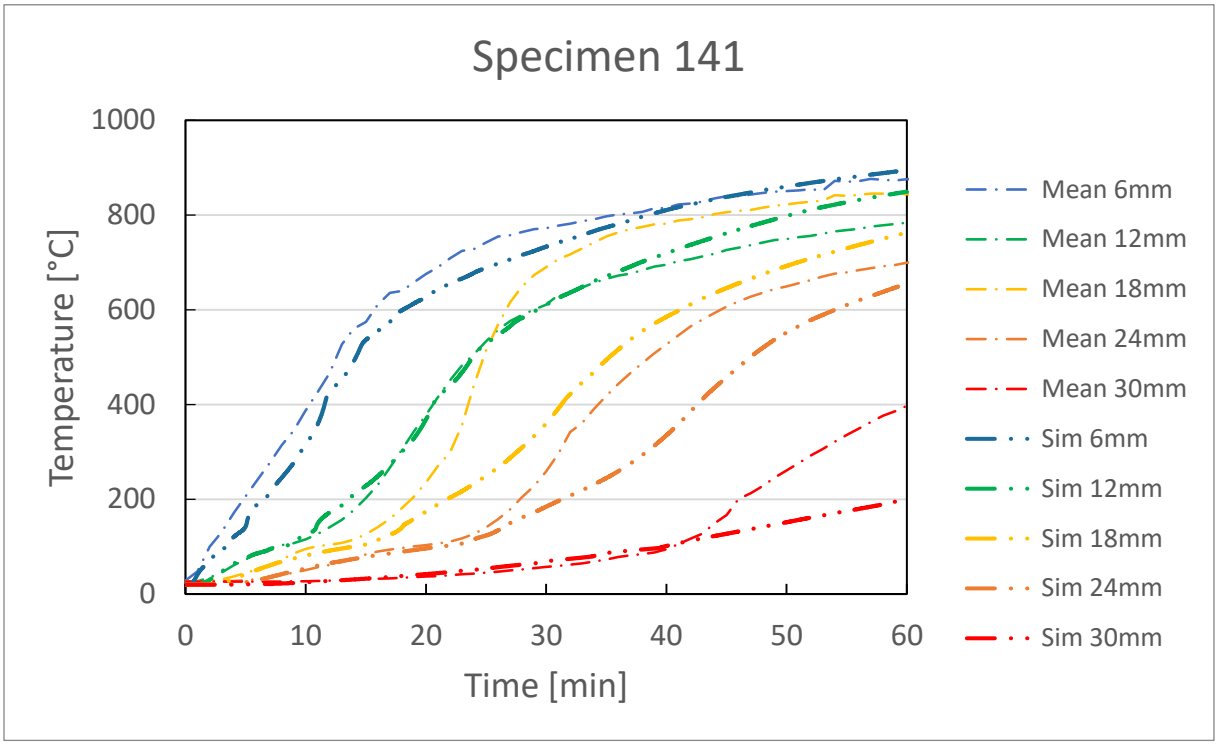

Figure 26: Comparison of test results (mean values) and simulation results for specimen 141 for the five measurement depths

The simulation results show that the assumptions and material parameters provide similar temperature profiles most of the time. There was increased charring in the tests compared to the generally applicable charring rate of 0.65 mm/min according to EN 1995-1-2. It is assumed that the joint between the specimens had an influence on the charring rate and was leading to a faster charring resulting in higher temperatures. The cooling effect on the rod is apparently overestimated by the simulation. Further tests are necessary to clarify how large the scope of the cooling effect actually is or whether the material parameters in this area may have to be adjusted.

5.3 Test series 2.2

In test series 2.2, eight test specimens were simulated. Four rods were glued transversely to the direction of the fibers in each test specimen. These rods had a diameter of 12 mm or 20 mm and a glue line thickness of 1 mm or 3 mm. The specimen setups are shown in Figure 27. A more detailed description of the specimens can be found in D3.4.

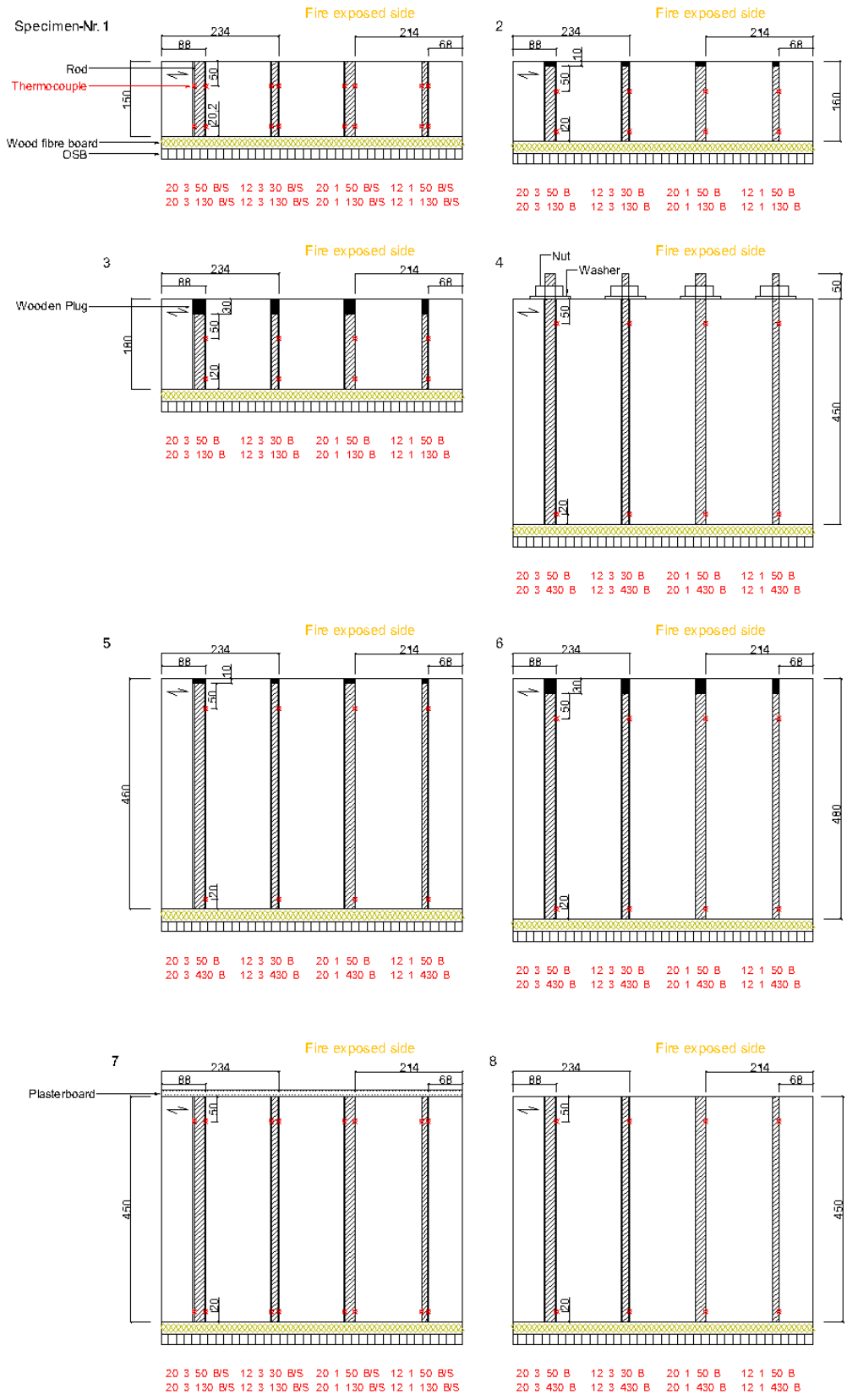

Figure 27: Sketches of the eight specimens of test series 2.2 (red are the names and the spots for temperature measurement)

For the simulation, each test specimen was divided into four sections in order to calculate one rod per model. The cross-sections were quartered by using symmetry effects (see Figure 28). The lateral faces were assumed to be perfectly insulated. The side facing the fire and the side unexposed of the fire were thermally loaded with the values described in Chapter 5.1. For the simulation duration of 60 minutes, the maximum time step was set to 0.1 seconds. The material parameters are listed in Chapter 3.

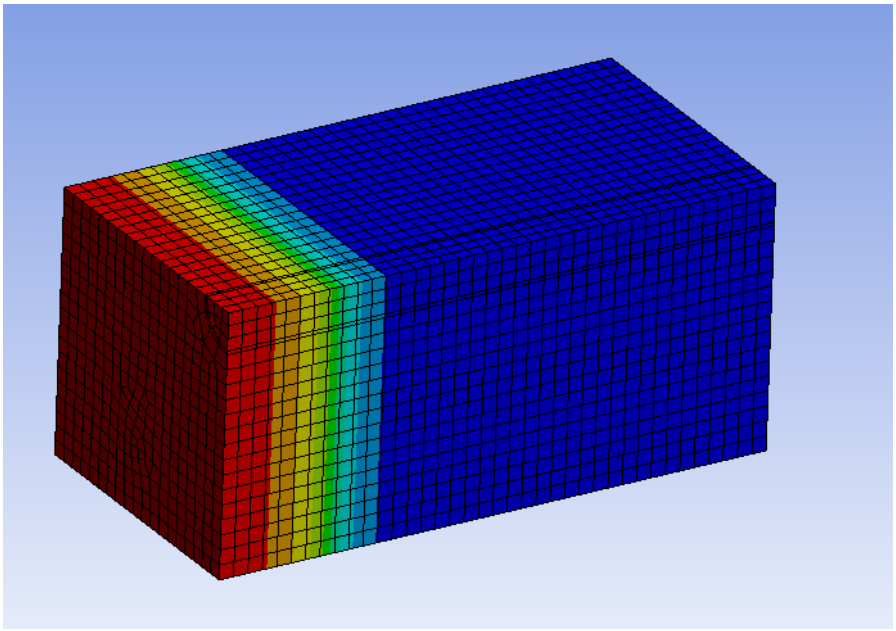

Figure 28: Temperature profile for a 3-dimensional model, with all parts simulated as timber

The temperatures at the actual measuring points were given from the simulation. The actual measuring points were used here, since most of the thermocouples in the test specimens deviated from their planned position by a few millimeters and were leading to more deviations between simulation and test.

The simulation results were then compared with the measuring points of the tests. The material parameters were initially calibrated on test specimen 1. Changes were carried out with the position of the thermocouples, the material parameters for wood and steel according to EN 1995-1-2 and EN 1993-1-2. Also, the influence of the grain direction as well as the parameters for adhesive and the initial temperatures as thermal load were changed during the validation.

In the case of specimen 7 with a gypsum plasterboard covering, falling off of the board was simulated. For this purpose, a time-dependent EKill function was programmed in ANSYS Workbench via an APDL command. As a result, the layer was deactivated when the failure time of the tests was exceeded.

After the layer has been deactivated by the EKill function, the thermal load with the Standard Fire Curve does not disappear. It has a direct effect on the timber which was protected before. It is now facing the thermal load directly. In order to represent the real temperature load as precisely as possible, a new curve corresponding to the effects of radiation and convection was used instead of the SFC. According to [15], the direct application of the SFC to the knots leads to a higher temperature load. Since the elements are not deleted via the EKill function, the radiation cannot be transmitted via the external radiation point, but must be applied directly to the new layer. Therefore, a time-dependent logarithmic function was developed, which applies the temperature profile due to convection and radiation to the nodes of the new layer.

$$T = 166.11 \cdot \ln(t) - 424.63 \quad (4)$$

Figure 29 shows the SFC and the logarithmic function for a comparison of the different temperatures.

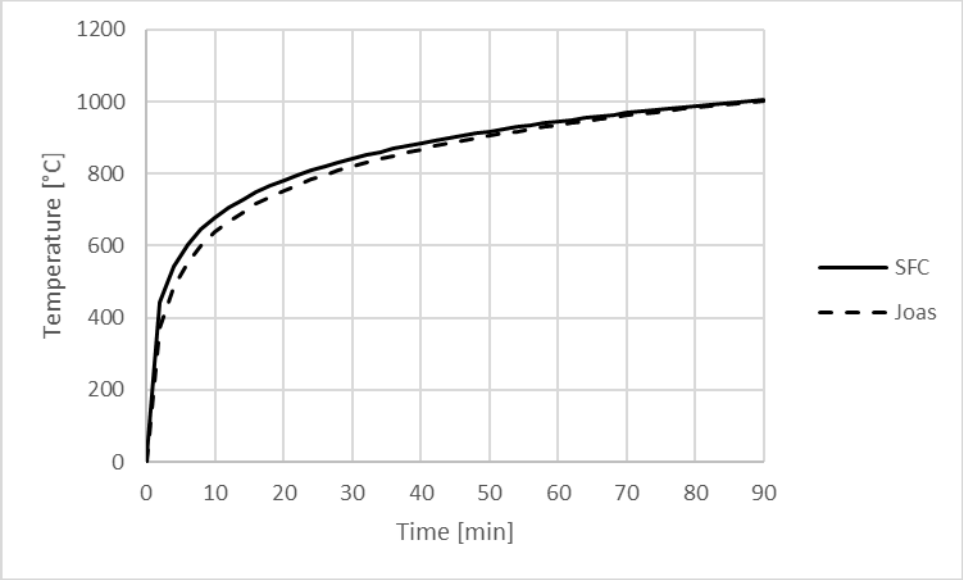

Figure 29: Comparison of the Standard Fire Curve and the adjusted curve from [15]

In some cases, a good agreement was reached with the test results. For other specimens like specimen 7 with the gypsum plasterboards the simulations showed too conservative results. It is assumed that the gypsum plasterboard has not fallen off completely due to the small surface area, but was still partially in front of the rod.

In Figure 30 the comparison of the simulation and test results of specimen1 is shown as an example. The rod had a diameter of 20 mm and a glue line thickness of 3 mm. The measuring points were either at the borehole (B) or at the threaded steel rod (S). The measuring depths were at a depth of 50 mm and 130 mm from the side facing the fire under the respective covering. The simulation provides similar curves as for the real measured values. In this case, the simulated curves for the rod are in a more conservative range, while the values at the borehole are slightly below the test results. The other curves of the individual configurations are shown in the Appendix B.2.

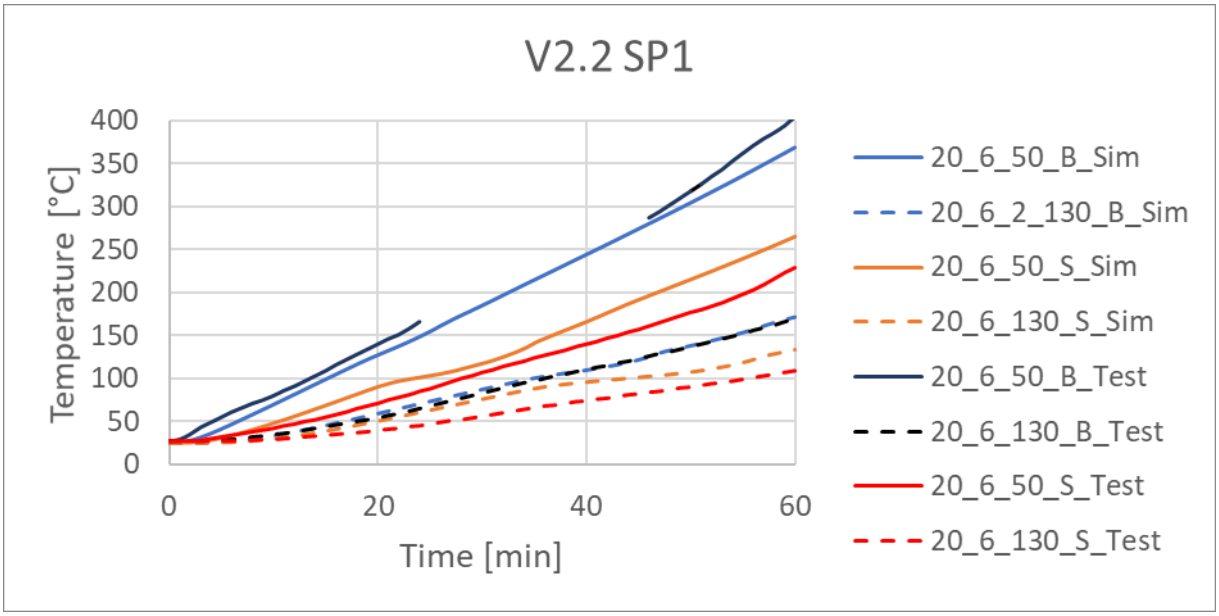

Figure 30: Temperature profile for specimen 1 in test series 2.2 with the simulated and measured curves

In order to obtain information about the accuracy of the simulation, the ratio of the final temperature (measured / simulated) was formed. In addition, the curve integrals were formed over the simulation time and also set in relation to each other. The results are shown in Table 7.

On average, the deviations for the end temperatures after 60 minutes are 1 % higher in the simulation for the boreholes than in the tests. Larger deviations of 4 % occurred for the measuring points directly placed at the rod. Overall, the standard deviation for the measuring points on the side facing the fire was significantly higher. The reason for this could be the uneven burning for wood, which has a greater influence when the measuring point is closer to the fire exposed side. Since there are large embedment lengths of 430 mm on the side unexposed from the fire for 5 test configurations and no temperature increases occurred there, there was better agreement between the simulated and measured results.

Table 7: Deviation of simulated temperature from the measured temperature curves in test series 2.2

		50_B		130_B/430_B		50_S		130_S/430_S	
Deviation		Final Temp.	Integral	Final Temp.	Integral	Final Temp.	Integral	Final Temp.	Integral
PK 1	12_2	108%	118%	114%	117%	112%	118%	91%	98%
	12_6	97%	102%			82%	99%	92%	105%
	20_2	139%		111%	107%	105%	107%	121%	116%
	20_6	91%		99%	98%	112%	114%	120%	119%
PK 2	12_2	118%	108%	116%	112%				
	12_6	72%							
	20_2	69%	75%	101%	100%				
	20_6	112%	112%						
PK 3	12_2	97%	101%	111%	103%				
	12_6	94%	98%	93%	93%				

	20_2			102%	99%				
	20_6	104%	94%	95%	95%				
PK 4	12_2			97%	94%				
	12_6	91%		98%	92%				
	20_2			113%	100%				
	20_6	103%		112%	99%				
PK 5	12_2	93%	90%	93%	90%				
	12_6	99%	95%	95%	92%				
	20_2			93%	90%				
	20_6	96%	96%	99%	93%				
PK 6	12_2	117%	114%	93%	89%				
	12_6	82%	98%	93%	89%				
	20_2	104%	105%	95%	92%				
	20_6	95%	98%	95%	92%				
PK 7	12_2	136%	131%	92%	92%	134%	134%	98%	95%
	12_6	83%	86%	97%	92%	70%	73%	97%	92%
	20_2			101%	93%	130%	132%	103%	93%
	20_6			101%	94%	87%	98%		
PK 8	12_2	122%	123%	103%	96%				
	12_6			99%	95%				
	20_2	92%	94%	113%	100%				
	20_6	104%	109%	115%	100%				
All	Mean	101%	102%	101%	96%	104%	109%	103%	103%
	Rel. Stand. Deviation+	17%	13%	8%	7%	22%	18%	12%	11%
SP1-3	Mean	100%	101%	105%	103%	103%	109%	106%	109%
	Rel. Stand. Deviation+	20%	13%	8%	8%	14%	8%	16%	9%
SP4-8	Mean	101%	103%	100%	94%	105%	109%	99%	93%
	Rel. Stand. Deviation+	15%	13%	7%	4%	30%	27%	3%	2%

5.4 Test series 2.3

In test series 2.3, three test specimens were simulated. All specimens were exposed to fire from all sides. A test specimen with a cross-section of 60 x 60 mm and an M12 rod (SP 211) and two test specimens with a cross-section of 100 x 100 mm and both an M12 (SP 212) and an M20 rod (SP 231) were tested with a glue line thickness of 1 mm. The exact test procedure can be seen in sub report D3.4. There were two measuring points per test specimen directly in the glue line (position A and B).

By using symmetry effects, two-dimensional models with a quarter cross-section of the specimen were generated. The edges were defined as "perfectly insulated" so that no heat transmission took place there. The temperature loads from Chapter 5.1 were applied over the test period of 60 minutes. The maximum time step per simulation was set to 0.1 seconds. Figure 31 shows the corresponding model. The temperature at the edge of the borehole (B) and at the steel rod (S) was evaluated.

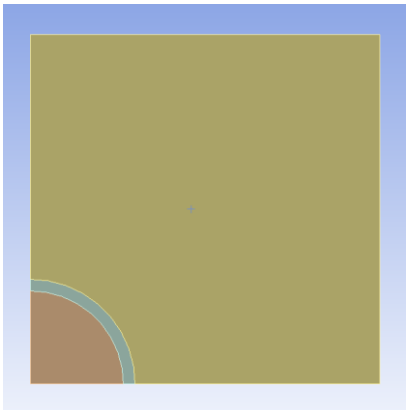

Figure 31: Model with a quarter cross-section used for test series 2.3

After the simulation, the results were compared with the temperature curves from the tests. The time is shown on the x-axis, while the temperatures are shown on the vertical axis. Since some of the thermocouples on SP 211 failed during the test, a validation was difficult. The curves are shown in the Appendix B.3.

The simulation for test specimen 212 provides slightly conservative values up to a temperature of 100 °C, but agrees well with the measured values from the tests (see Figure 32). In the range of 100 °C, the temperatures from the tests are briefly above the simulation results. At the higher temperatures, however, the simulation again assumes a faster temperature rise afterwards. Especially for the range from 60 – 80 °C, in which the adhesive loses a lot of its strength, good matches are achieved with the selected material parameters.

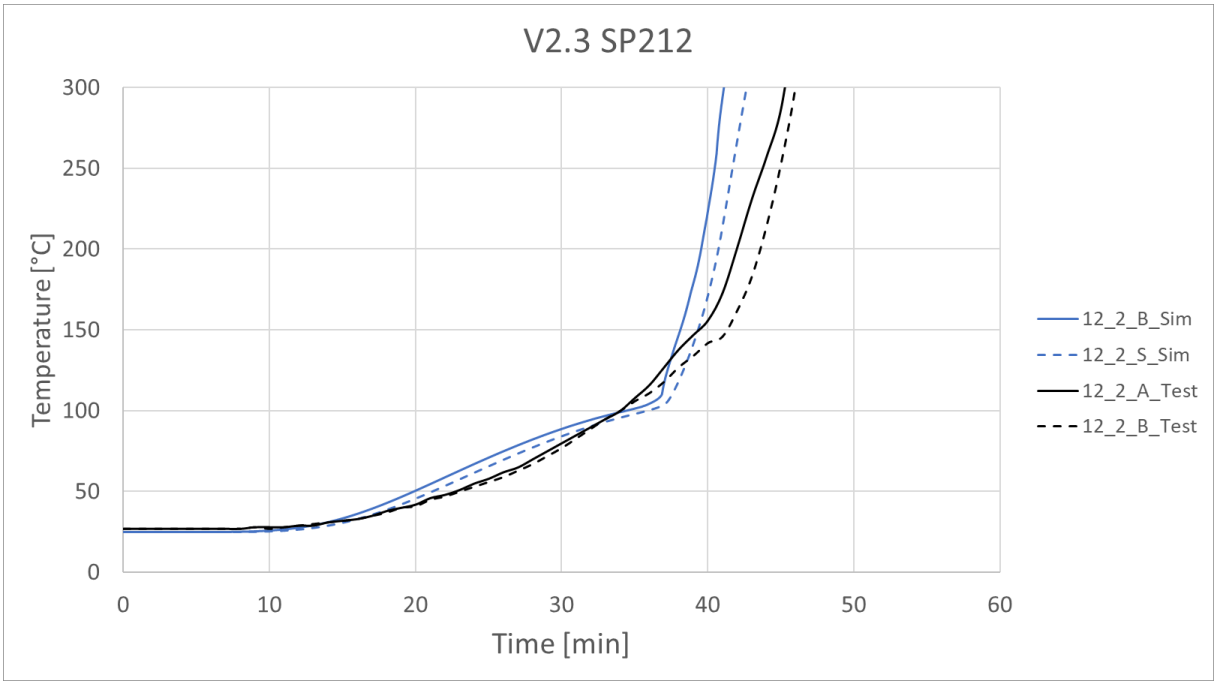

Figure 32: Temperature curve of test specimen 212 in test series 2.3 with simulated and measured results

The simulation also provides similar temperature curves as the measured results for test specimen 231 (see Figure 33). However, the calculated temperature is below the measured values for a short time at around 80 °C. Only after exceeding 140 °C does the simulation show higher or more conservative values again. The selected material parameters thus deliver acceptable results and are verified again by test series 4.

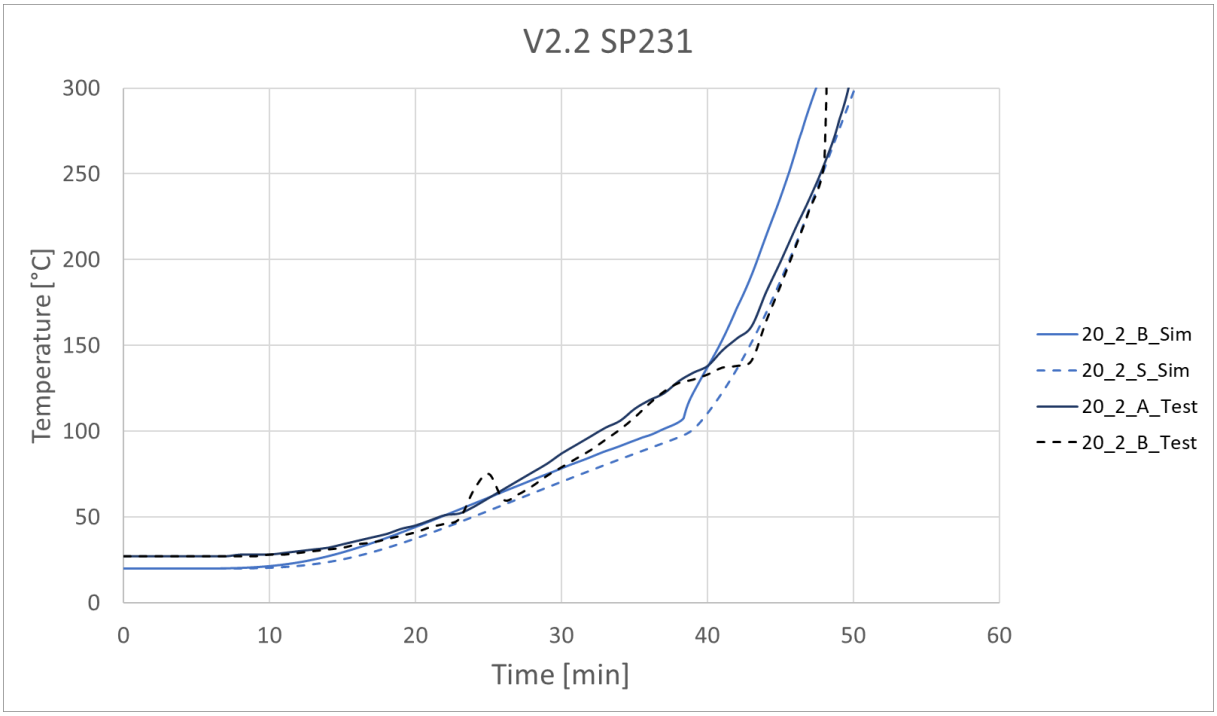

Figure 33: Temperature curve of test specimen 231 in test series 2.3 with simulated and measured results

6 Test series 4

The results of each test series have shown that the adhesive is the weak point of the connection when exposed to temperature. This should not exceed an adhesive-dependent critical temperature limit. For this reason, a wooden covering is recommended, which acts as fire protection. The temperature limit was derived from test series 3. With the help of the simulation models of test series 2.3, it was checked when this critical temperature is exceeded. The material characteristics from Chapter 3 were used here. On this basis the specimens for test series 4 were planned. The specimens had the same design as in test series 3. They were exposed to fire on all sides under a constant tension load.

Rods with diameters of 12 mm and 20 mm were used for the fire tests. In addition, both previous adhesives were used. These were set according to test series 3 with the 20 % -quantiles of all specimens which showed failure in the glue line. For Adhesive 1 (2K-Epoxy) a critical temperature limit of 69 °C and for Adhesive 2 (2K-PUR) a temperature limit of 79 °C was derived and defined.

Quarter models from test configuration 2.3 were used in the model to determine the necessary minimum timber cover. For these, a parametric study was used with a change in the cross-section in order to obtain the temperature profile at the edge of the borehole after the fire load of 30, 60 and 90 minutes. Based on these simulations, the minimum wood cover for the two rod diameters was selected depending on the adhesive system. With this procedure, the necessary minimum wood cover can be calculated exactly. This method is disadvantageous since it is time-consuming in practice. There are also uncertainties, since the temperature range in which the adhesive fails is relatively small. Since wood has an anisotropic material behavior, there is no exact match with the simulations, which is why additional safety measures are necessary.

The calculated cross-sections were increased to the next highest side length used in praxis for the tested specimens, whereby the simulated minimum wood cover was exceeded and a fire

exposure duration of more than 30 minutes should be ensured. A total of four test specimens were examined. The structure is given in Table 8. Further details on the testing process as well as on the evaluation and production are presented in sub report D3.4.

Table 8: Setup of the four test specimens in test series 4

Number	Rod diameter [mm]	Adhesive Type	Cross section [mm x mm]	Failure Time [min]
1	12	1	120 x 120	33
2	12	2	100 x 100	34,2
3	4*12	1	180 x 180	32,1
4	20	1	120 x 120	30,1

In addition to the test specimen under tensile load, an identical reference test specimen was placed in the oven, which should record the temperatures inside the specimen. The measuring depth was increased by 6 mm from the surface and finally measured directly at the rod. The test specimens themselves each had a sheathed thermocouple placed directly at the rod.

In order to be able to compare the measurement results with the simulations, sheathed thermocouples were placed near the surface of the specimen and the reference specimen to measure the air temperature. These values were used in the numerical simulation as thermal load and the temperature profile within the specimen was calculated.

Figure 34 shows the temperature curve for reference test specimen 1. The dashed lines represent the measured values from the tests. The complete simulations for all measuring depths are shown in the Appendix C. For the test specimen 1, good agreement is achieved in the temperature profile between the measured values and the simulation. In this case, the simulation values are partly on the safe side and indicate larger values for the selected input parameters. The simulation also achieves good agreement for the other test specimens. However, in some cases lower temperatures are also achieved through the simulation. It should also be noted that the measured values in the range of approx. 10 - 15 minutes showed a sharp rise in temperature, which then dropped back to the expected temperature level. The reason for this could not be clarified. The measuring device has been checked and showed no errors. Even changing the measuring channels in the device did not bring any improvement. For this reason, the temperatures recorded in this time duration were removed until the temperature increased again.

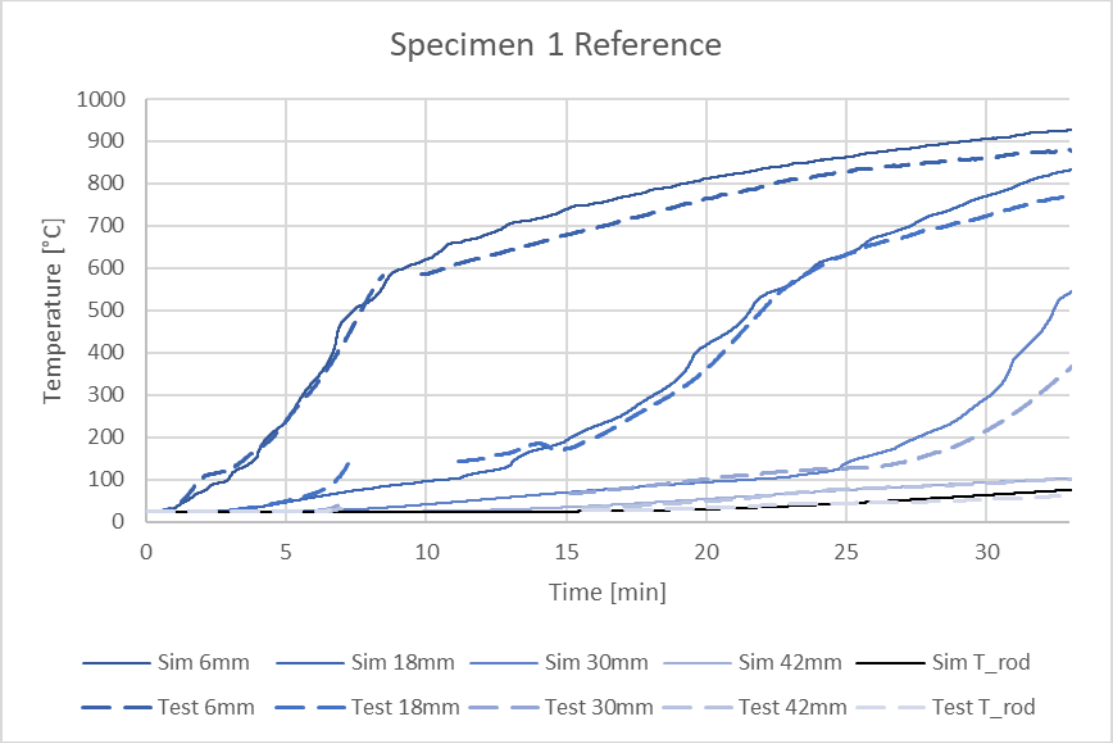

Figure 34: Temperature curves for simulated and measured results for reference specimen 1

In the low temperature range of the critical adhesive temperature between 60 °C and 80 °C, the curves are illustrated again in Figure 35. Good agreement is achieved, especially for the measuring points with a higher embedding depth. In the area of the rod a faster heat development is predicted by the simulation for the reference specimen than was actually measured. The simulation is therefore on the safe side.

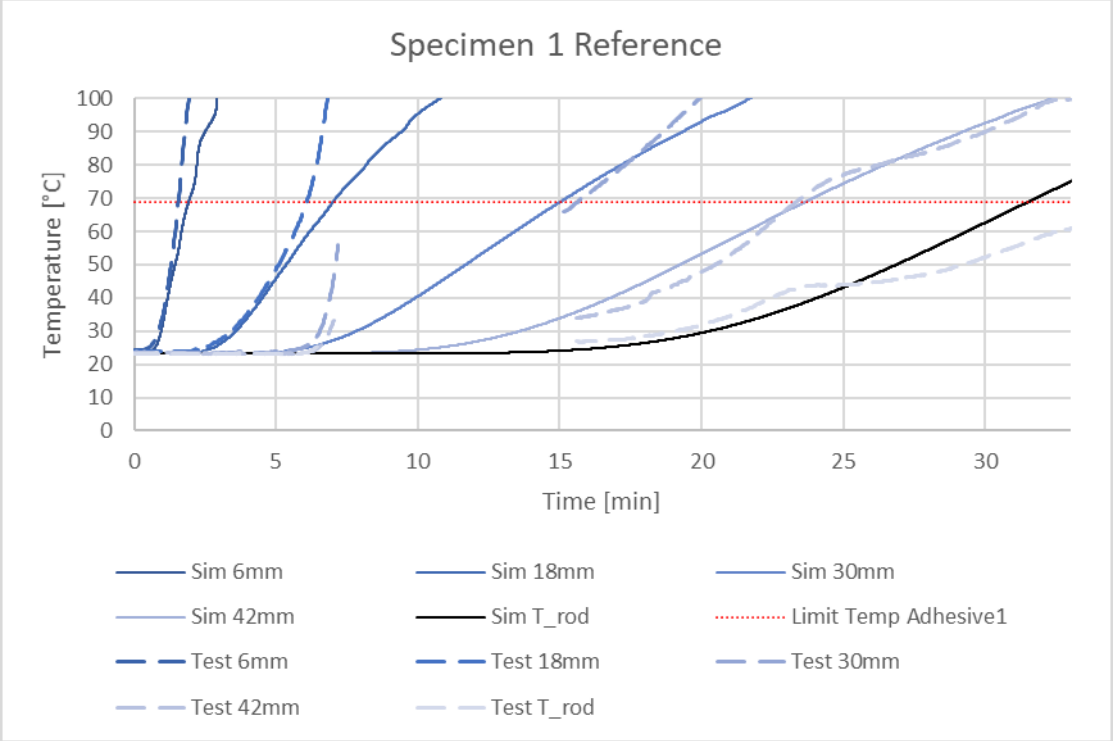

Figure 35: Temperature curves for simulated and measured results for reference specimen 1 in a temperature range of up to 100 °C

For the test specimen 1 the measurement during the test shows that it reaches the critical temperature level faster than in the simulation at the rod (see Figure 36). At 30 minutes, the curves are only about 8 °C apart. The other series of tests have shown that only a few degrees of temperature difference are sufficient to greatly reduce the adhesive strength. To ensure the load-bearing capacity, either higher limit temperatures for the adhesive are necessary or higher temperatures must be applied by the design model.

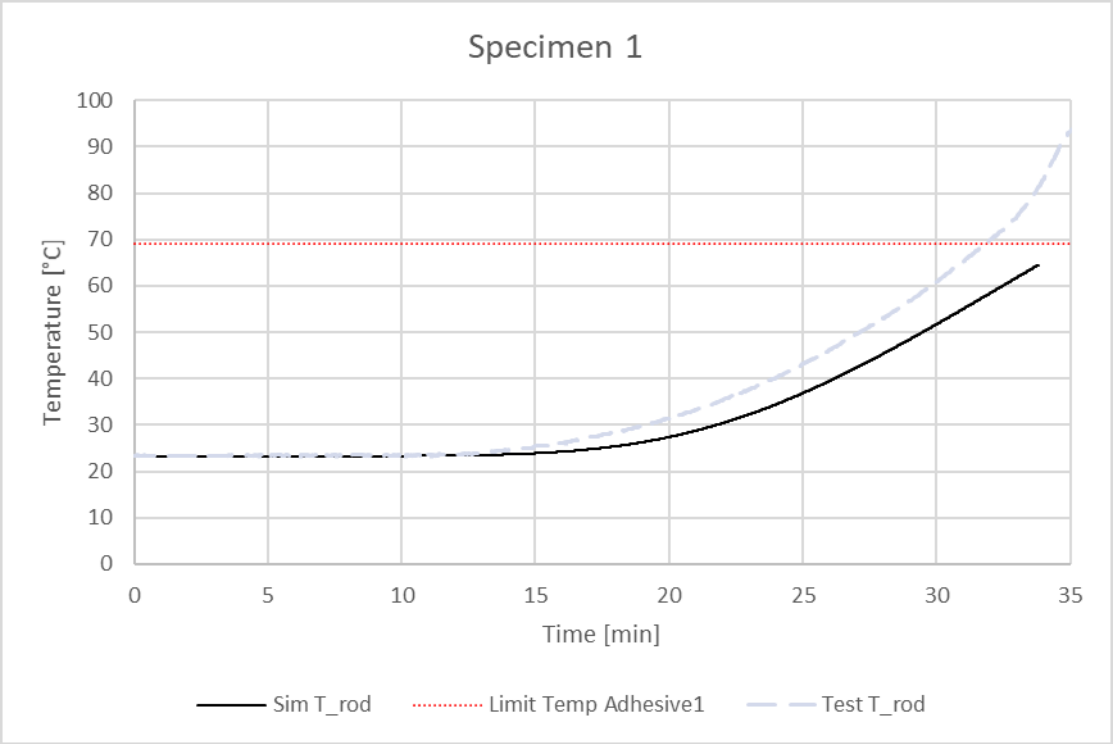

Figure 36: Temperature curves for simulated and measured results at the rod for specimen 1 in a temperature range of up to 100 °C

Similar results are obtained with reference specimen 2. Here, the temperatures in the test at a depth of 12 mm are above those of the simulation (see Figure 37). However, at the larger measuring depths, the simulation results are on the safe side and exceed the measured values. Significantly higher temperatures are calculated for the rod in particular than occurred in the test. However, in the event of a failure after 34 minutes, these two temperatures converge again. In both cases, the critical adhesive temperature of 79 °C for Adhesive 2 was already exceeded.

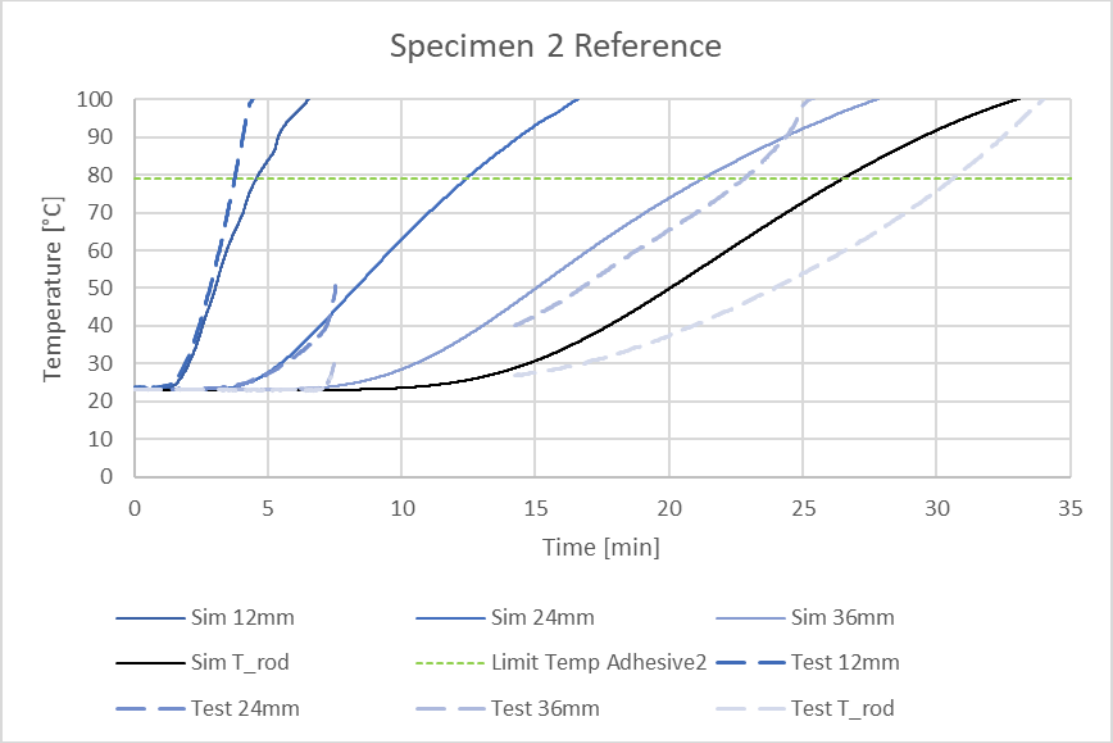

Figure 37: Temperature curves for simulated and measured results for reference specimen 2 in a temperature range of up to 100 °C

Higher temperatures are measured for the rod in the test specimen 2 than in the simulation (see Figure 38). However, both are in a similar range. At the point of failure, the temperature between the two graphs is about 6 °C apart. In both measurements/calculations, the specified limit temperature of 79 °C is exceeded after approx. 27 minutes.

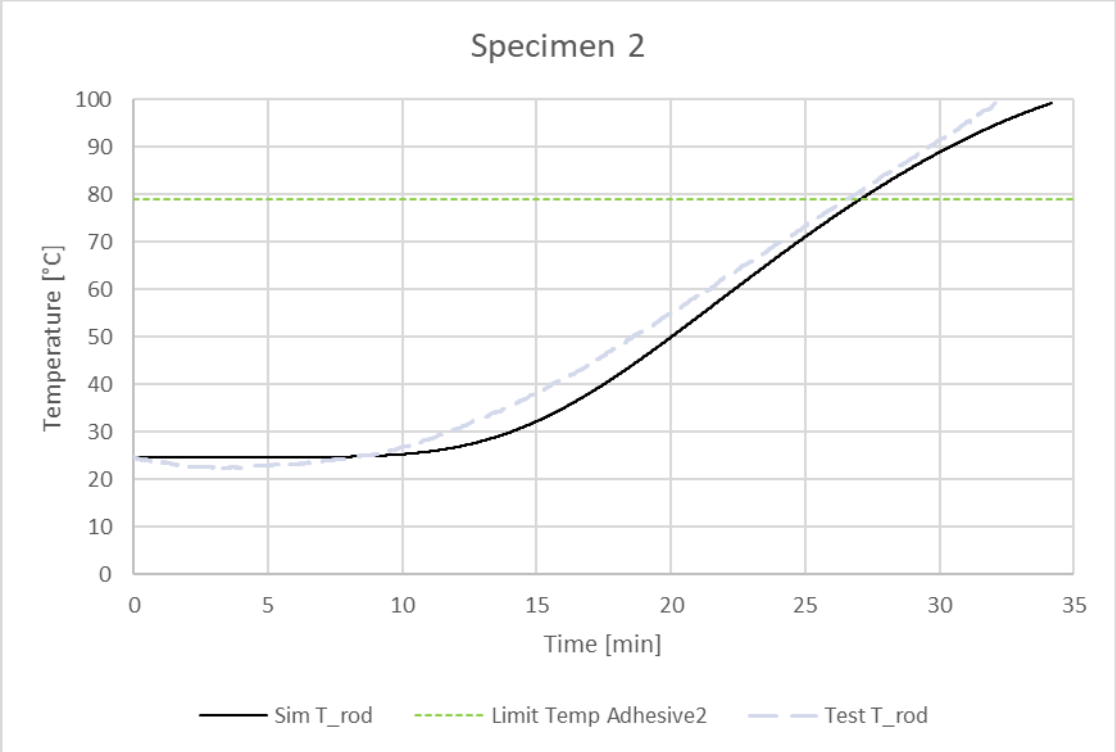

Figure 38: Temperature curves for simulated and measured results for specimen 2 in a temperature range of up to 100 °C

Four rods with a diameter of 12 mm were glued into reference specimen 3. Here, 2 rods with Adhesive 1 and a coverage of 46 mm were used. The other two rods were glued with Adhesive 2 and only had a coverage of 43 mm due to its greater thermal resistance.

Similar results to those of the previous reference specimens are again obtained for Adhesive 1 (see Figure 39). However, the simulation results for all measuring depths are below the measured values. The only exception are the measurement points at the two rods. Here the simulation exceeds both measuring points by more than 20 °C at the time of failure. Since the same coverage occurs here as with reference specimen 1 and test specimen 1, the differences are probably to be found in the material. Due to uneven combustion of the wood temperature differences are common during a fire. The high thermal load differences in this scale are common. However, the temperature range in which adhesive failure occurs is very small (between 60 °C and 90 °C for the two adhesives tested). Therefore, safety margins have to be planned in order to consider the uneven rise in temperature in the event of a fire.

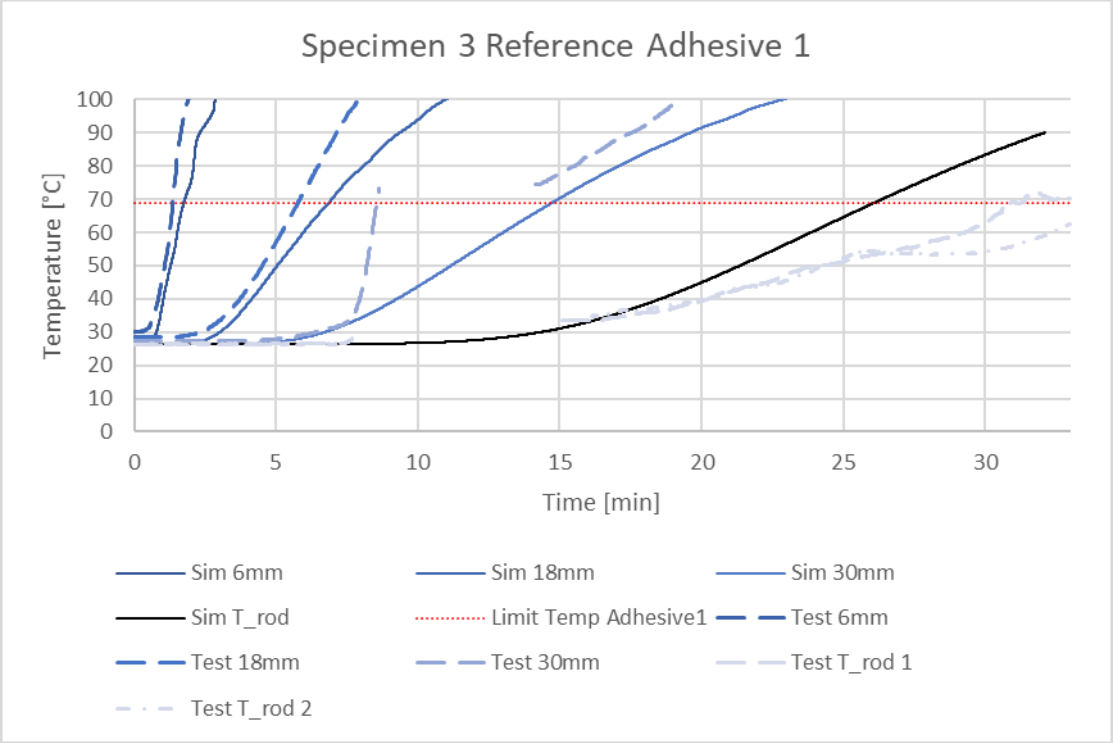

Figure 39: Temperature curves for simulated and measured results for reference specimen 3 in a temperature range of up to 100 °C for Adhesive 1

Approximately the same temperature curves as for Adhesive 1 are achieved for the measuring points in the wood for Adhesive 2 (see Figure 40). The simulation provides similar curves. However, these are below the measurement results in the temperature range of up to 100 °C. The measured values are only exceeded by the simulation at higher temperatures (see also Appendix C). With Adhesive 2, there was a 3 mm smaller wood cover for the rod. Logically, therefore, higher or faster rising temperatures were expected at the rod. After 30 minutes, the measurement results are approx. 50 °C below the simulation results. In addition, despite the smaller coverage, they are about 10 °C lower than for Adhesive 1. It can therefore be assumed that the adhesive type only has an insignificant role in the heat development of the rod and that it is much more dependent on the anisotropic properties of the wood.

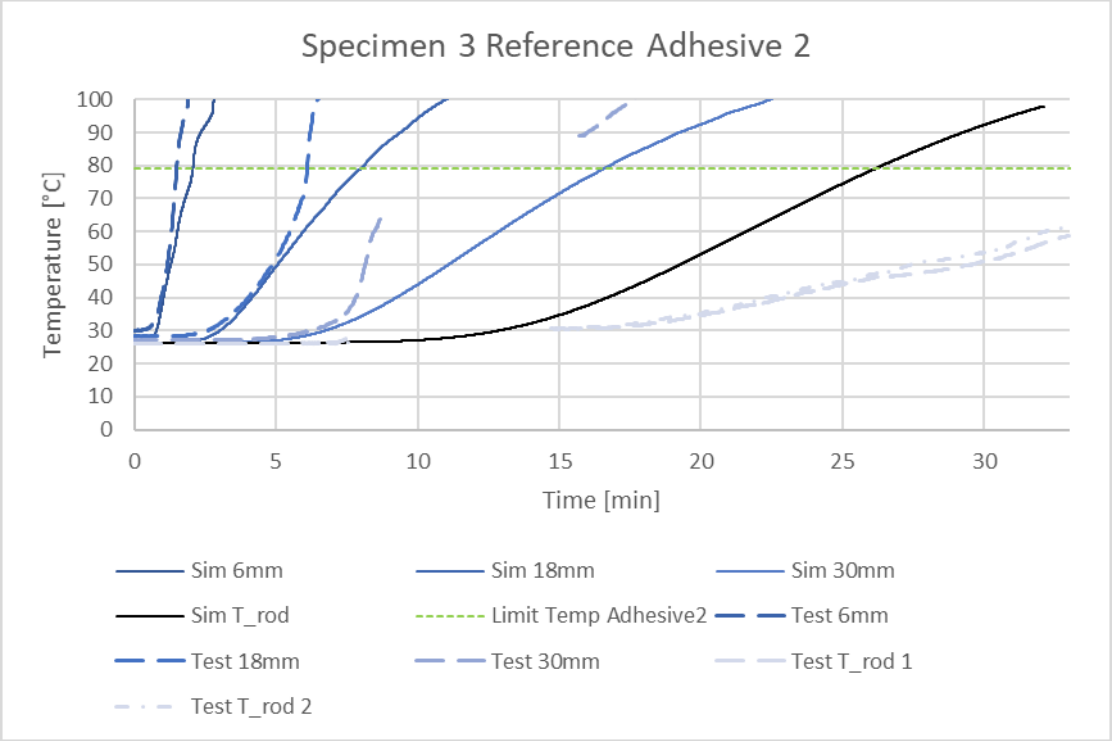

Figure 40: Temperature curves for simulated and measured results for reference specimen 3 in a temperature range of up to 100 °C for Adhesive 2

The temperature on all four rods of the test specimen was measured with the help of sheathed thermocouples. The wood cover in this case was 46 mm for all the rods because the same adhesive was used for all rods deviating from the reference specimen. Only at rod 3 do the measured values significantly exceed the simulation results (see Figure 41). After 30 minutes, they are approx. 20 °C higher. The other three rods, on the other hand, have significantly lower temperatures than in the simulation. After 30 minutes of exposure to fire, they are approx. 10 °C or 20 °C below the simulated values. The specified limit temperature for Adhesive 1 is exceeded by the rods 3 and 4. The difference in temperature may be caused by the uneven combustion. Since rod 3 exceeds the limit temperature of 69 °C very early it is assumed that the load bearing capacity mostly no longer exists. The mechanical load is therefore redistributed on the other rods which caused an earlier failure below the set temperature limit of 69 °C for the rods 1 and 2.

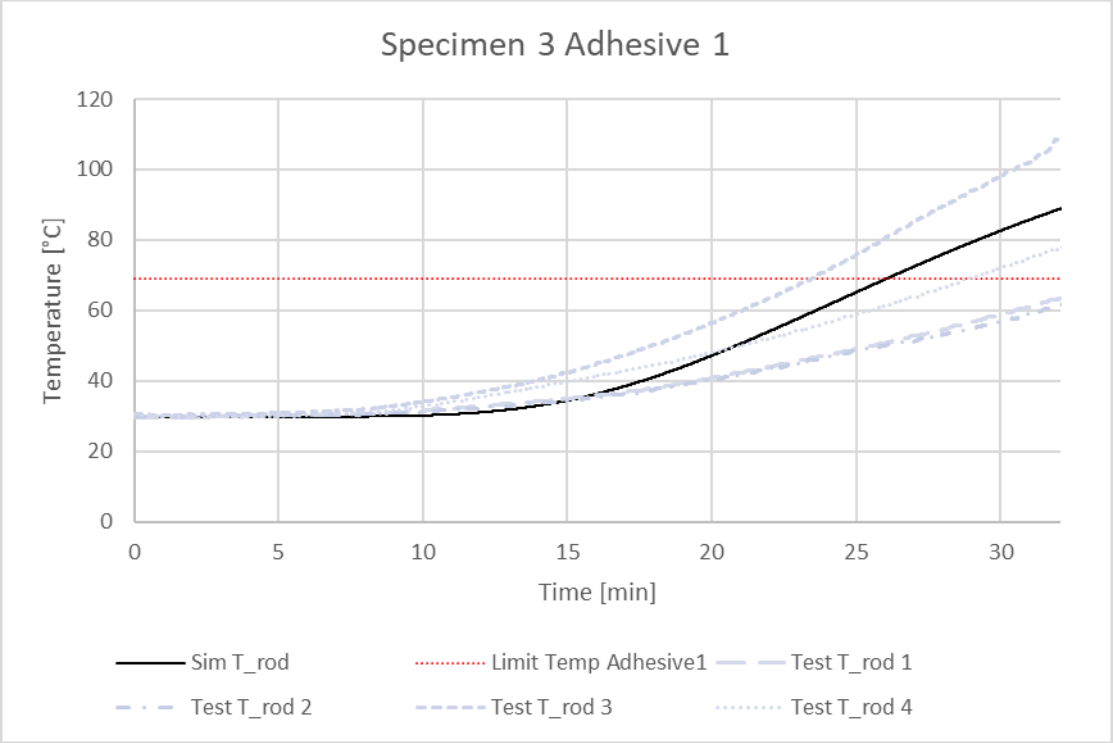

Figure 41: Temperature curves for simulated and measured results for specimen 3 in a temperature range of up to 100 °C

During the test of specimen 4 the measurement of the air temperature showed an error during the time of 21 s until 313 s. The values for the thermal load were therefore filled in with the measured temperatures from test specimen 2 for the test specimen 4 and from reference specimen 1 for the reference specimen 4 because these curves showed the most similar air temperature curves.

In the case of reference specimen 4, the simulation curves are slightly exceeded by the measured values at depths of up to 30 mm in the temperature range of up to 100 °C (see Figure 42). For the rod the simulation calculates about 15 °C lower temperatures after 30 minutes than occurred in the test. The only exception is the measuring depth of 42 mm from the surface. Here, higher temperatures are reached in the simulation. At the higher temperatures above 100 °C, the simulation curves for all measuring depths are again higher and therefore on the safe side (see also Appendix C). After 30 minutes, the critical temperature limit of the adhesive is exceeded in the simulation.

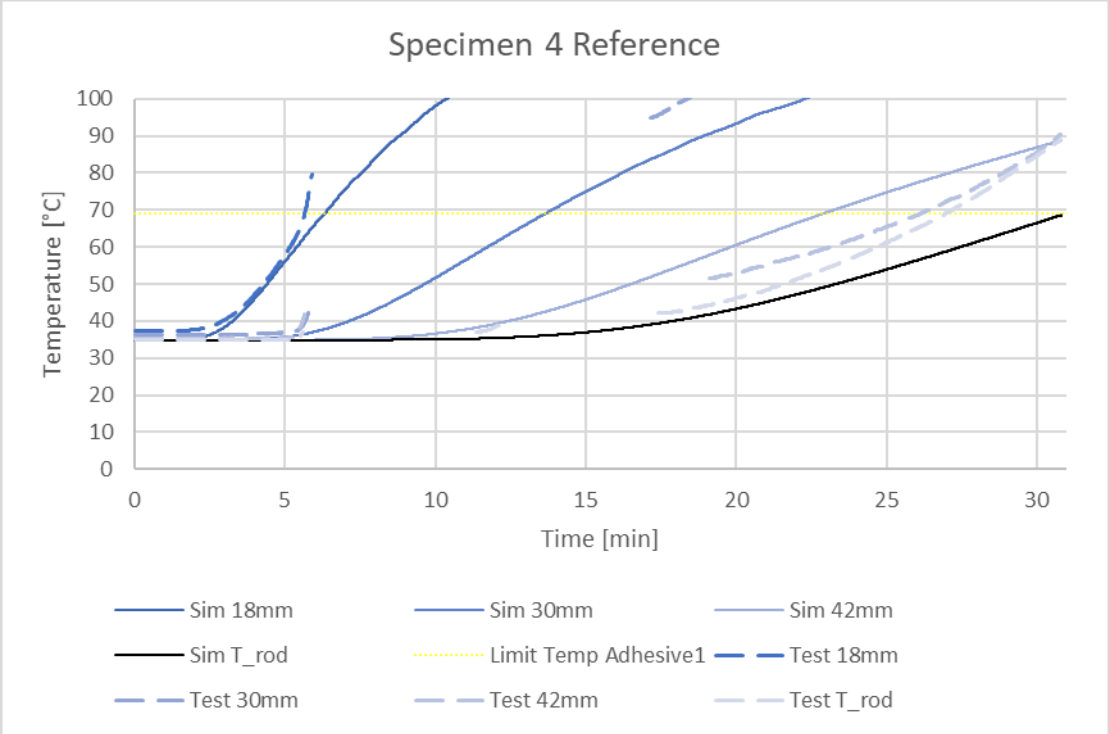

Figure 42: Temperature curves for simulated and measured results for reference specimen 4 in a temperature range of up to 100 °C

Test specimen 4, on the other hand, shows an almost congruent curve for the simulation and for the measured values of the rod (see Figure 43). After 30 minutes of exposure to fire, both curves reach the critical temperature limit.

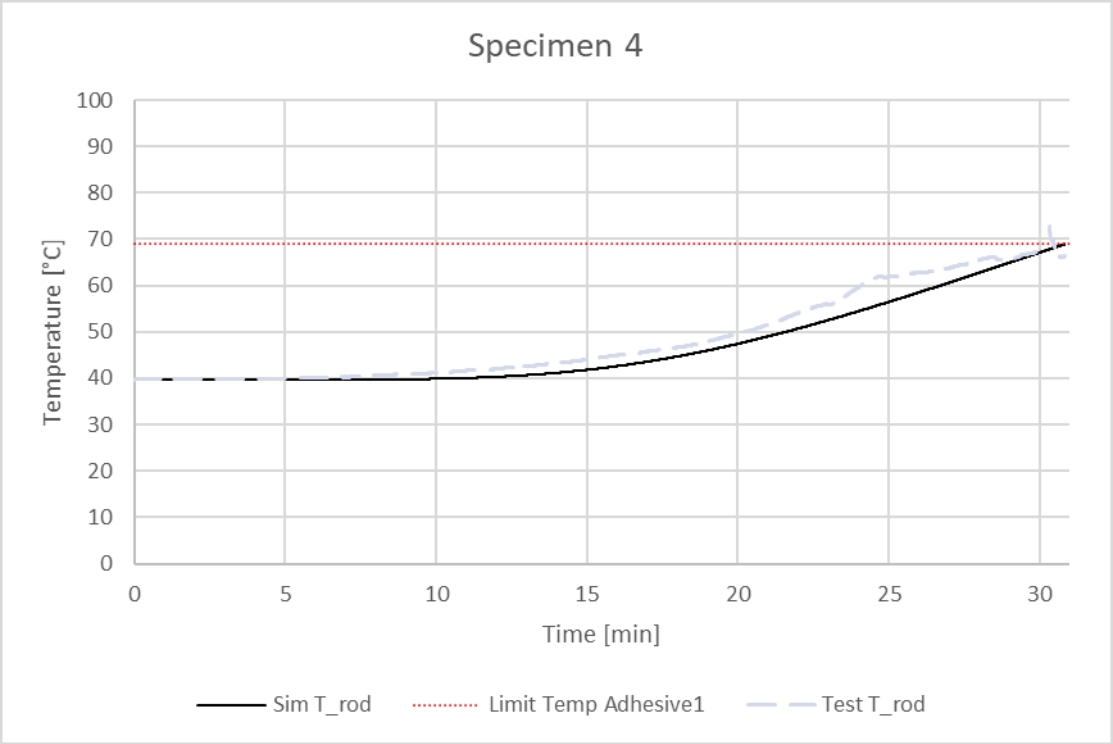

Figure 43: Temperature curves for simulated and measured results for specimen 4 in a temperature range of up to 100 °C

The tests have shown that the selected simulation parameters lead to a good correlation of the temperature development of a specimen with a glued in rod. The simulation results are usually on the safe side, especially at temperatures in the range of over 100 °C. In the temperature range below 100 °C, there are steeper temperature rises within the test specimens, especially in the areas near the surface, which exceed the simulation curves. Further adjustments to the material parameters are conceivable in order to achieve more precise results.

In the area of the rod, partly different results were achieved in the reference test specimens and test specimens. The following temperature deviations from the test results compared to the simulation results after 30 minutes are shown in Table 9.

Table 9: Deviation of temperatures after 30 minutes SFC fire load between simulation and measured values (+ measured value larger than simulation; - measured value smaller than simulation)

Specimen	Rod 1	Rod 2	Rod 3	Rod 4
SP 1	+10	-	-	-
SP 2	+2	-	-	-
SP 3	-20	-20	+20	-10
SP 4	0	-	-	-
Reference				
R1	-10	-	-	-
R2	-15	-	-	-
R3	-20	-26	-40	-40
R4	+20	-	-	-

In most cases, the simulation is on the safe side. However, the loss of strength of the adhesive only takes place in a small temperature range. Since the tests have shown that the temperature development is primarily dependent on the anisotropic material wood, additional safety factors should be planned in order to prevent the critical adhesive temperature limit from being exceeded. In addition, the temperature measurements in the test specimens only represent individual points. The temperature in the glue line can differ over the entire embedment length due to the wood characteristics as well as knots and other wood defects. Therefore, some parts of the connection can already be weakened whereas other parts of the glue line still have the full strength.

7 Design Model

The tests have shown that the current adhesives are decisive for the failure of a connection with glued in rods under the influence of fire. For this reason, the critical limit temperature of the adhesive should not be exceeded in order to ensure the load-bearing capacity for the required fire resistance duration. The idea of the analytical design model provides the possibility to determine the temperature in the glue line for different design durations under fire load. This makes it possible to determine the wood cover required to protect the adhesive from exceeding the critical temperature limit.

For this purpose, the analytical approaches presented in [10, 11, 16, 17] for determining the time dependent temperature in a cross-section of wooden beam were examined. The following formulas were suggested by the various authors for one-sided fire exposure. A charring rate of 0.7 mm/min is always assumed. The formulas 5 - 7 are based on the charring limit at the 200 °C - isotherm. Formula 8 assumes a charring limit of 300 °C:

$$T(x) = 20 + 180 \cdot ((\beta \cdot t/x)^{\alpha}) \quad (5)$$

With: $\alpha = 0{,}398 \cdot t^{0{,}62}$

$$T(x) = 20 + 180 \cdot \left(1 - \frac{x}{25}\right)^2 \quad (6)$$

$$T(x) = 20 + 180 \cdot ((\beta \cdot t/x)^{\alpha}) \quad (7)$$

With: $\alpha = 0{,}025 \cdot t + 1{,}75$

$$T(x) = T_i + (T_p - T_i) \cdot (1 - \frac{x}{a})^2 \quad (8)$$

With: a = 40 mm

In the case of fire exposure from at least two sides, the following formula is suggested by [18]. Here, too, the 200 °C charring limit is taken as a basis.

$$T(x) = 20 + (180 \cdot (\beta \cdot t)^{\alpha}) \cdot \{(\frac{1}{x})^{\alpha} + (\frac{1}{(b-x)})^{\alpha} + (\frac{1}{y})^{\alpha}\} \quad (9)$$

With: $\alpha = 0{,}025 \cdot t + 1{,}75$

The formulas shown were compared with the numerical simulation curves with parameters based on the test series 2 and 4 for different fire durations of 30, 60 and 90 minutes. The measuring point in the simulation was the edge of the borehole. This can be considered in the analytical calculation by adjusting the x and y values. Afterwards they were adapted to the numerical model.

Based on the validation and the optimization approach, the following analytical design formula is proposed to determine the necessary borehole cover / side length:

$$T(x) = 20 + (280 \cdot (\beta \cdot t)^{\alpha}) \cdot \{(\frac{1}{x})^{\alpha} + (\frac{1}{(b-x)})^{\alpha} + (\frac{1}{y})^{\alpha} + (\frac{1}{(h-y)})^{\alpha}\} \quad (10)$$

With: $\alpha = 0{,}4 \cdot t^{0{,}6}$

charring rate $\beta_n = 0{,}7$ $[\frac{\text{mm}}{\text{min}}]$

time t [min]

width of the cross section b [mm]

height of the cross section h [mm]

depth measured from original width x [mm]

depth measured from original height y [mm]

The area of application is a test specimen exposed to fire on all sides. The dimensional variables are shown in Figure 44. The proposed design model is applicable for the following boundary conditions:

- Softwood
- No exposed steel components
- Close jointed connections
- Time t > 20 minutes

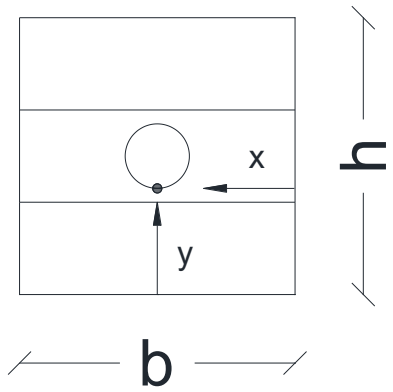

Figure 44: Sketch for the application of formula 10 with fire load on all sides

With this calculation approach, it is possible to adapt the connection or the cross-section to the critical adhesive temperature limit for certain adhesives and to reduce the necessary coverage. It should be noted that the critical temperature limit determined in the tests for the adhesives used is not generally applicable. A critical temperature of 60°C according to the application limits in EN 1995-1-1 is therefore recommended for other adhesives for now. [19]

The following diagrams show a comparison of the temperature calculated with the help of the proposed formula (10) and the simulated temperature in a component with a correspondingly square cross-section. For comparison purposes, a simulation was carried out for a solid wood cross-section and with an M12 and M20 rod. The glue line thickness was 1 mm.

Test specimens with a side length of 120 mm each were examined with a 30-minute Standard Fire Curve. Temperatures are plotted on the vertical axis (see Figure 45).

A depth of 60 mm corresponds exactly to the middle of the cross-section and thus shows the lowest temperatures. The charring limit of 300 °C is at a depth of approx. 24 mm. This means that at lower depths it can be assumed that the wood is completely burnt. The proposed design model shows very good agreement with the simulation results for a solid wood cross-section. The values of the analytical method are always higher than the simulated temperature curves and deliver slightly more conservative results. In the tests, the critical adhesive temperature limit was between 69 °C and 79 °C. Very good approximations are provided for this range by the analytical calculation. In the simulation with glued in rods, significant reductions in the temperature level can be seen in the area of the rod. These differences are due to the cooling effect of the steel rod in the simulation, which however, could not be clearly demonstrated in the tests. It is assumed that the influence of the wood cover has a significantly higher influence on the adhesive temperature, which is why this effect is not considered in the analytical design approach to be on the safe side.

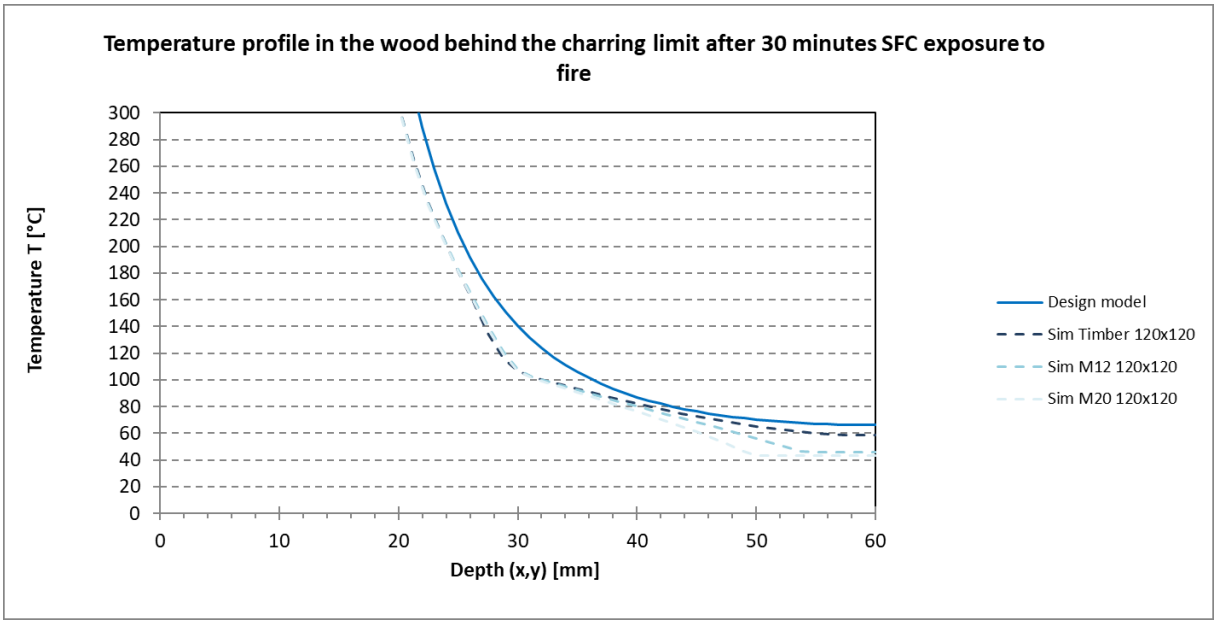

Figure 45: Comparison of the temperature profile for after 30 minutes SFC exposure to fire between the design model and the numerical simulation

For a thermal load of 60 minutes under the Standard Fire Curve, good agreement between the analytical calculation and the numerical simulation is also achieved (see Figure 46). In this example, a cross-section of 180 mm x 180 mm was considered. For temperatures above 100 °C there are greater differences between the simulation and the design model than for a 30-minute exposure to fire. However, since the critical adhesive temperature is below this temperature range for both tested adhesives, no further adjustment of the formula is necessary. For the numerical model with rods, lower temperatures are calculated in the area of the rod than for a solid wood cross-section. However, the influence is only limited to the immediate vicinity of the rod. The area of the borehole edge lies at 83 mm for the M12 rod and at 79 mm for the M20 rod.

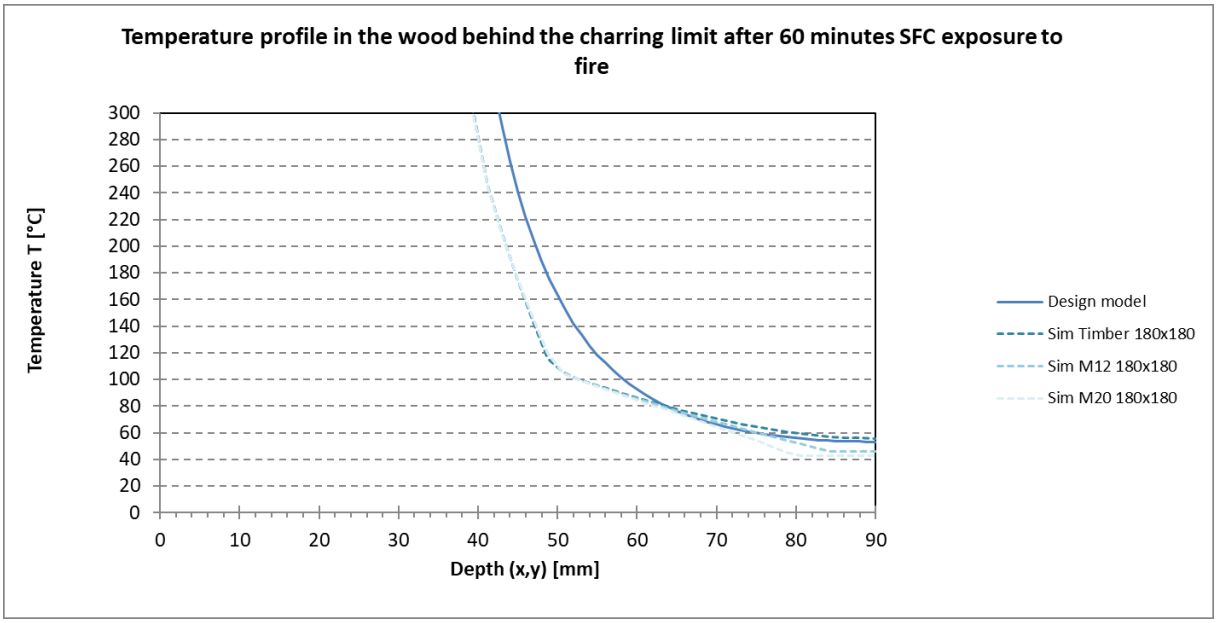

Figure 46: Comparison of the temperature profile for after 60 minutes SFC exposure to fire between the design model and the numerical simulation

A cross-section of 240 mm x 240 mm was considered for a 90-minute simulation period. Very good approximations between simulation and analytical calculation are achieved in the range below 80 °C (see Figure 47). The calculation provides slightly more conservative results. For higher temperatures, the distance between the two curves increases and the calculation based on the design model delivers more conservative results. It is noticeable that the cooling effect of a rod predicted by the simulation decreases with increasing time. The temperature differences aren't as big between the model with a glued in rod and a wooden model anymore. The borehole edge for the M12 rod lies at 113 mm and for the M20 rod at 109 mm.

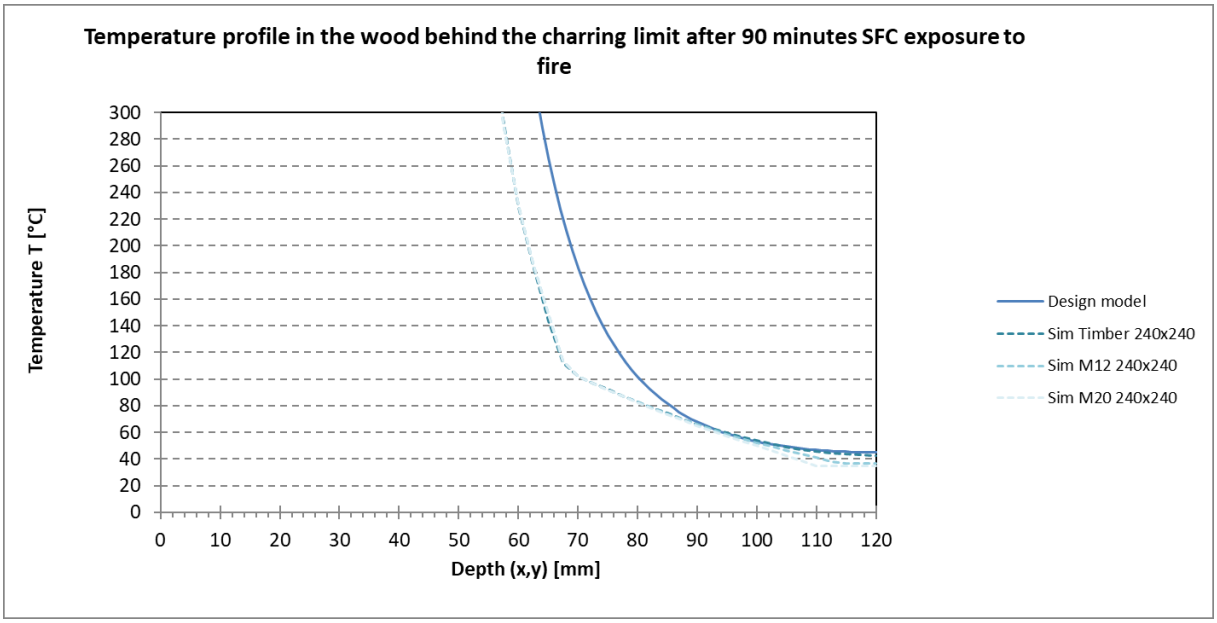

Figure 47: Comparison of the temperature profile for after 90 minutes SFC exposure to fire between the design model and the numerical simulation

The following Table 10 shows a comparison of the temperature of the test results from test series 4 with the calculated results from the design proposal (10) and from the numerical simulation for the failure time. The corresponding temperatures are from the measuring points on the rod of the individual specimens and reference specimens. In addition, the expected temperatures from the design model are given for the failure times and respective cross-sections.

For the numerical simulations (FEM) the input variables were changed accordingly. In addition to the Standard Fire Curve, the measured air temperatures of both the test specimen and the respective reference specimen were used as the thermal load. It is noticeable that the temperatures using the Standard Fire Curve are significantly below the test results. The reason for this is the inert behavior of the thermo plates and the initial control of the furnace, which exceeds the Standard Fire Curve in the first ten minutes (see also report D3.4). With the exception of rod 3 for test specimen 3 the proposed design model delivers results on the safe side. Also, specimen 1 exceeds the calculated temperature with only 0.1 °C.

In comparison, the calculations with the numerical simulation are more often below the failure temperatures in the test or in an approximately same range. Since larger temperature fluctuations are possible due to the anisotropic material properties of the wood, the design method should be more on the safe side in order to guarantee the load-bearing capacity.

Table 10: Comparison of failure temperatures in the test, in the design model and with the numerical simulation for specimens and reference specimens

	Time	Test		Design Model	FEM		
	Failure	Specimen	Reference		SFC	Specimen	Reference
	[min]	[°C]	[°C]	[°C]	[°C]	[°C]	[°C]
SP1	33	74,9	60,8	74,8	58,5	61,8	74,9
SP2	34,2	106,9	101,3	130,8	93,3	99,3	103
SP3	32,1	63,5	56,5	100,3*	58,5*	88,9*	90**
		61,7	59,8				
		109	70,9				97,9**
		75,4	59,1				
SP4	30,1	68,2	85,1	74,7	46,1	67,3	66,7

* Due to the same wood cover for all four threaded rods of the test specimen 3, only one temperature is obtained for the FEM and the analytical calculation.

**Rods 3 and 4 in the reference specimen 3 had a smaller wood cover because of the higher critical temperature limit of Adhesive 2. Two different adhesives were used in the reference specimen.

For an easier assessment, nomograms were created that show a minimum side length for square cross-sections for fire durations of 30, 60 and 90 minutes (see Figure 48, Figure 49, and Figure 50). A large borehole needs a larger cross-section respectively a larger side length for the same coverage.

The critical adhesive temperature limit can be freely selected. The creep tests in test series 3 resulted in a limit temperature of 69 °C for Adhesive 1 and 79 °C for Adhesive 2. If the temperature limit of the adhesive is not known, a temperature of 60 °C is recommended based on the application limits of EN 1995-1-1. The diagrams apply to a centrally inserted rod.

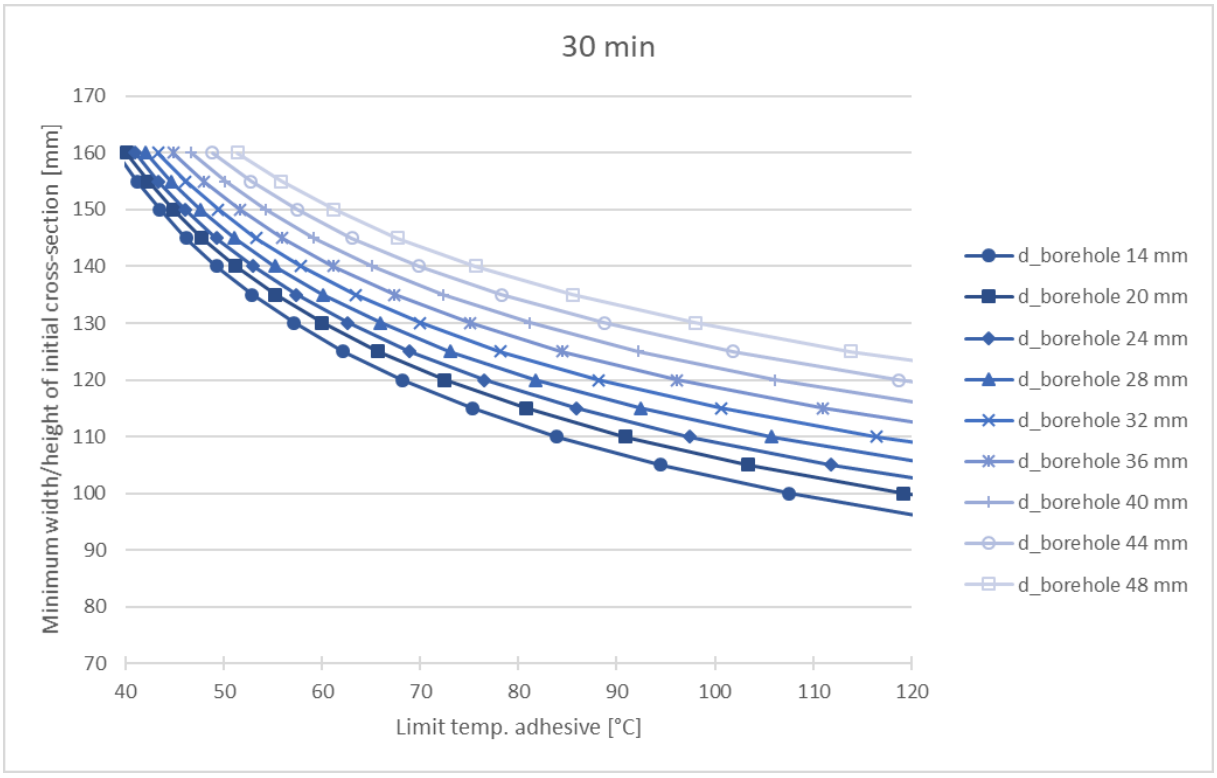

Figure 48: Nomogram for a fire load of 30 minutes with the proposed design model

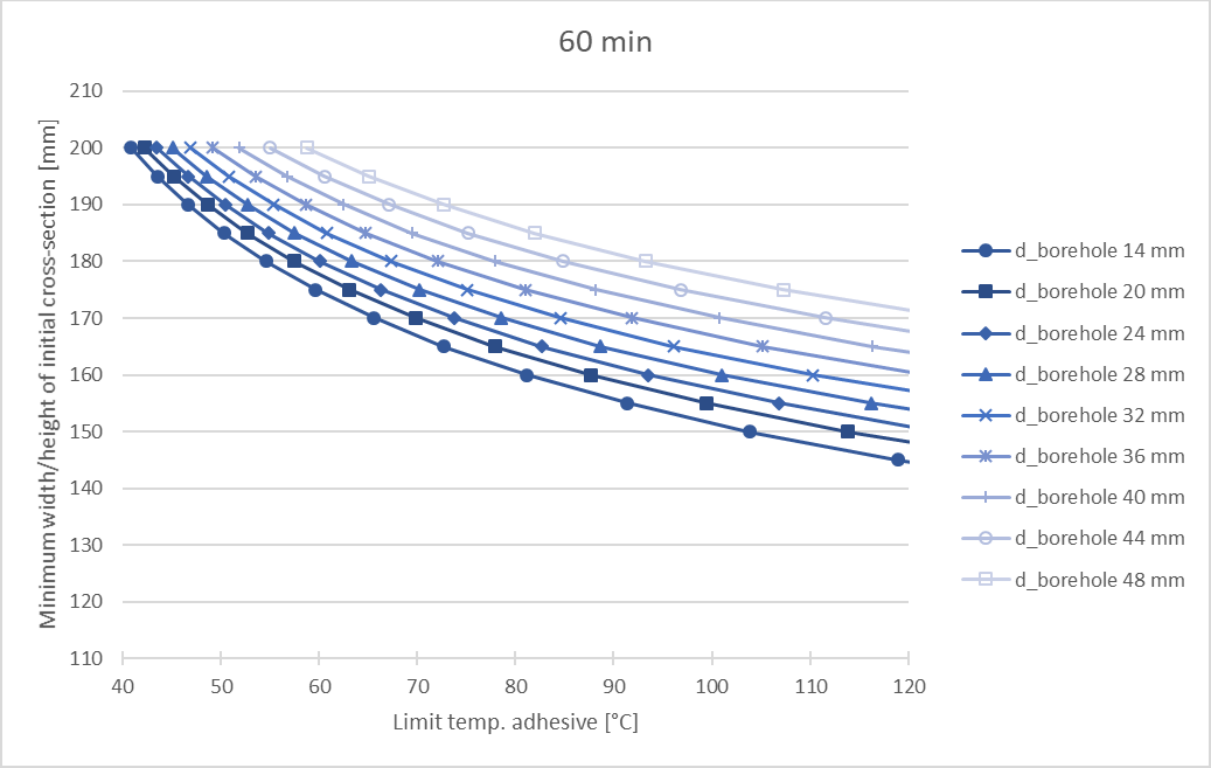

Figure 49: Nomogram for a fire load of 60 minutes with the proposed design model

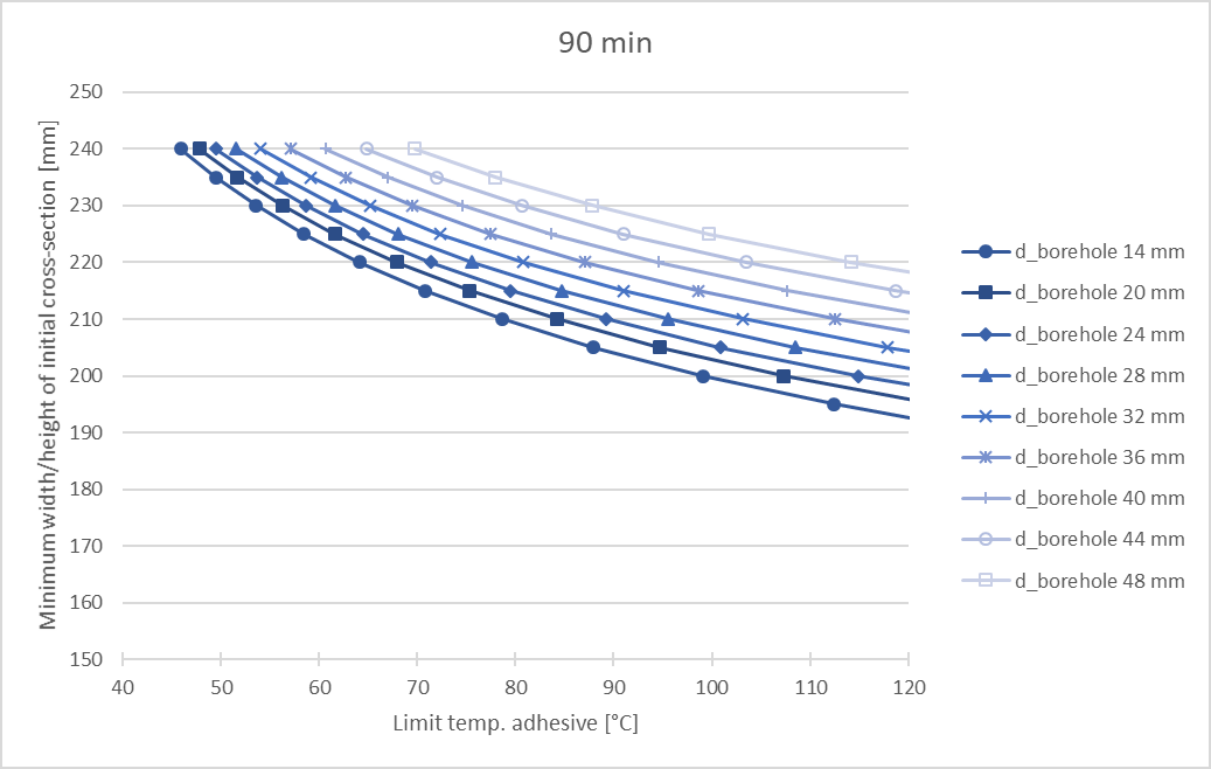

Figure 50: Nomogram for a fire load of 90 minutes with the proposed design model

8 Summary

On the basis of the four test series, numerical simulations for the temperature development within specimens with glued in rods were carried out. Therefore, sensitivity analyzes and parameter studies on the individual parameters for wood, gypsum, steel and adhesive were performed.

The numerical models for the test specimens in which the rod was inserted parallel to the fiber direction of the wood could be created as two-dimensional models. By exploiting the symmetry conditions only a quarter of the original cross-section was needed. The models of test series 2.2 with rods that were inserted perpendicular to the grain had to be created as a 3D model due to the anisotropic material properties.

In the simulation of test series 2.2, the fire protection coverings consisting of wooden plugs provided good agreement with the real test results. The simulation was also able to take account of the falling off of gypsum plasterboards. However, there were major discrepancies here. It is assumed that due to the small component dimensions, a complete fall off was partially prevented, which is why lower temperatures occurred in some of the tests. In the numerical simulation, on the other hand, the covering was completely deactivated and the free surface including the rod was subjected to an adapted fire curve.

The test specimens of test series 4 were planned on the basis of these simulations. The fire tests should validate the numerical simulation models in this regard. During the evaluation it was noticeable that for the majority of the test specimens, the numerical simulation delivered results on the safe side and therefore exceeded the temperatures from the tests. Only at the measuring points close to the surface in the temperature range up to 100 °C the tests showed steeper rises, which is why further adjustments to the material parameters could be possible.

From the tests it was deduced that the adhesive represents the critical point of the connection when put under thermal load. It should not exceed a critical temperature level in order to prevent failure. For this reason, the thermal development within the specimens and in the glue line is essential to predict failure.

Based on already existing formulas for determining the temperature in a solid wood cross-section in the case of a one-sided or multi-sided fire load, a design model was developed. With the proposed formula the temperature of the adhesive joint of a beam with a glued in rod can be calculated. The design model was adapted on the basis of the numerical models and the results of test series 4. Since larger temperature fluctuations are possible due to the anisotropic material properties of wood, the design model should have a certain level of safety, since the critical adhesive temperature limit lies in a small temperature range. Also, temperature changes in the range of 10 °C can be sufficient to lead to a connection failure. Therefore, the design approach was adjusted to be higher than the numerical simulation models.

The advantage of the design model is the possibility to adjust the cross-section based on the critical temperature limit of the adhesive. This makes it possible to obtain smaller coverings with thermally resistant adhesives and with thermally post-treated adhesives (tempering).

As a planning aid, nomograms based on the design model were created, which enable an initial estimation of the required side length for specific borehole diameters and fire resistance durations. There is a freely selectable critical temperature limit of the adhesive. However, it must be considered that the adhesives examined in this research project and the specified critical temperature limits are not generally applicable to other adhesives of the same type, since these differ in their composition depending on the manufacturer and can therefore react differently to the effects of heat. If no data is available, the application limit of 60 °C is recommended as the critical temperature for the adhesive based on EN 1995-1-1.

References

[1] HERWIG, Heinz ; MOSCHALLSKI, Andreas: *Wärmeübertragung : Physikalische Grundlagen ; illustrierende Beispiele ; Übungsaufgaben mit Musterlösungen*. 3., erw. und überarb. Aufl. Wiesbaden : Springer Vieweg, 2014 (Lehrbuch)

[2] BOCKH, Peter ; WETZEL, Thomas: *Warmeubertragung : Grundlagen und Praxis*. 7., aktualisierte u. uberarb. Aufl. 2017 edition. Berlin : Springer, 2018

[3] GROTH, Clemens ; MÜLLER, Günter ; STELZMANN, Ulrich: *FEM für Praktiker : Basiswissen und Arbeitsbeispiele zur Finite-Element-Methode mit dem FE-Programm ANSYS Rev. 5.5 ; mit ... Installationsanleitung und zahlreichen Beispielen*. 7. Aufl. Renningen : expert-Verl., 2002 (Edition expertsoft 23)

[4] GROTH, Clemens ; MÜLLER, Günter: *Temperaturfelder : Basiswissen und Arbeitsbeispiele zu FEM-Anwendungen der Temperaturfeldberechnung ; Lösungen mit dem FE-Programm ANSYS ; mit CD-ROM und zahlreichen Beispielen*. 5., neu bearb. Aufl. Renningen : expert-Verl., 2009 (Edition expertsoft 45)

[5] BAEHR, Hans Dieter ; STEPHAN, Karl: *Wärme- und Stoffübertragung*. 10. Auflage 2019. Berlin, Heidelberg : Springer Berlin Heidelberg, 2019

[6] *DIN EN 1991-1-2:2010-12, Eurocode_1: Einwirkungen auf Tragwerke_- Teil_1-2: Allgemeine Einwirkungen_- Brandeinwirkungen auf Tragwerke; Deutsche Fassung EN_1991-1-2:2002_+ AC:2009*

[7] H. H., Bosshard: *Holzkunde : Aspekte der Holzbearbeitung und Holzverwertung*. 2., überarbeitete Auflage. [Place of publication not identified] : Birkhauser Basel, 2013 (Reihe der Experimentellen Biologie 20)

[8] *DIN EN 1995-1-2:2010-12, Eurocode_5: Bemessung und Konstruktion von Holzbauten_- Teil_1-2: Allgemeine Regeln_- Tragwerksbemessung für den Brandfall; Deutsche Fassung EN_1995-1-2:2004_+ AC:2009*

[9] SCHLEIFER, Vanessa: *Zum Verhalten von raumabschliessenden mehrschichtigen Holzbauteilen im Brandfall*. ETH Zurich. 2009

[10] DEUTSCHE GESELLSCHAFT FÜR HOLZFORSCHUNG: *Holz-Brandschutz-Handbuch*. 3. Aufl. / unter Federführung von Claus Scheer und Mandy Peter. Berlin : Ernst, 2009 (Informationsdienst Holz)

[11] FRANGI, Andrea: *Brandverhalten von Holz-Beton-Verbunddecken*. 2001

[12] CLANCY, P.: *Advances in modelling heat transfer through wood framed walls in fire*. In: *Fire and Materials* 25 (2001), Nr. 6, S. 241–254

[13] *DIN EN 1993-1-2:2010-12, Eurocode_3: Bemessung und Konstruktion von Stahlbauten_- Teil_1-2: Allgemeine Regeln_- Tragwerksbemessung für den Brandfall; Deutsche Fassung EN_1993-1-2:2005_+ AC:2009*

[14] LEONARDO DA VINCI PILOT PROJECT CZ/02/B/F/PP-134007: *Design of buildings for the fire situation*. 2005 (Development of skills facilitating implementation of Eurocodes Handbook 5)

[15] JOAS, Carla: *Numerische Beurteilung des Abbrandverhaltens von Holzbauteilen*. München, 2016

[16] KÖNIG, Jürgen: *Die Bemessung von Holzbauten für den Brandfall nach ENV 1995-1-1*. Düsseldorf, 1995

[17] JANSSENS, Marc L. ; WHITE, Robert H.: *Short communication: Temperature profiles in wood members exposed to fire*. In: *Fire and Materials* 18 (1994), Nr. 4, S. 263–265

[18] RÖLL, H.: *Untersuchungen über das Abbrandverhalten von Fichten- und Eichenholz in Abhängigkeit von Rohdichte, Jahrringsorientierung und Zeit*. 1984

[19] *DIN EN 1995-1-1:2010-12, Eurocode_5: Bemessung und Konstruktion von Holzbauten_- Teil_1-1: Allgemeines_- Allgemeine Regeln und Regeln für den Hochbau; Deutsche Fassung EN_1995-1-1:2004_+ AC:2006_+ A1:2008*

A Sensitivity analysis

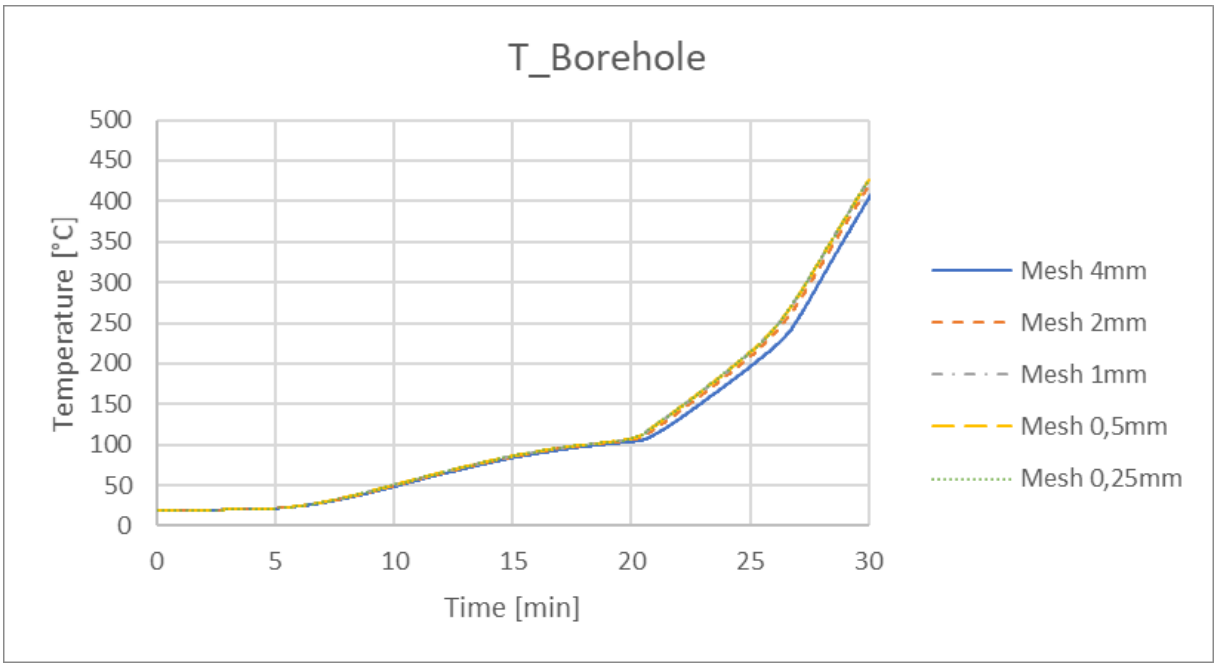

Figure 51: Influence of the mesh density on the temperature curve for a wooden cross-section

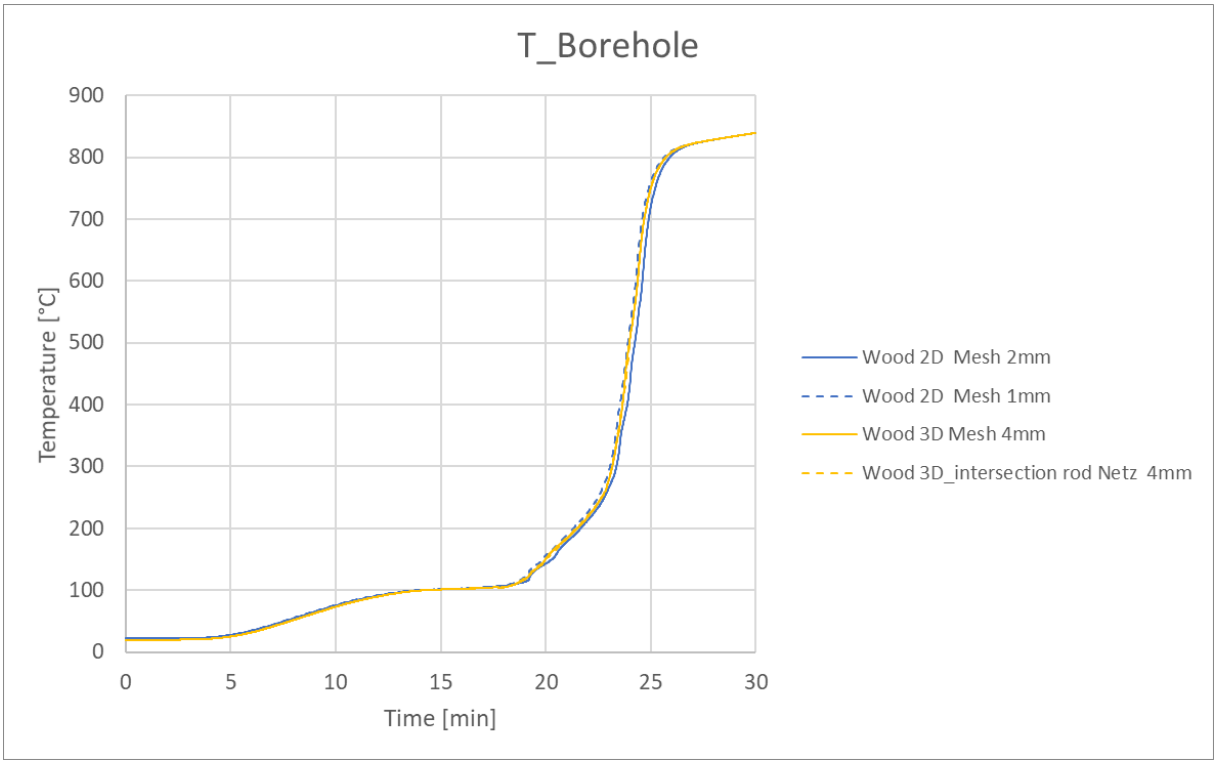

Figure 52: Influence of the mesh density on the temperature curve for a 2-dimensional and a 3-dimensional model with a cross-section of 60 mmx 60 mm with only timber

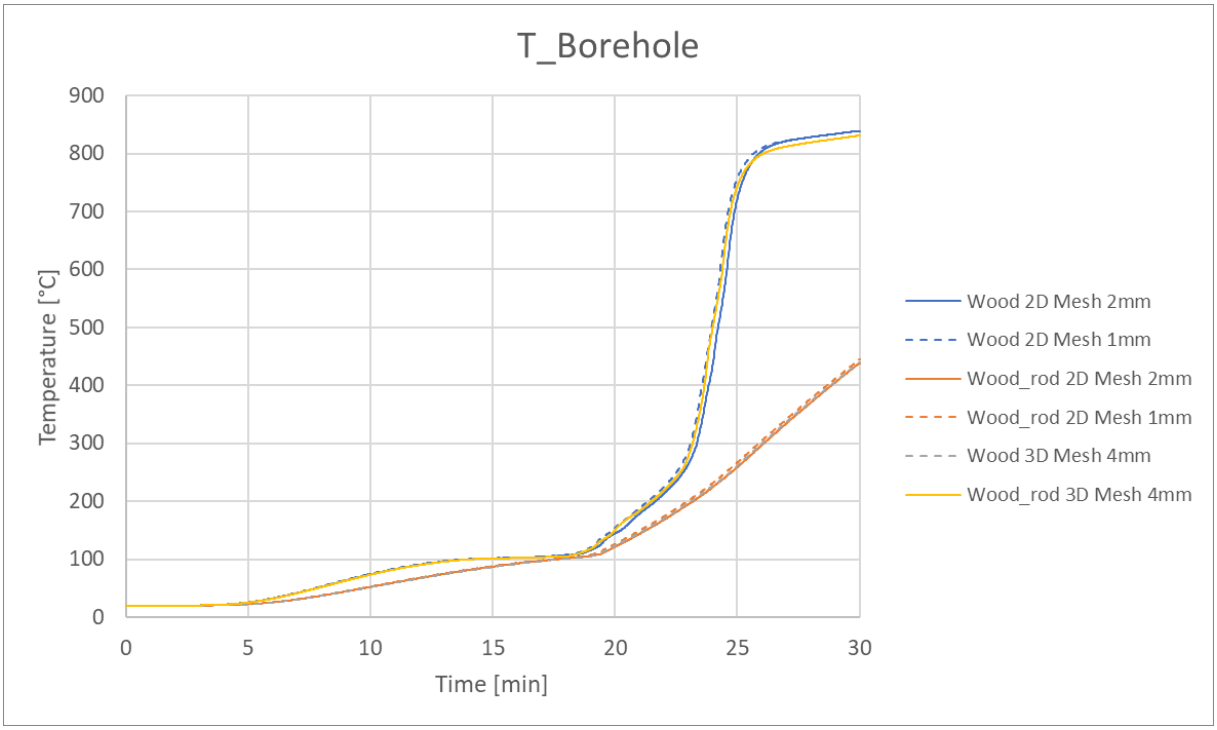

Figure 53: Influence of the mesh density on the temperature curve for a 2-dimensional and a 3-dimensional model with a cross-section of 60 mmx 60 mm with timber and with a glued in rod

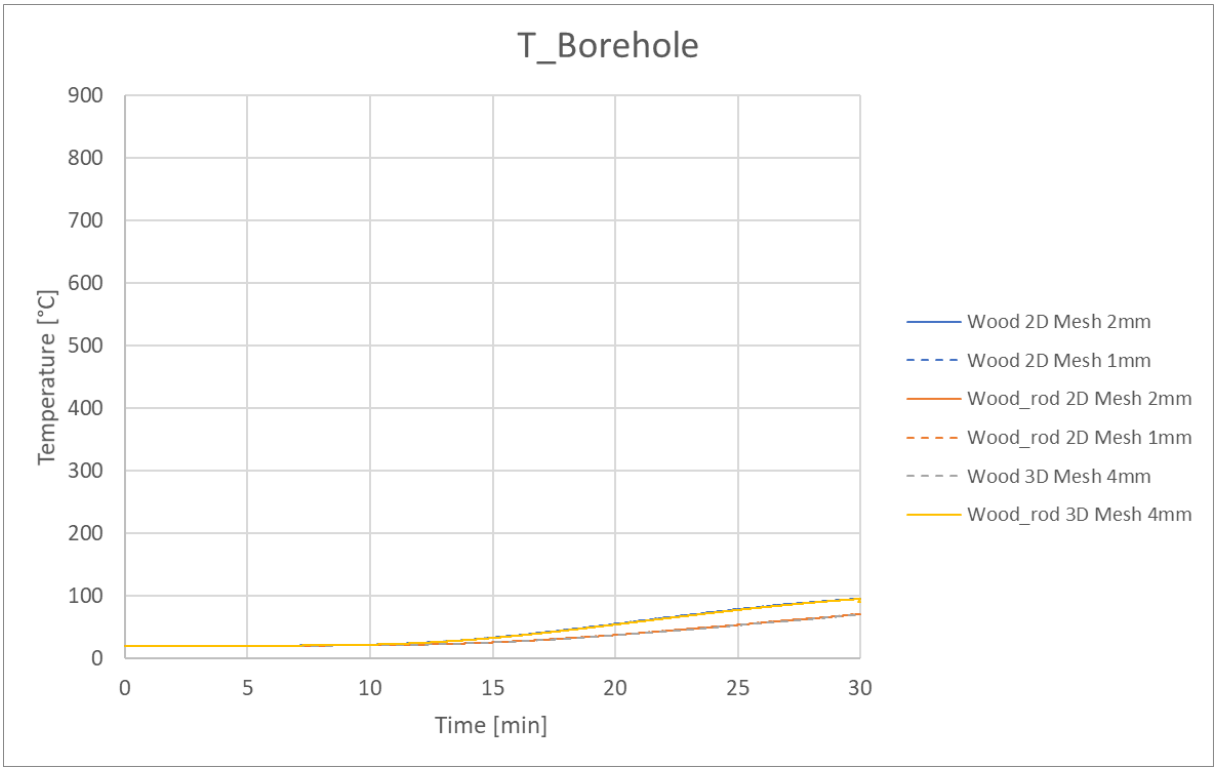

Figure 54: Influence of the mesh density on the temperature curve for a 2-dimensional and a 3-dimensional model with a cross-section of 100 mmx 100 mm with timber and with a glued in rod

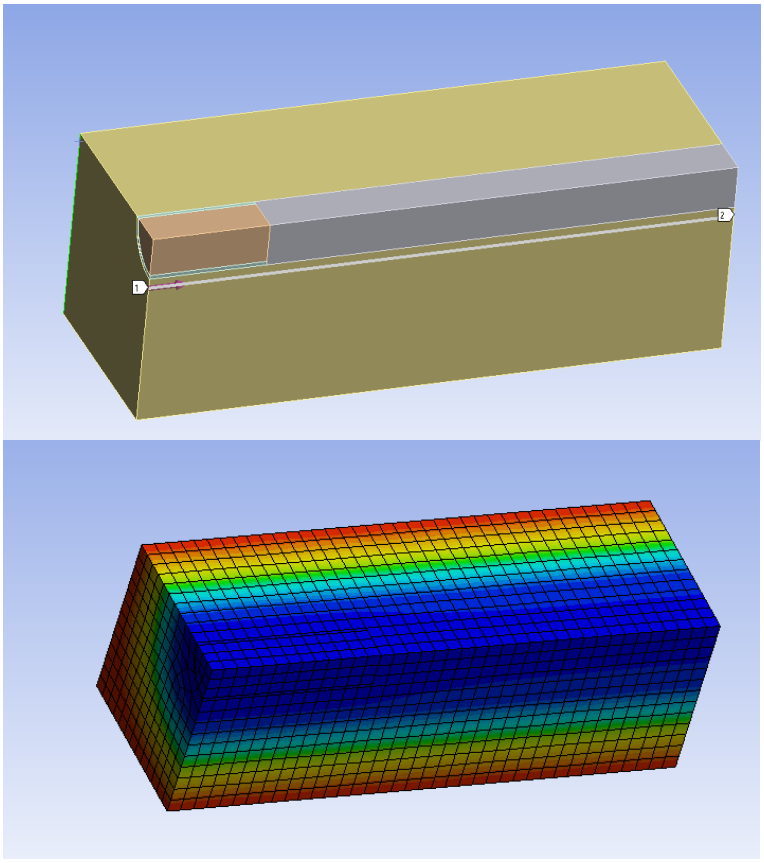

Figure 55: Temperature profile of a 3-dimensional model with a glued in rod M20 (blue colder than red)

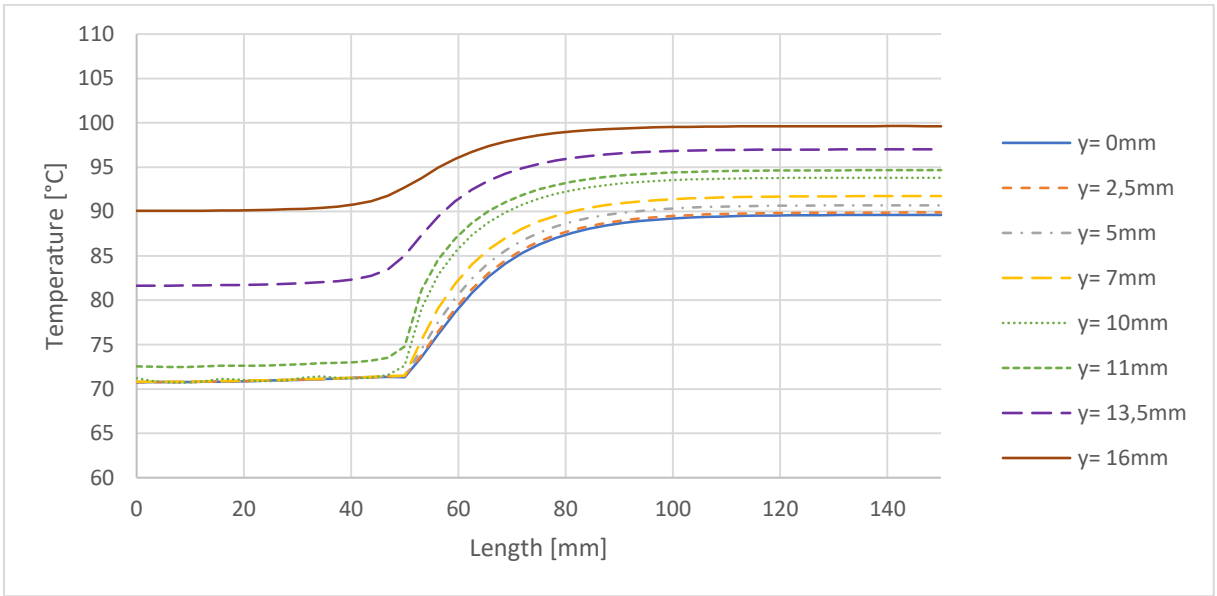

Figure 56: Temperature profile for different depths of a 3-dimensional model with a glued in rod after 30 minutes of fire load with Standard Fire Curve with a cross-section of 100 mm x 100 mm and a rod diameter of 20 mm

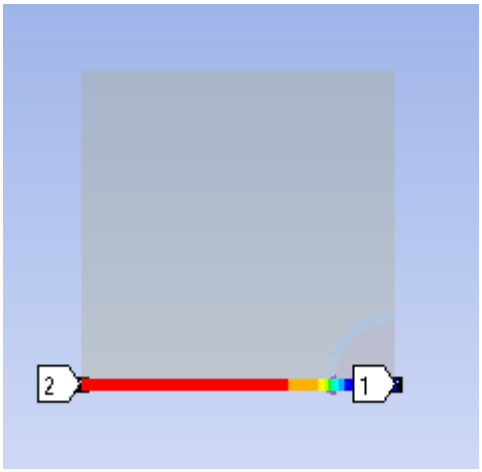

Figure 57: Sketch of temperature profile alongside the edge

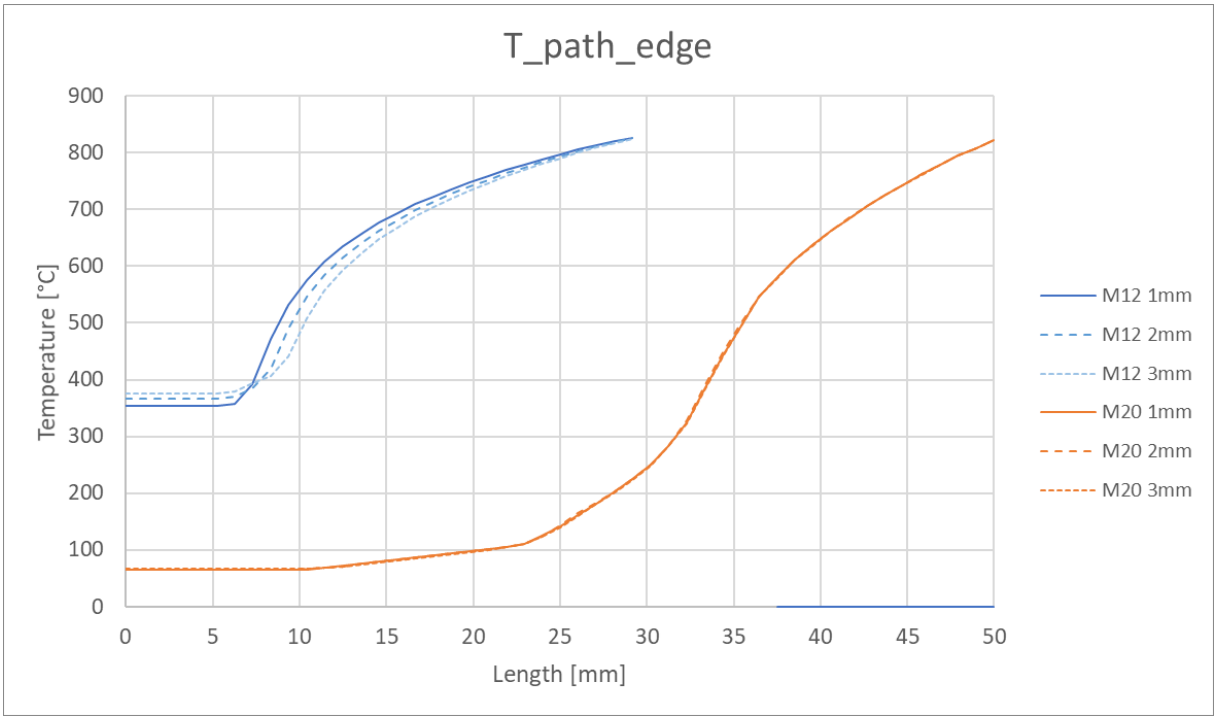

Figure 58: Temperature profile of numerical simulation along the edge for different glue line thicknesses

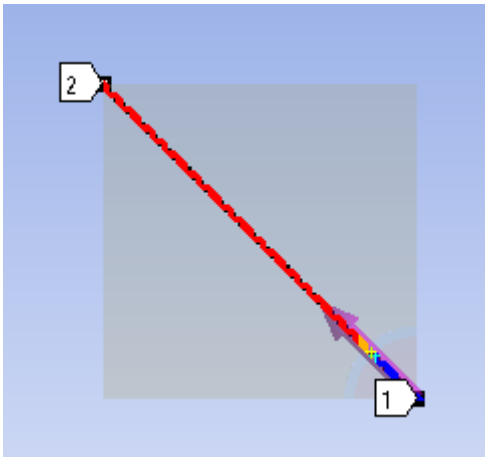

Figure 59: Sketch of temperature profile alongside the diagonal

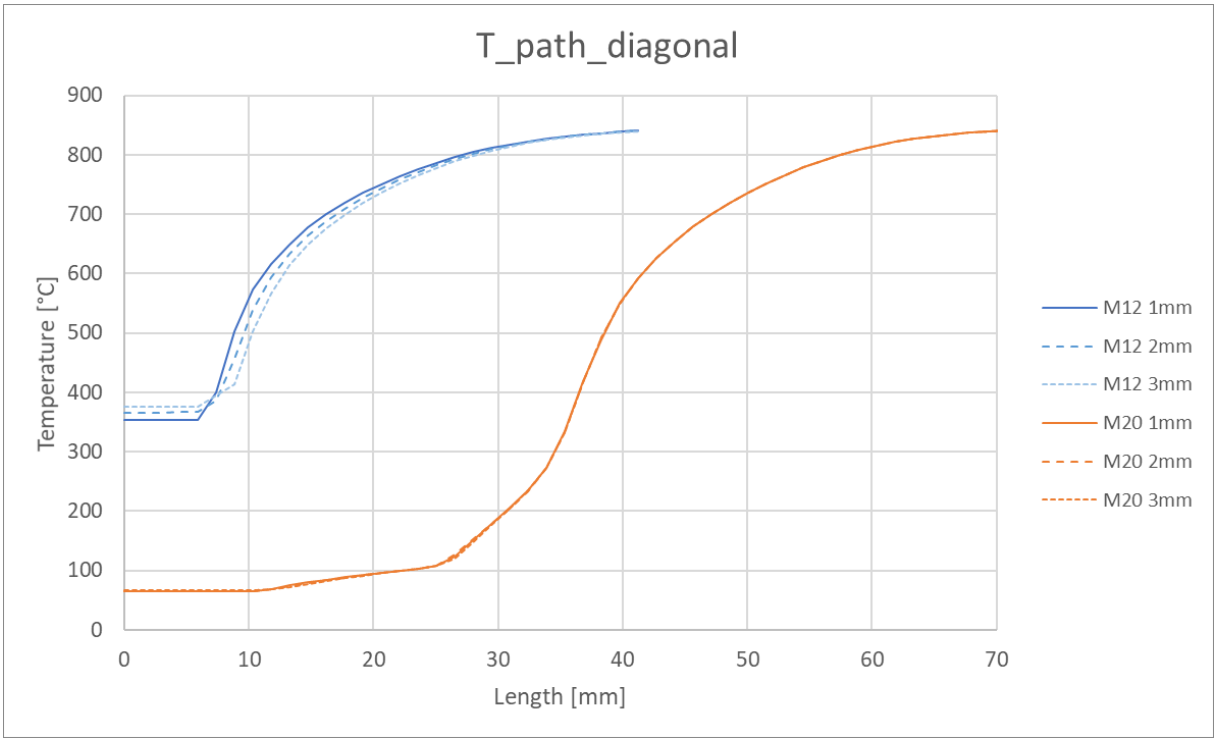

Figure 60: Temperature profile of numerical simulation along the diagonal for different glue line thicknesses

B Test series 2

B.1 Test series 2.1

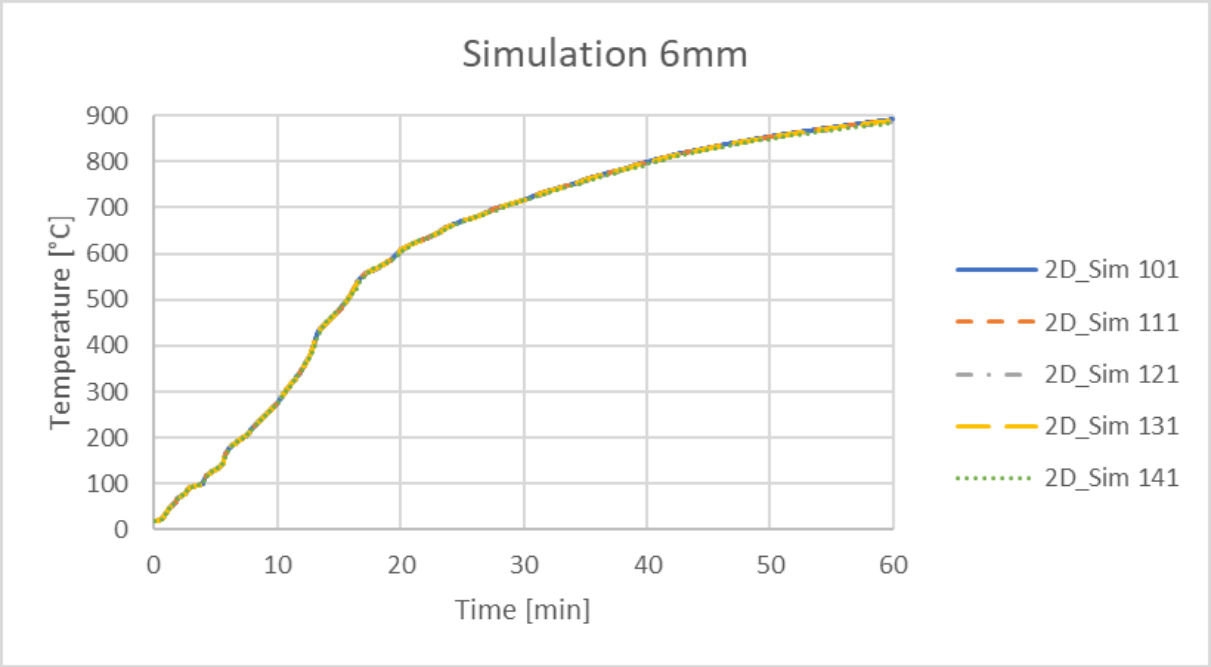

Figure 61: Simulation of temperature for test series 2.1 in a depth of 6 mm below the surface

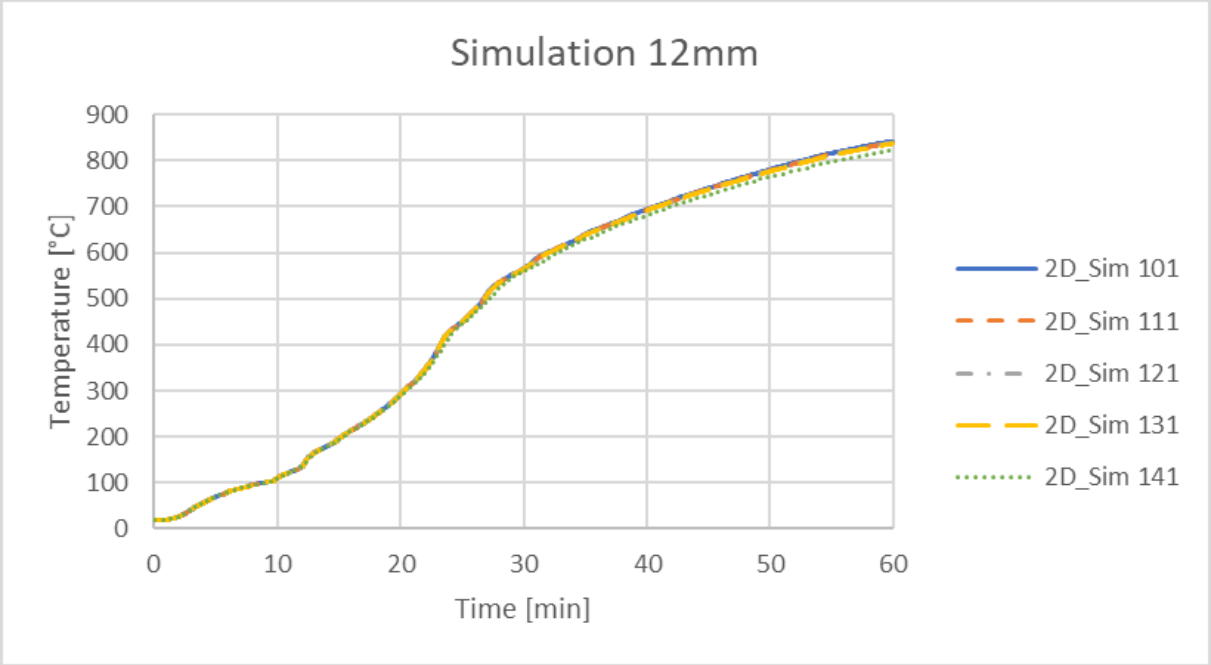

Figure 62: Simulation of temperature for test series 2.1 in a depth of 12 mm below the surface

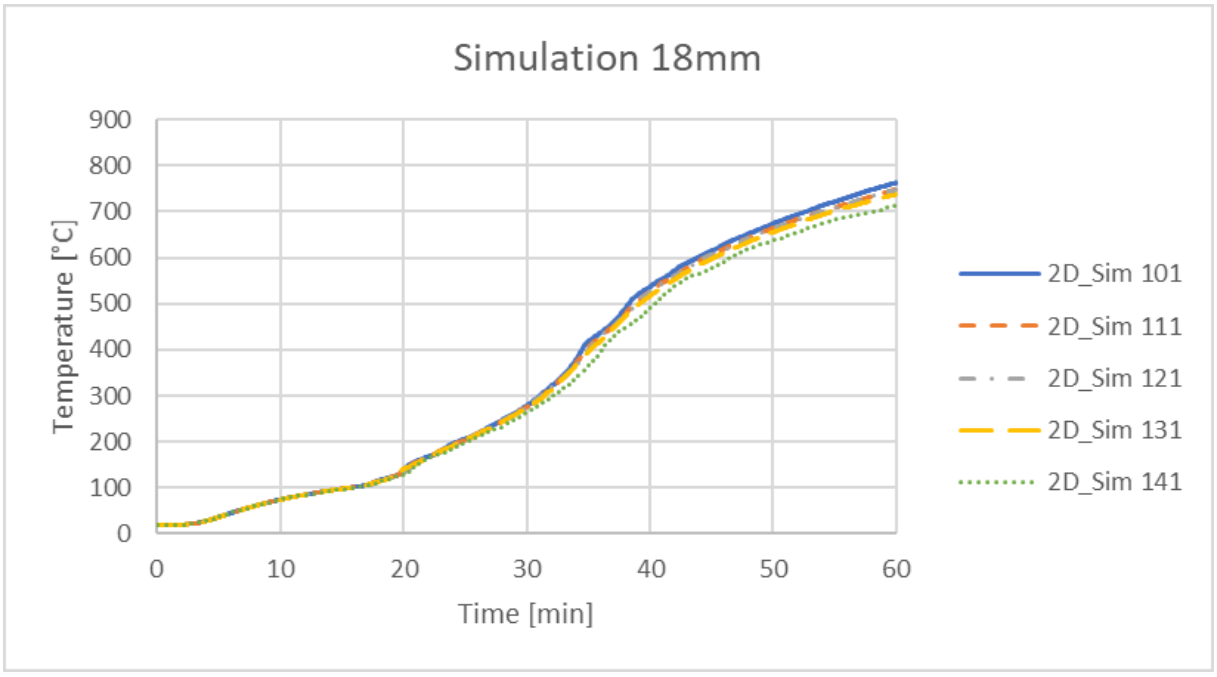

Figure 63: Simulation of temperature for test series 2.1 in a depth of 18 mm below the surface

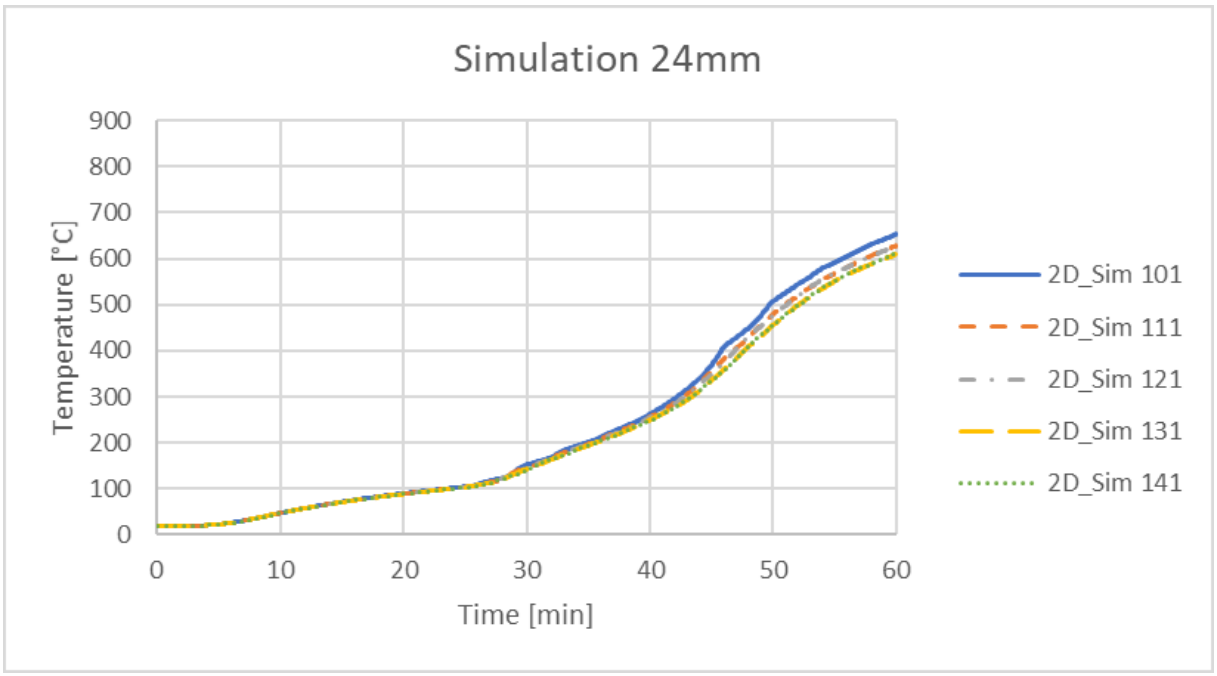

Figure 64: Simulation of temperature for test series 2.1 in a depth of 24 mm below the surface

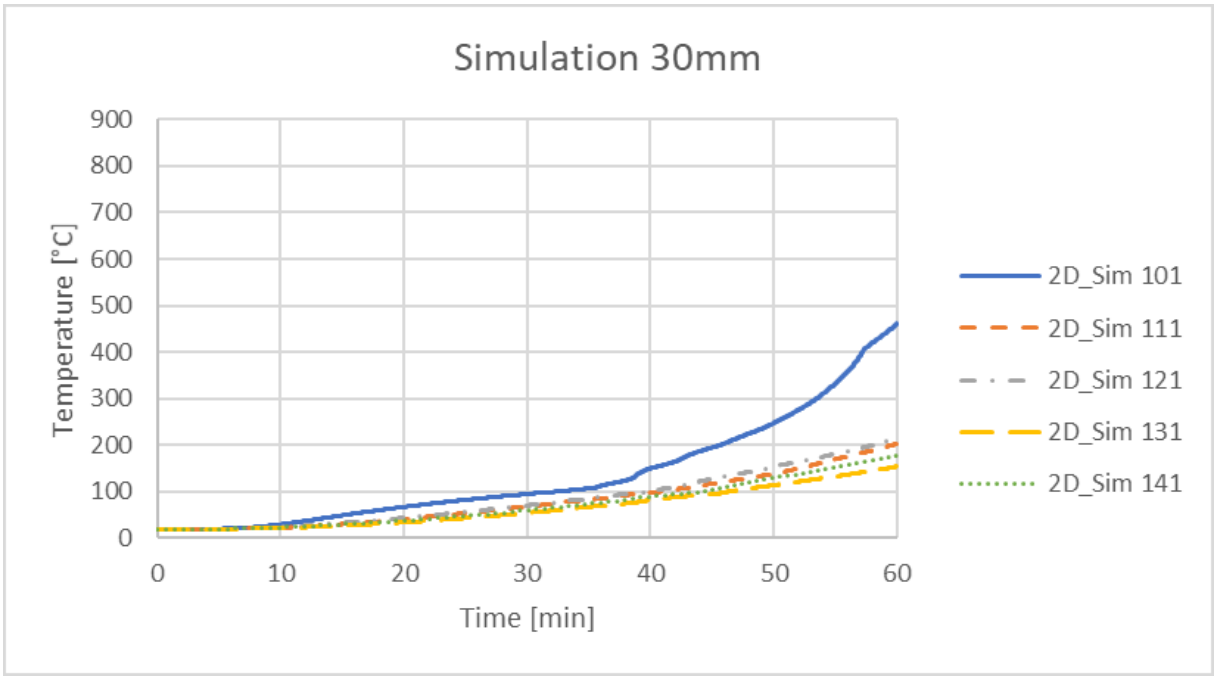

Figure 65: Simulation of temperature for test series 2.1 in a depth of 30 mm below the surface

B.2 Test series 2.2

Specimen 1

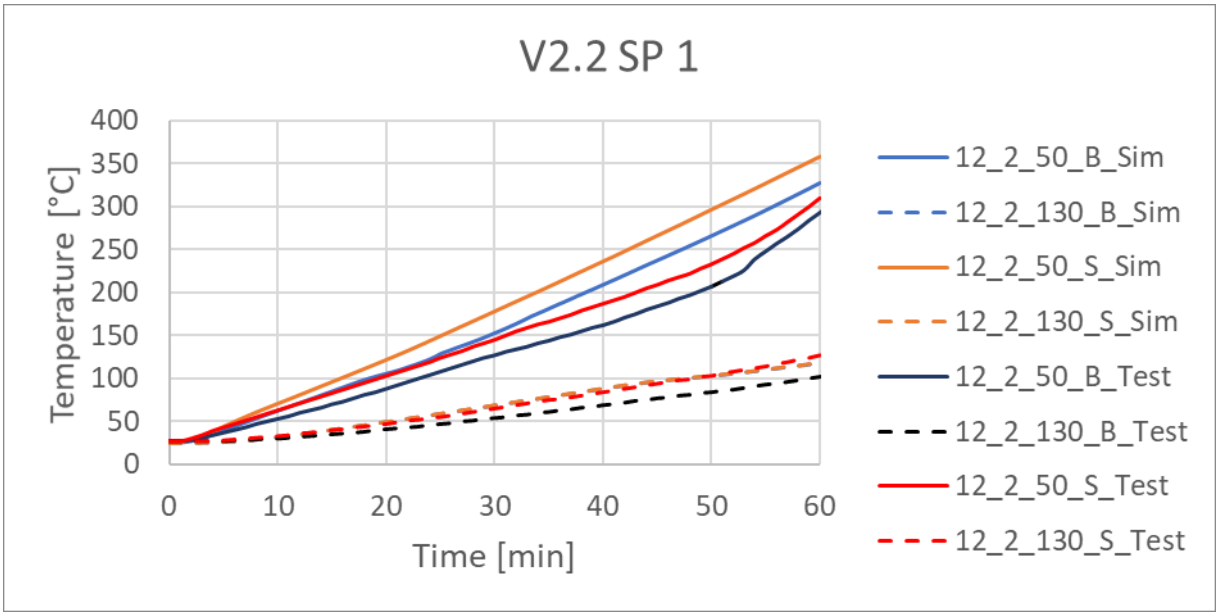

Figure 66: Comparison of temperature curves for measured and simulated results of specimen 1 and a 12 mm rod diameter with a glue line thickness of 1 mm

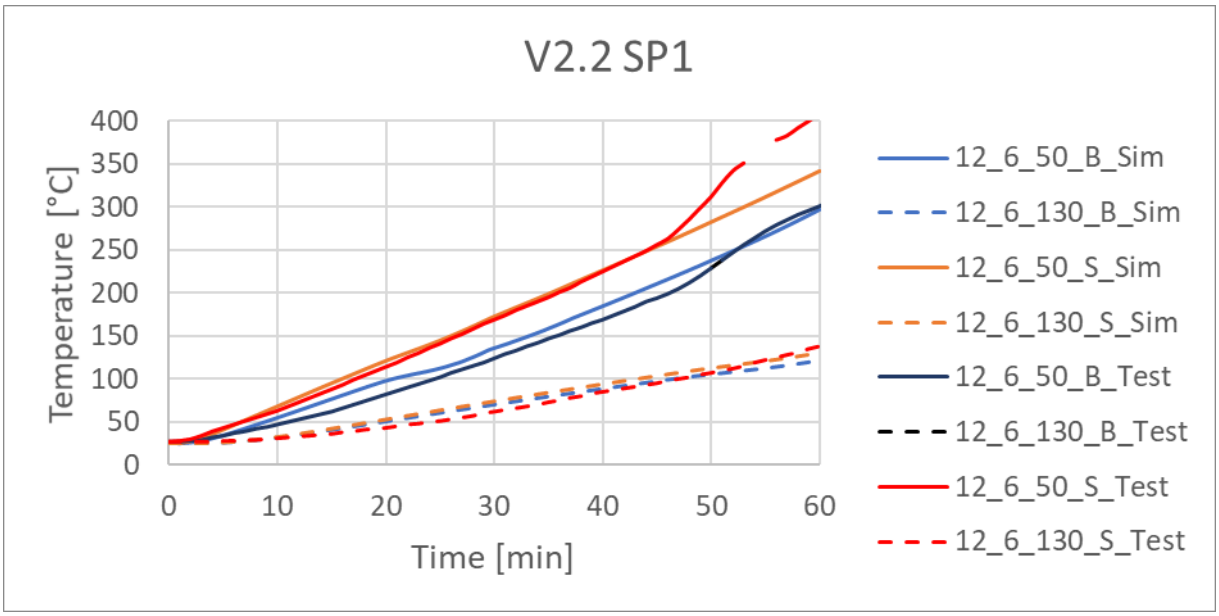

Figure 67: Comparison of temperature curves for measured and simulated results of specimen 1 and a 12 mm rod diameter with a glue line thickness of 3 mm

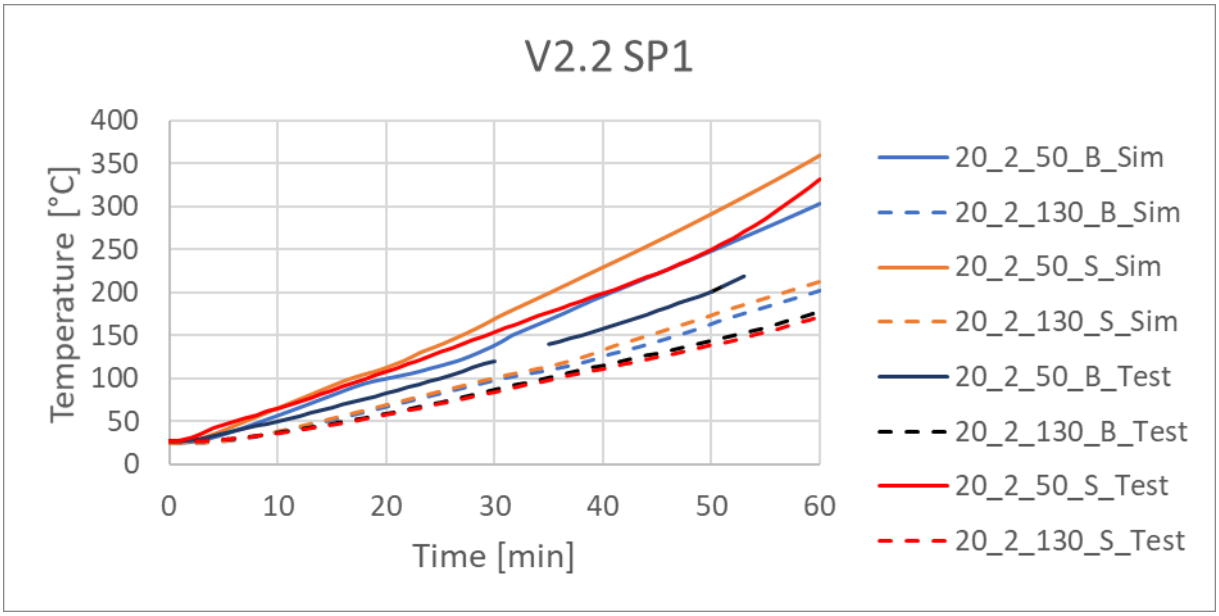

Figure 68: Comparison of temperature curves for measured and simulated results of specimen 1 and a 20 mm rod diameter with a glue line thickness of 1 mm

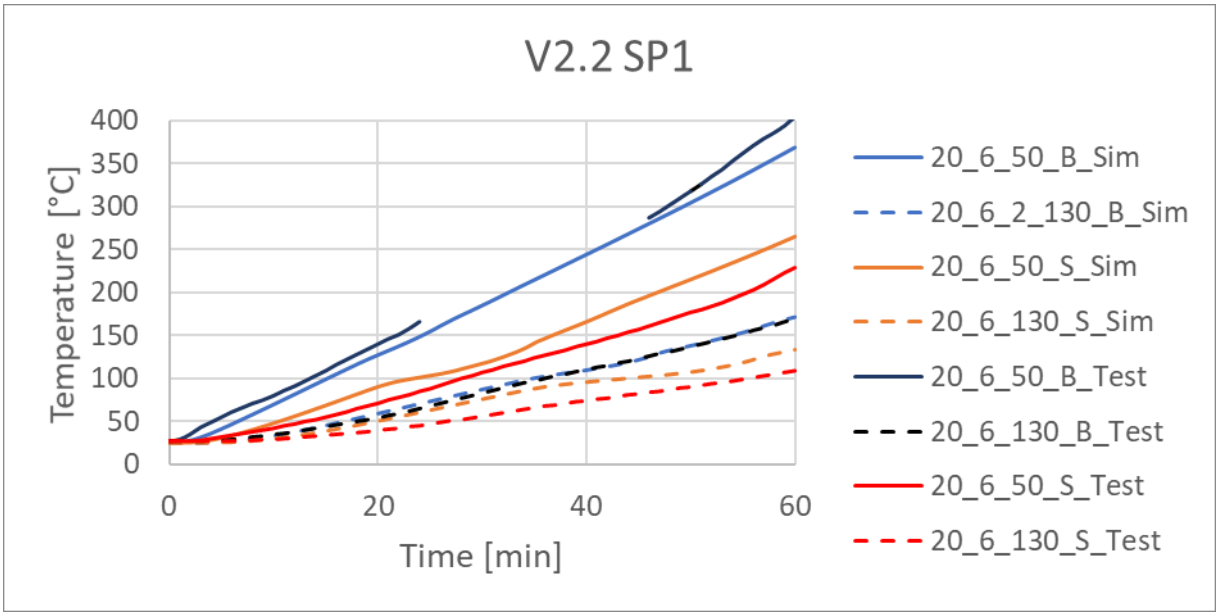

Figure 69: Comparison of temperature curves for measured and simulated results of specimen 1 and a 20 mm rod diameter with a glue line thickness of 3 mm

Specimen 2

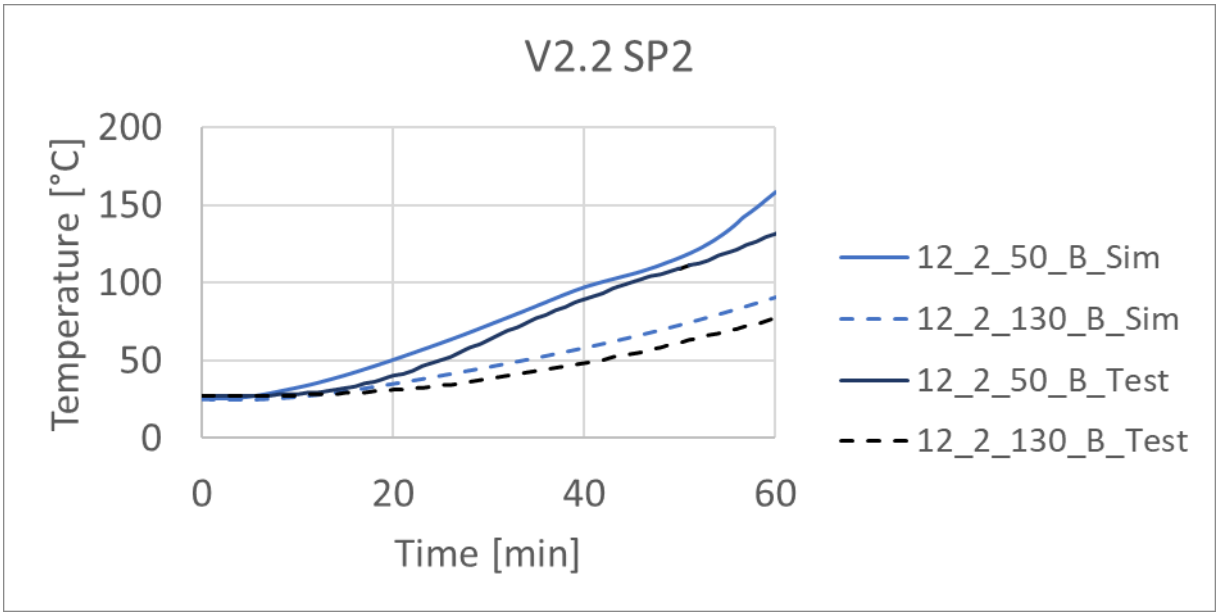

Figure 70: Comparison of temperature curves for measured and simulated results of specimen 2 and a 12 mm rod diameter with a glue line thickness of 1 mm

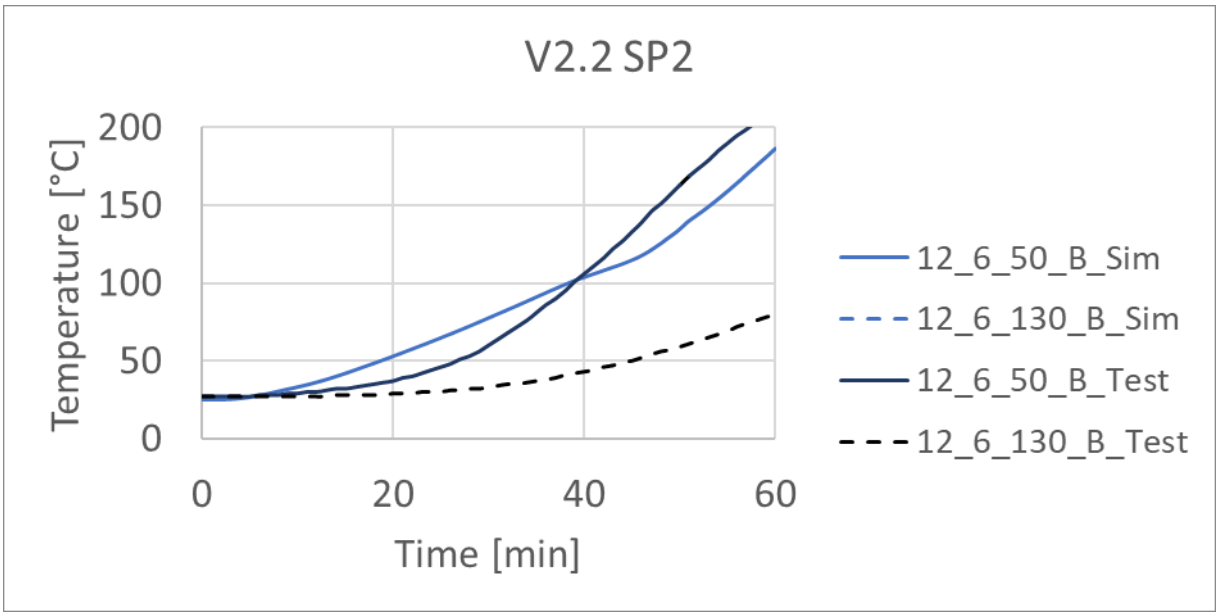

Figure 71: Comparison of temperature curves for measured and simulated results of specimen 2 and a 12 mm rod diameter with a glue line thickness of 3 mm

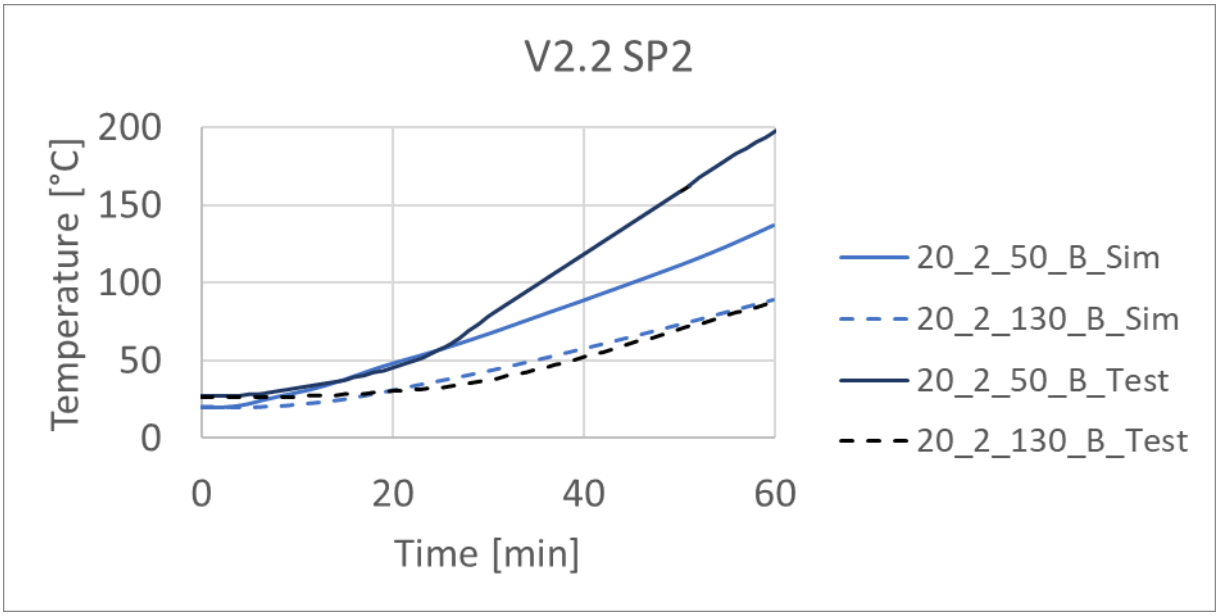

Figure 72: Comparison of temperature curves for measured and simulated results of specimen 2 and a 20 mm rod diameter with a glue line thickness of 1 mm

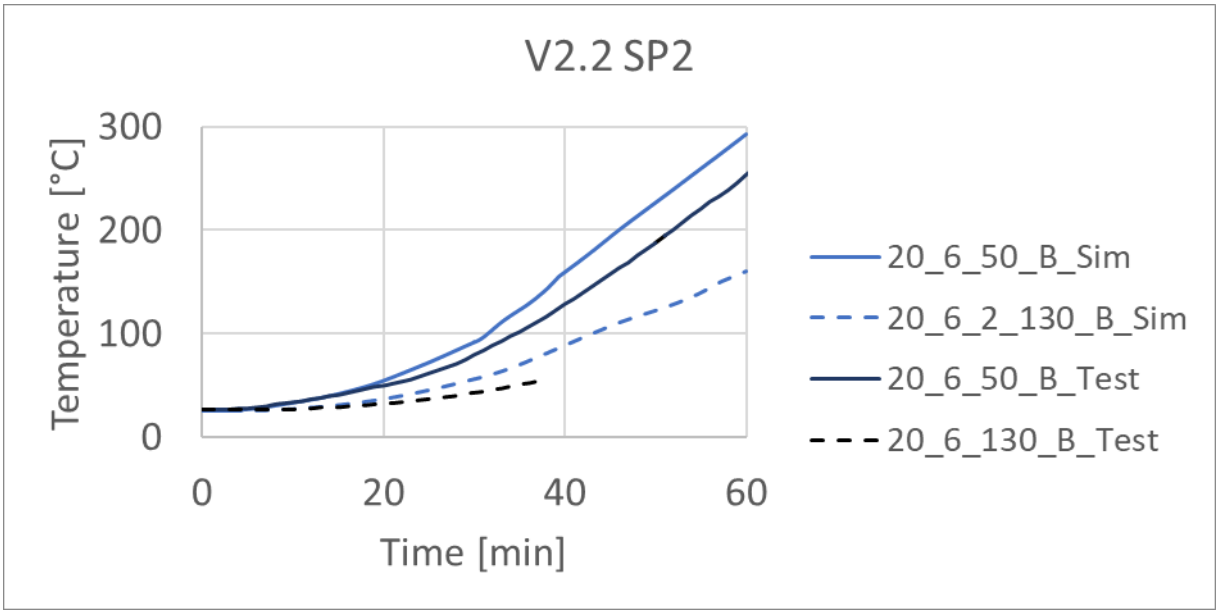

Figure 73: Comparison of temperature curves for measured and simulated results of specimen 2 and a 20 mm rod diameter with a glue line thickness of 3 mm

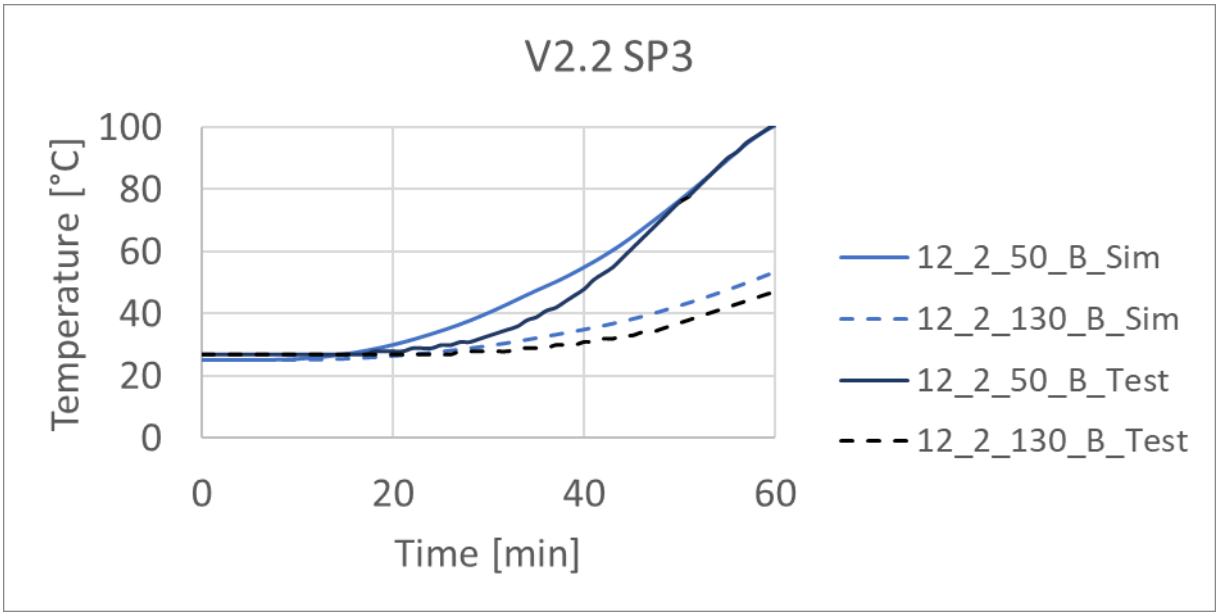

Figure 74: Comparison of temperature curves for measured and simulated results of specimen 3 and a 12 mm rod diameter with a glue line thickness of 1 mm

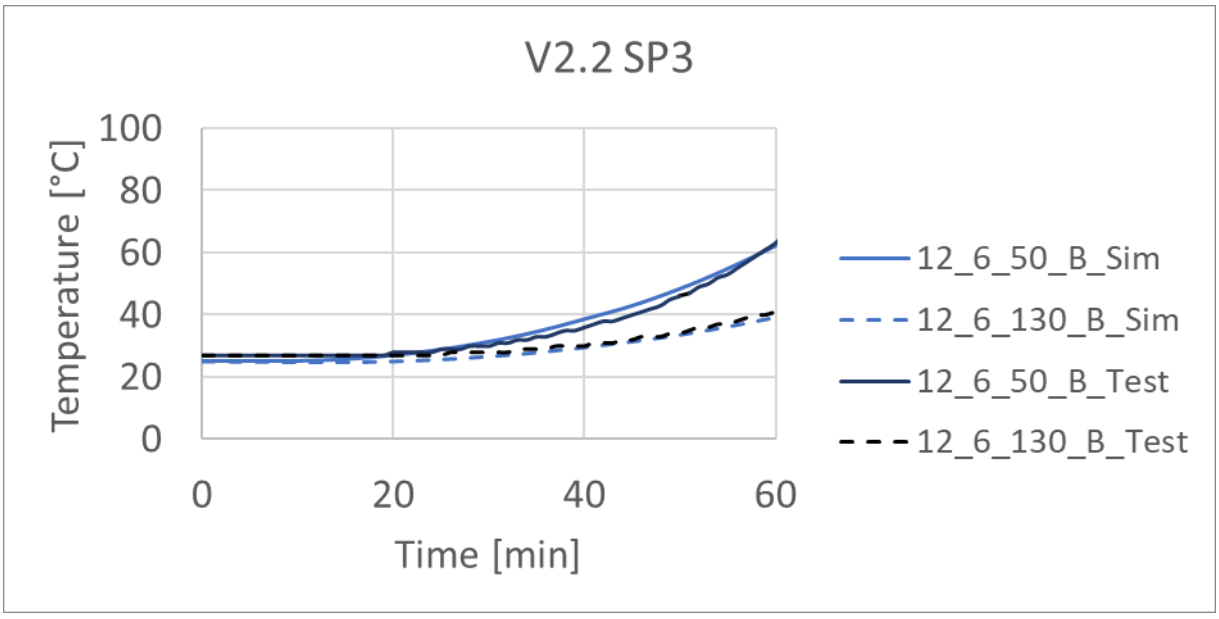

Figure 75: Comparison of temperature curves for measured and simulated results of specimen 3 and a 12 mm rod diameter with a glue line thickness of 3 mm

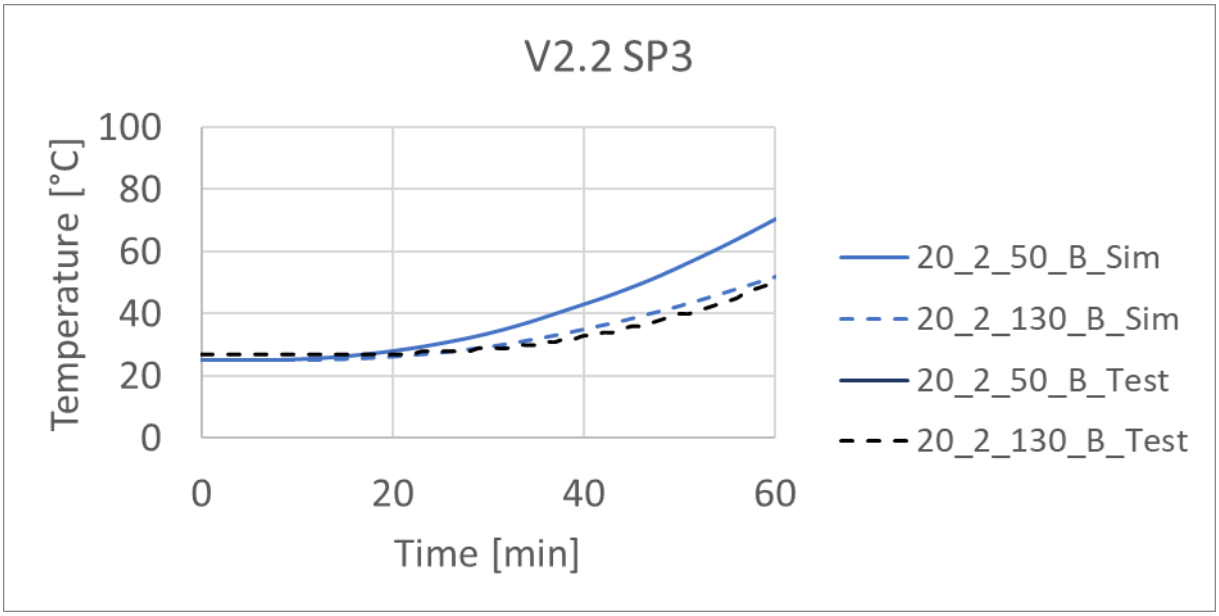

Figure 76: Comparison of temperature curves for measured and simulated results of specimen 3 and a 20 mm rod diameter with a glue line thickness of 1 mm

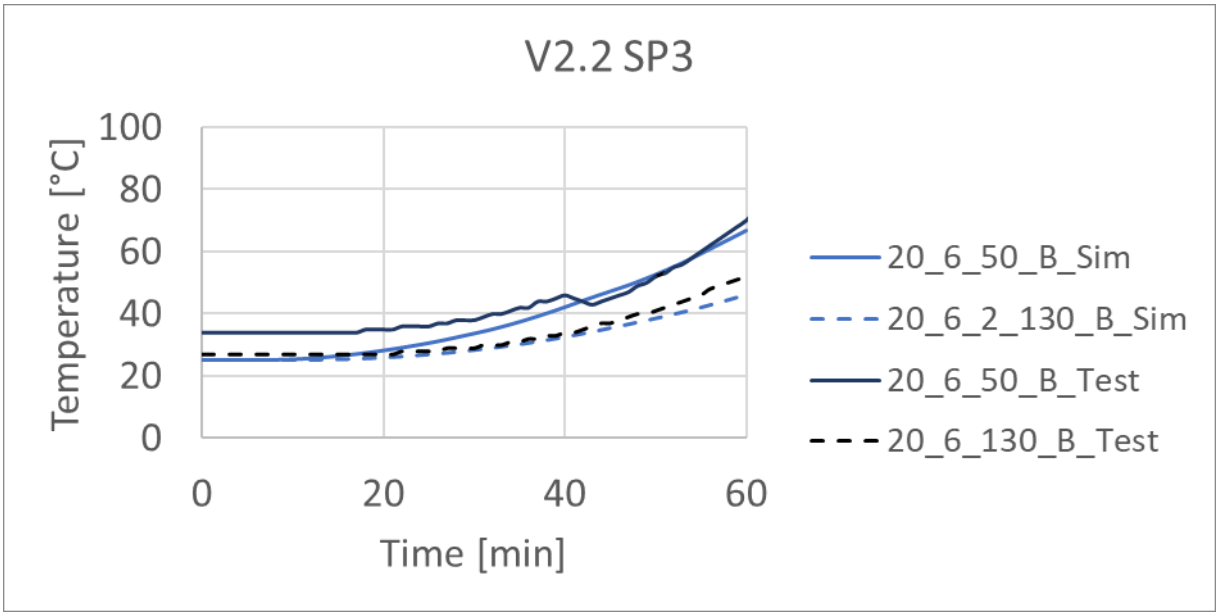

Figure 77: Comparison of temperature curves for measured and simulated results of specimen 3 and a 20 mm rod diameter with a glue line thickness of 3 mm

Specimen 4

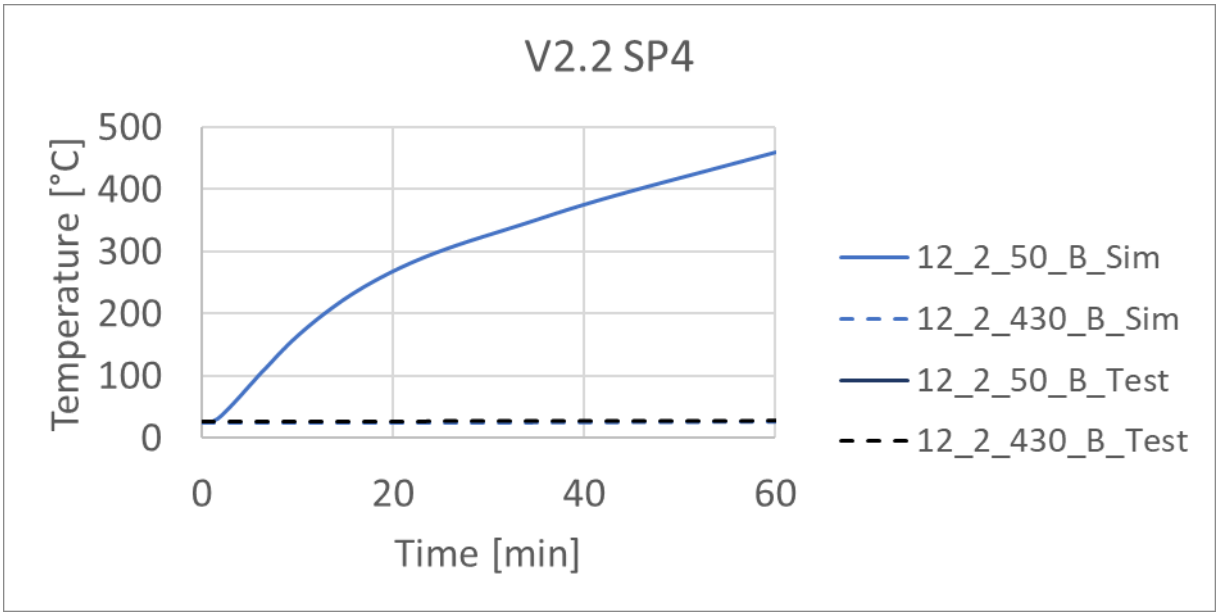

Figure 78: Comparison of temperature curves for measured and simulated results of specimen 4 and a 12 mm rod diameter with a glue line thickness of 1 mm

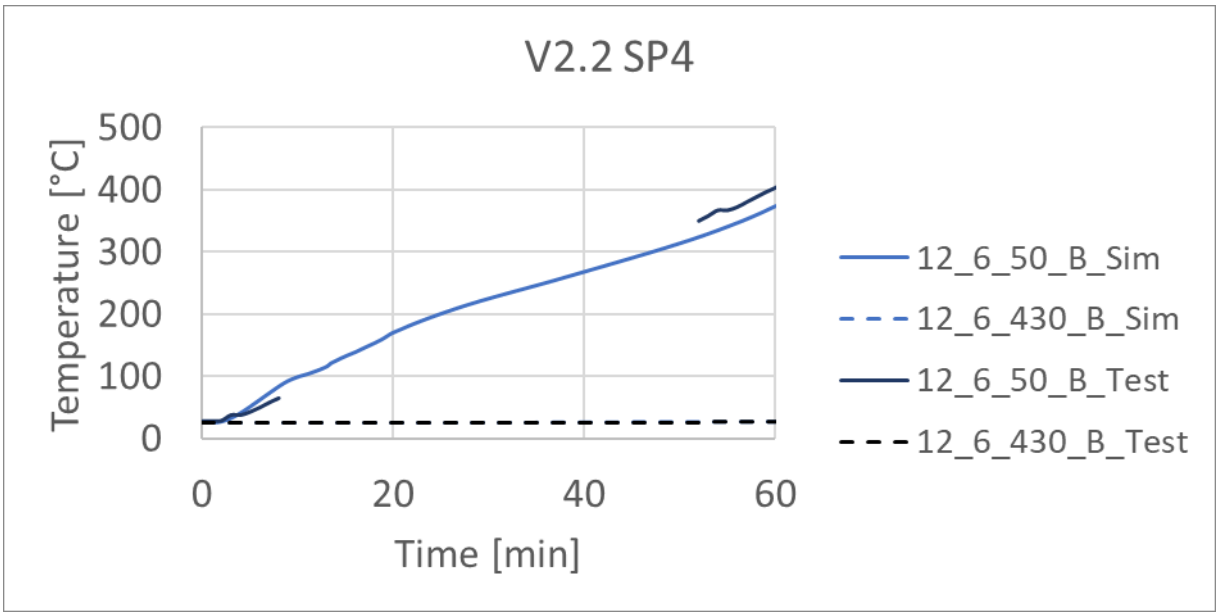

Figure 79: Comparison of temperature curves for measured and simulated results of specimen 4 and a 12 mm rod diameter with a glue line thickness of 3 mm

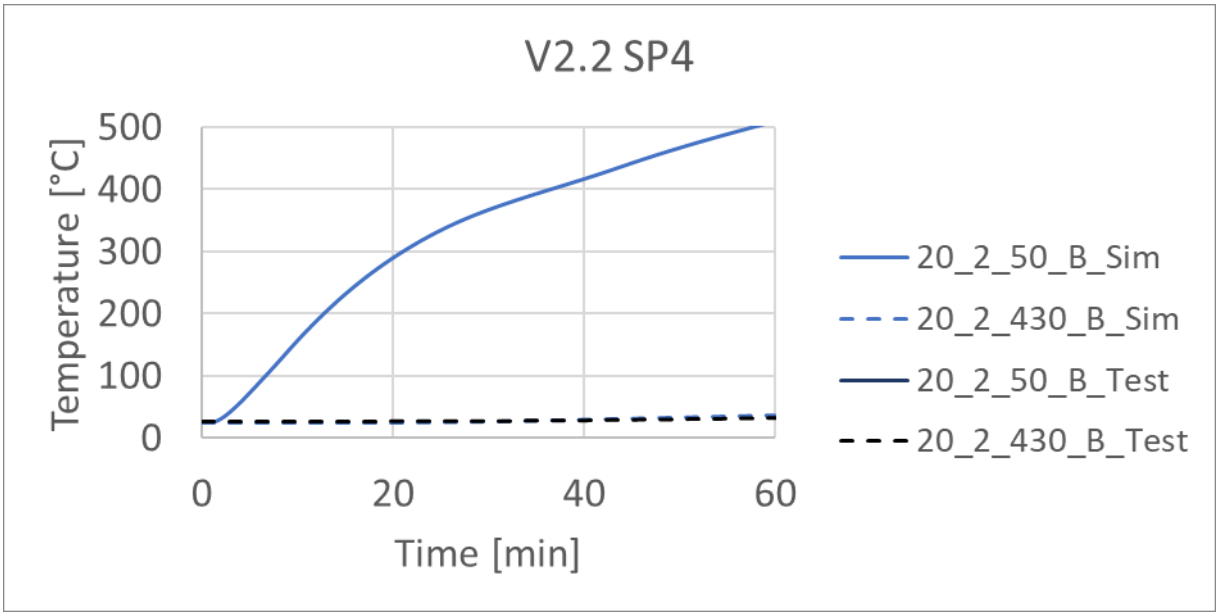

Figure 80: Comparison of temperature curves for measured and simulated results of specimen 4 and a 20 mm rod diameter with a glue line thickness of 1 mm

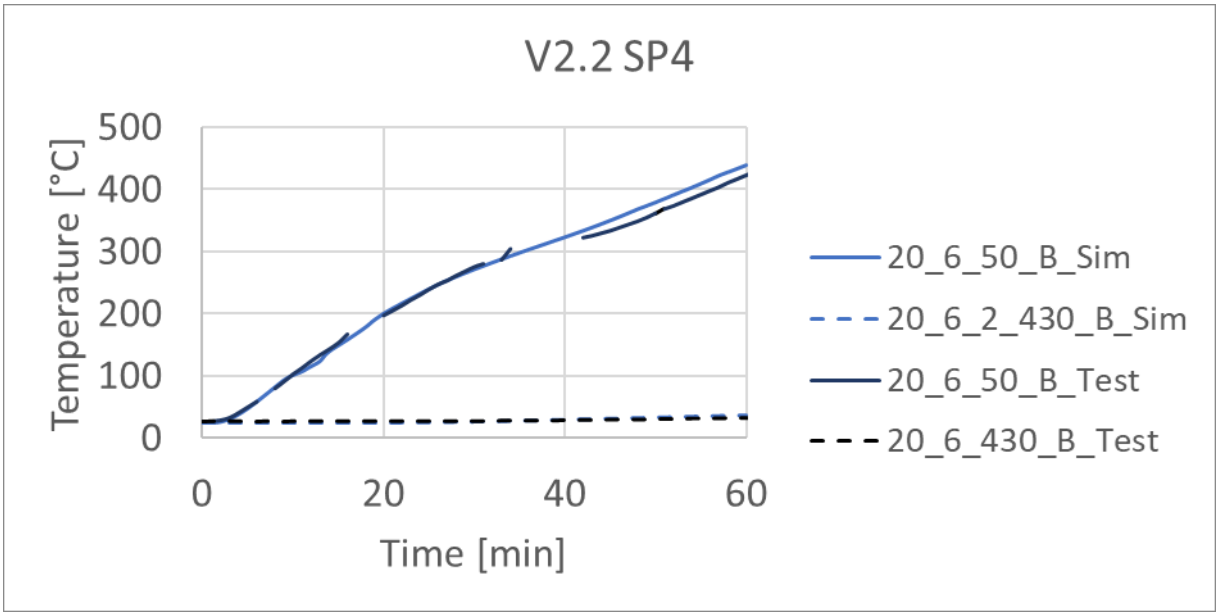

Figure 81: Comparison of temperature curves for measured and simulated results of specimen 4 and a 20 mm rod diameter with a glue line thickness of 3 mm

Specimen 5

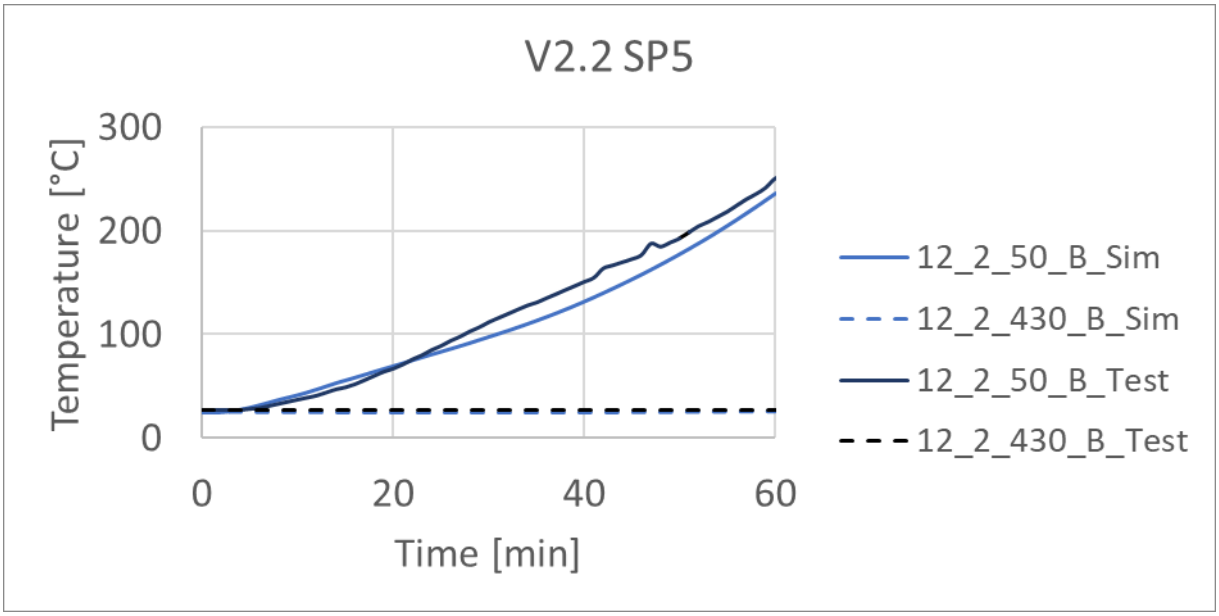

Figure 82: Comparison of temperature curves for measured and simulated results of specimen 5 and a 12 mm rod diameter with a glue line thickness of 1 mm

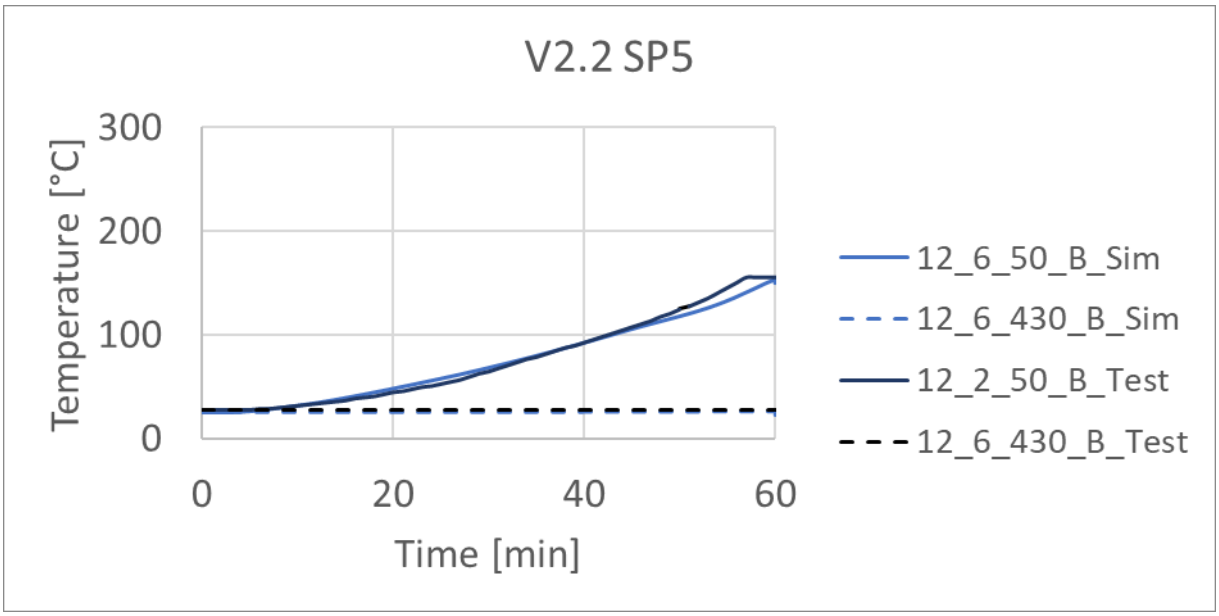

Figure 83: Comparison of temperature curves for measured and simulated results of specimen 5 and a 12 mm rod diameter with a glue line thickness of 3 mm

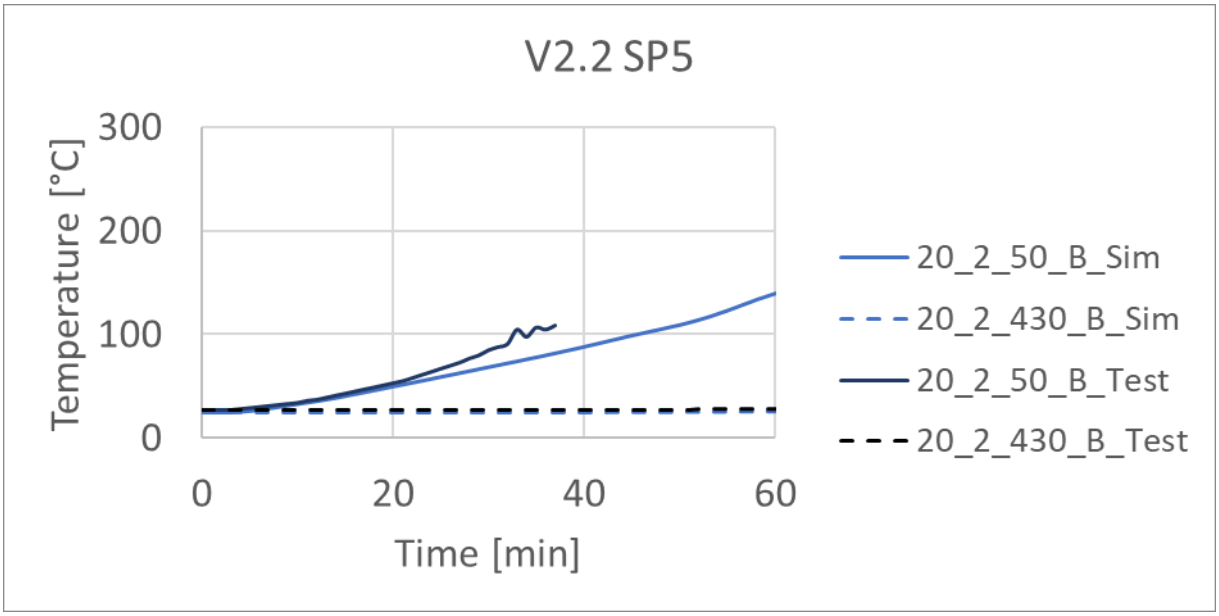

Figure 84: Comparison of temperature curves for measured and simulated results of specimen 5 and a 20 mm rod diameter with a glue line thickness of 1 mm

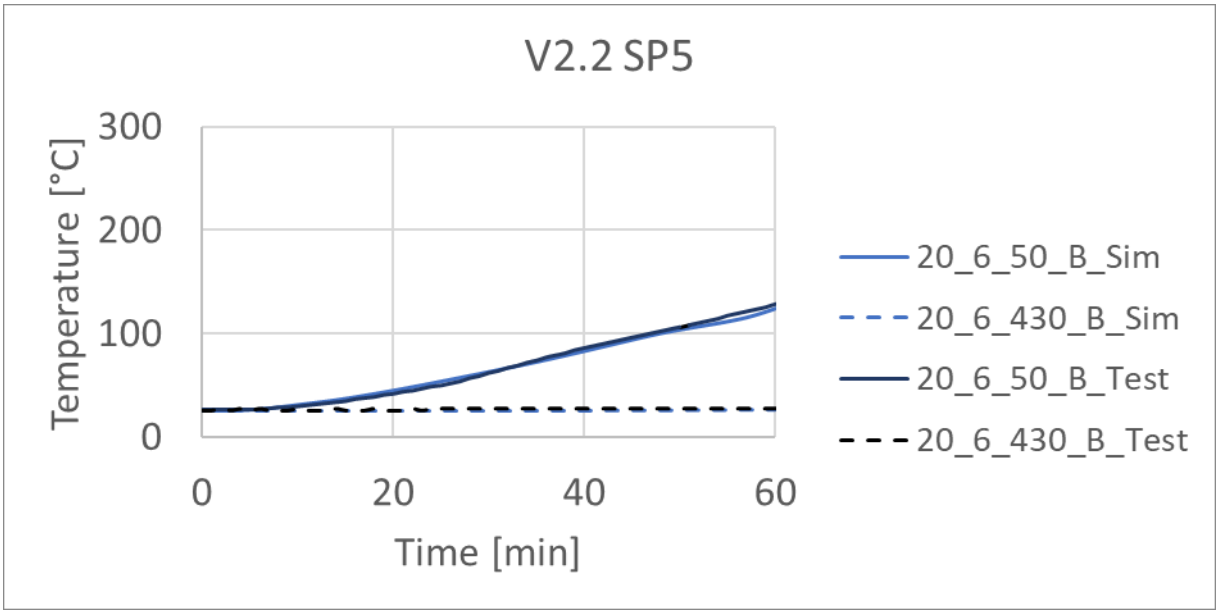

Figure 85: Comparison of temperature curves for measured and simulated results of specimen 5 and a 20 mm rod diameter with a glue line thickness of 3 mm

Specimen 6

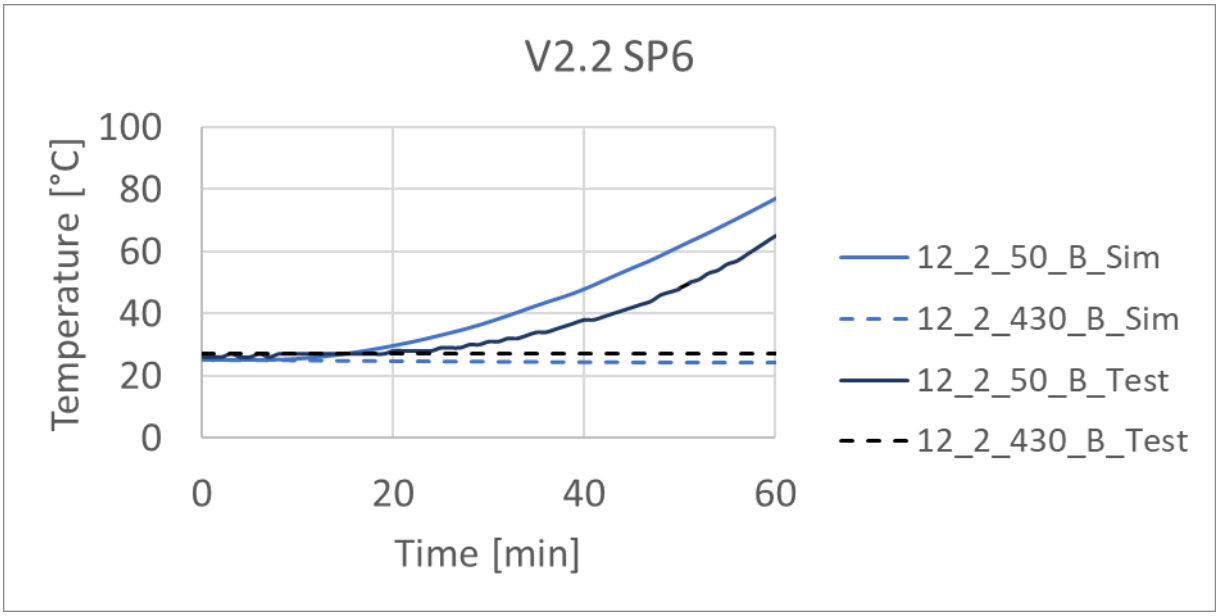

Figure 86: Comparison of temperature curves for measured and simulated results of specimen 6 and a 12 mm rod diameter with a glue line thickness of 1 mm

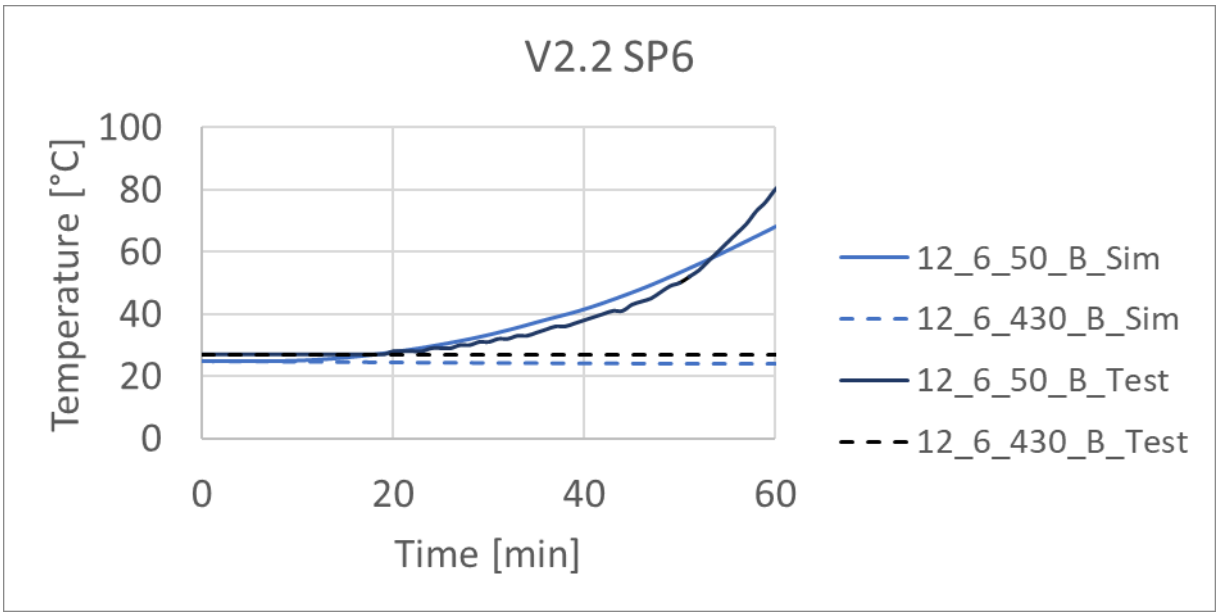

Figure 87: Comparison of temperature curves for measured and simulated results of specimen 6 and a 12 mm rod diameter with a glue line thickness of 3 mm

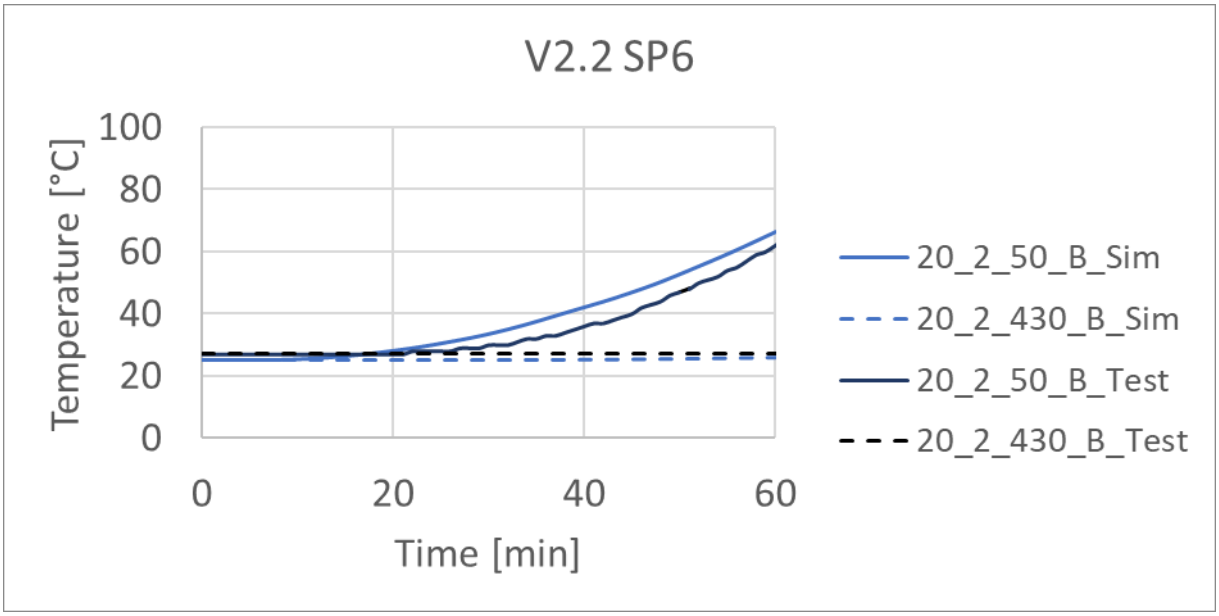

Figure 88: Comparison of temperature curves for measured and simulated results of specimen 6 and a 20 mm rod diameter with a glue line thickness of 1 mm

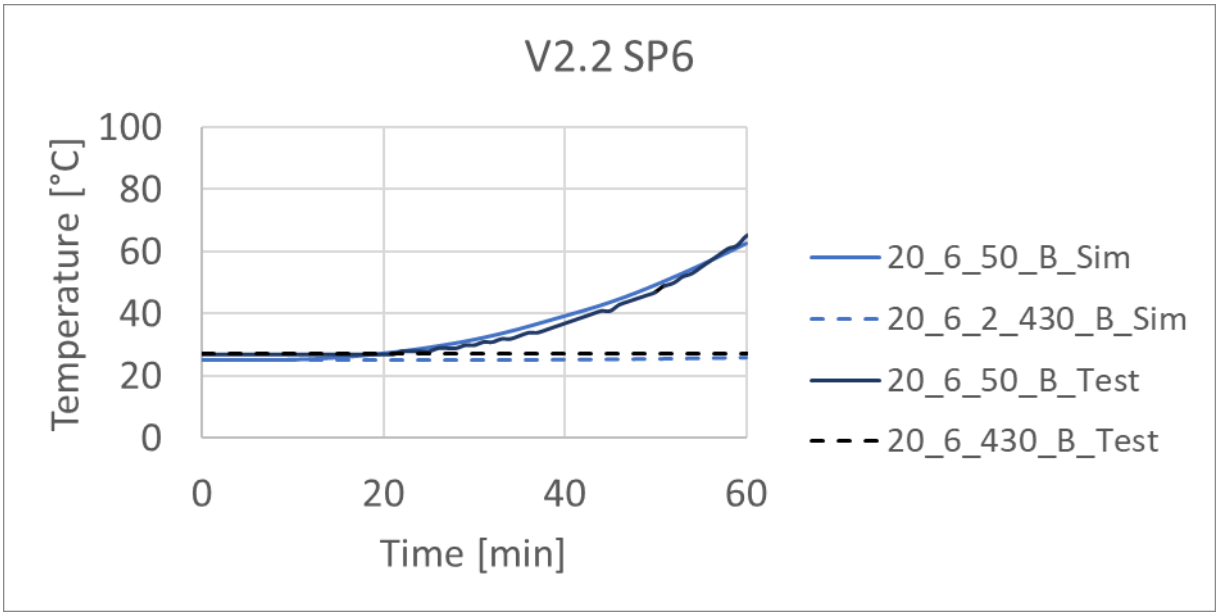

Figure 89: Comparison of temperature curves for measured and simulated results of specimen 6 and a 20 mm rod diameter with a glue line thickness of 3 mm

Specimen 7

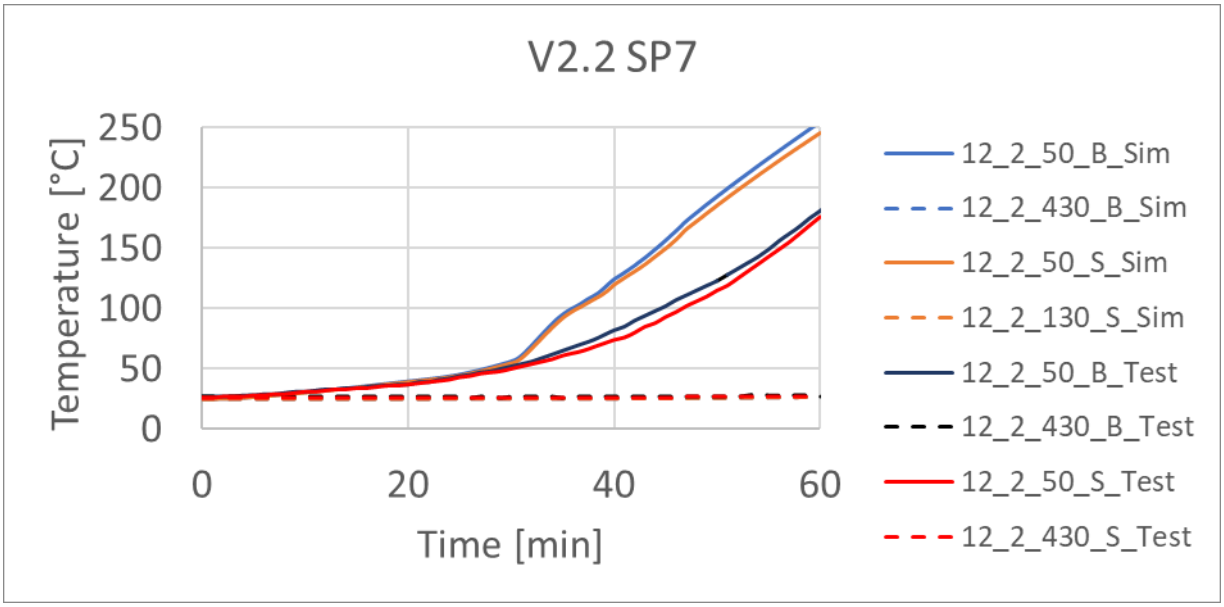

Figure 90: Comparison of temperature curves for measured and simulated results of specimen 7 and a 12 mm rod diameter with a glue line thickness of 1 mm

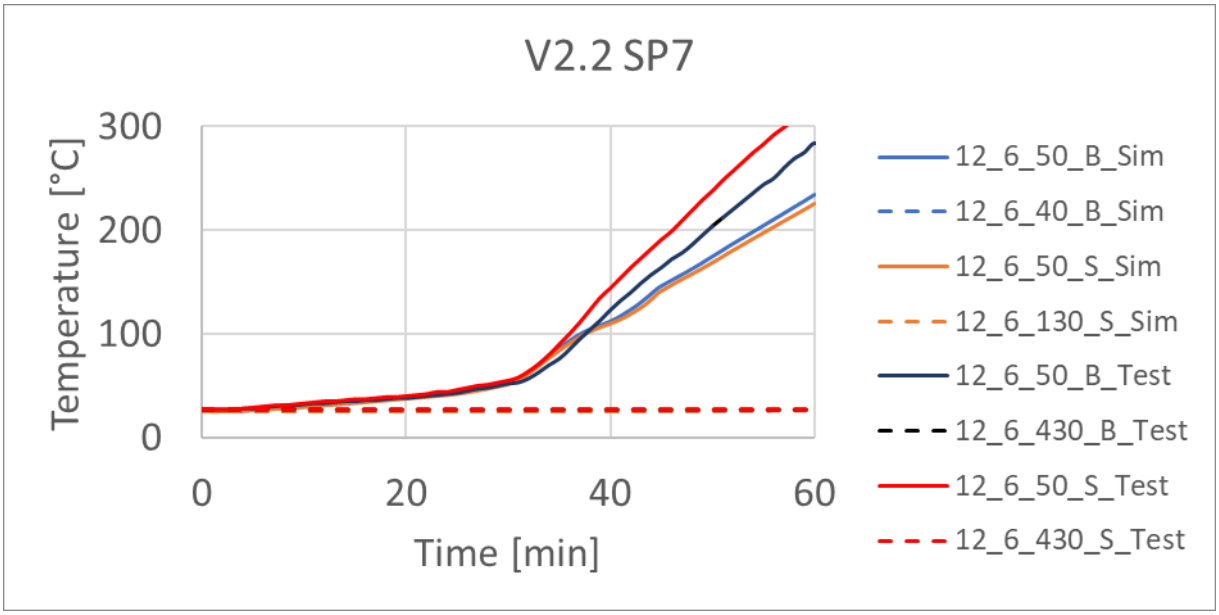

Figure 91: Comparison of temperature curves for measured and simulated results of specimen 7 and a 2 mm rod diameter with a glue line thickness of 3 mm

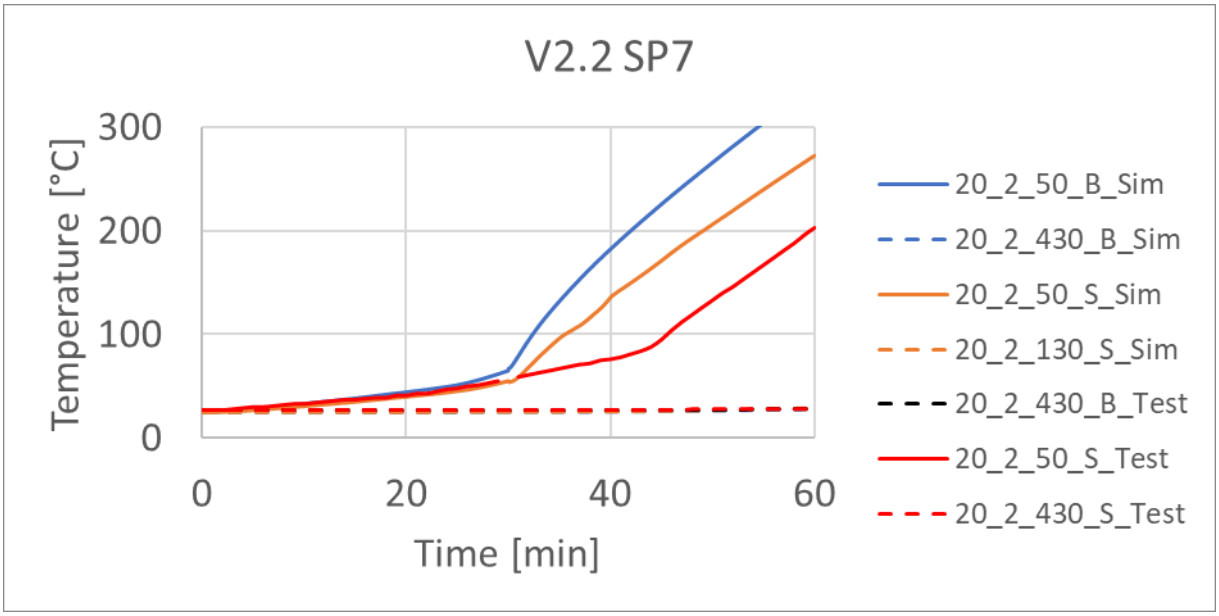

Figure 92: Comparison of temperature curves for measured and simulated results of specimen 7 and a 20 mm rod diameter with a glue line thickness of 1 mm

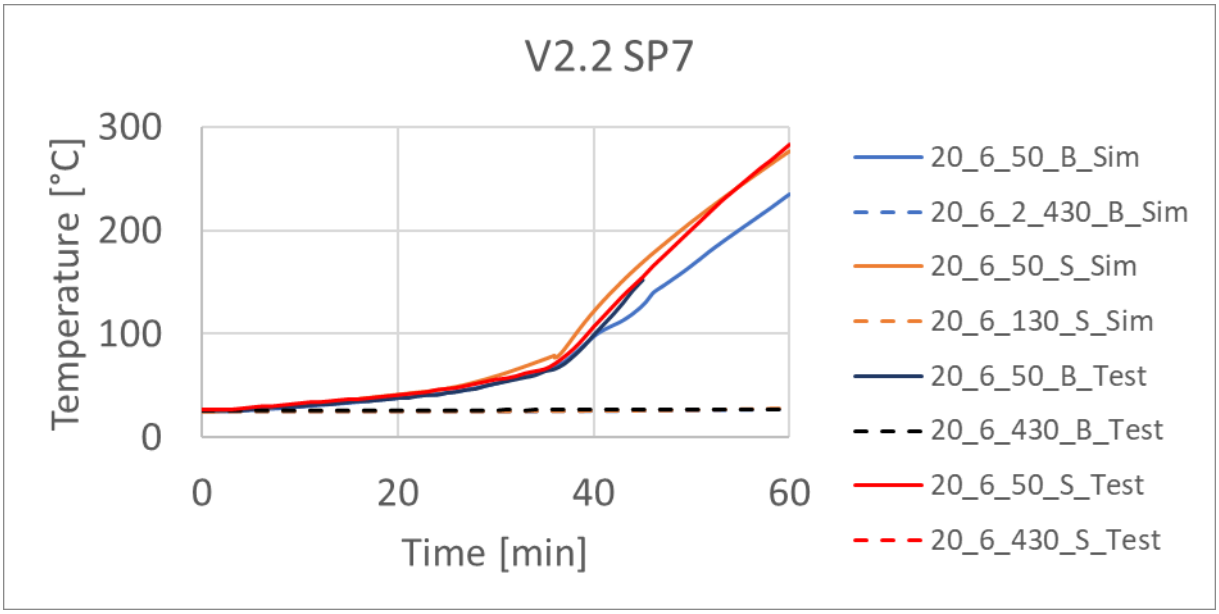

Figure 93: Comparison of temperature curves for measured and simulated results of specimen 7 and a 20 mm rod diameter with a glue line thickness of 3 mm

Specimen 8

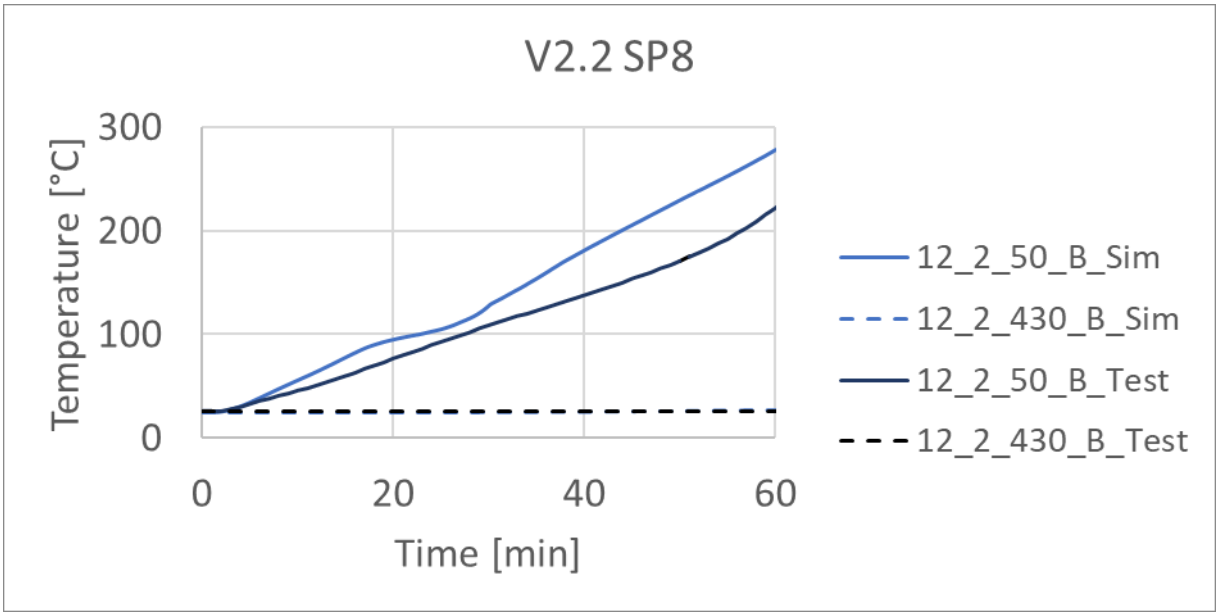

Figure 94: Comparison of temperature curves for measured and simulated results of specimen 8 and a 12 mm rod diameter with a glue line thickness of 1 mm

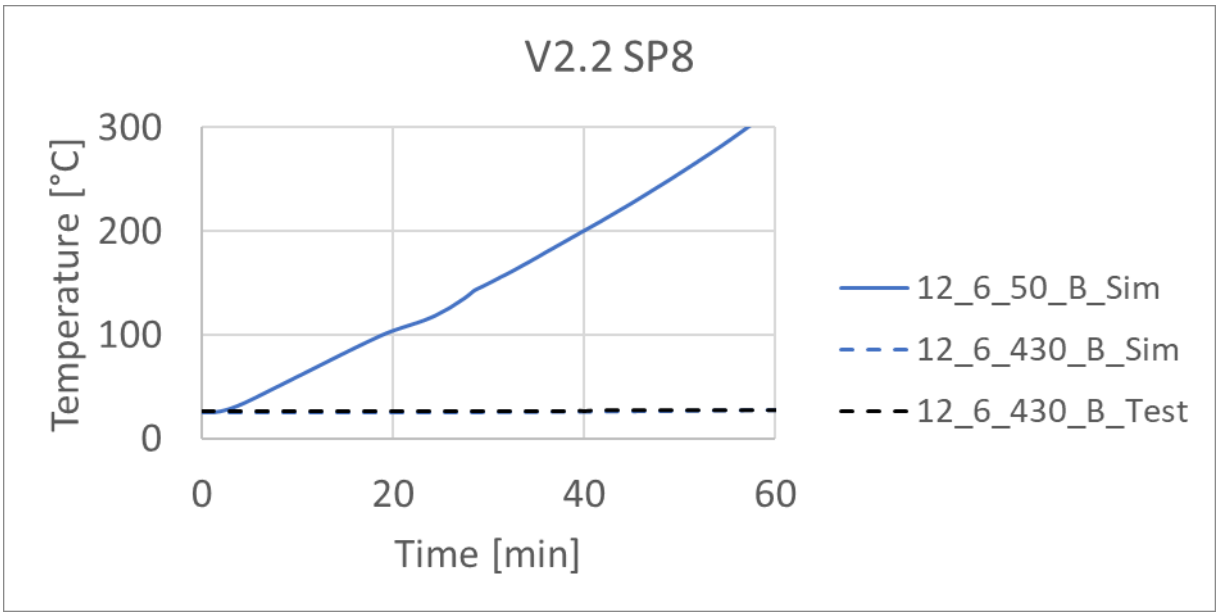

Figure 95: Comparison of temperature curves for measured and simulated results of specimen 8 and a 12 mm rod diameter with a glue line thickness of 3 mm

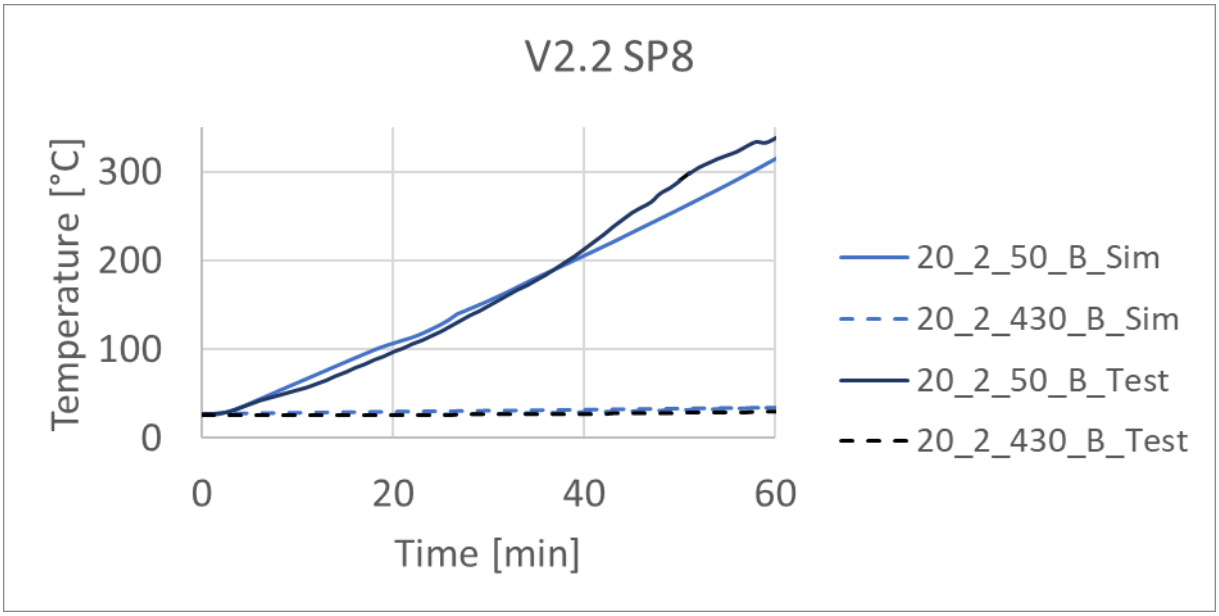

Figure 96: Comparison of temperature curves for measured and simulated results of specimen 8 and a 20 mm rod diameter with a glue line thickness of 1 mm

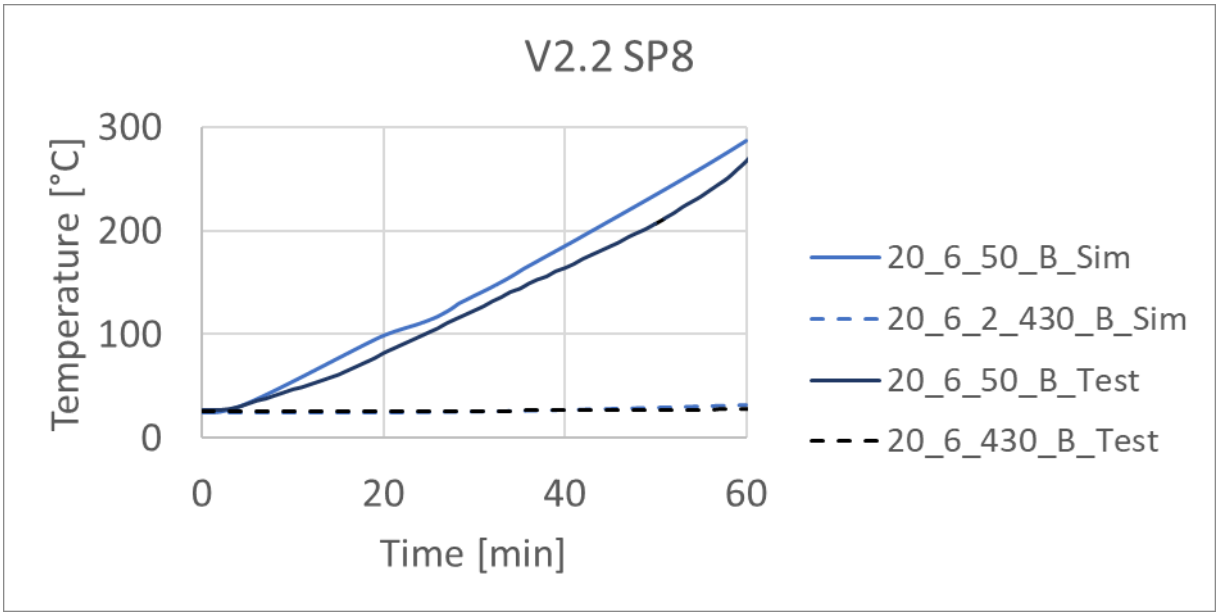

Figure 97: Comparison of temperature curves for measured and simulated results of specimen 8 and a 20 mm rod diameter with a glue line thickness of 3 mm

B.3 Test series 2.3

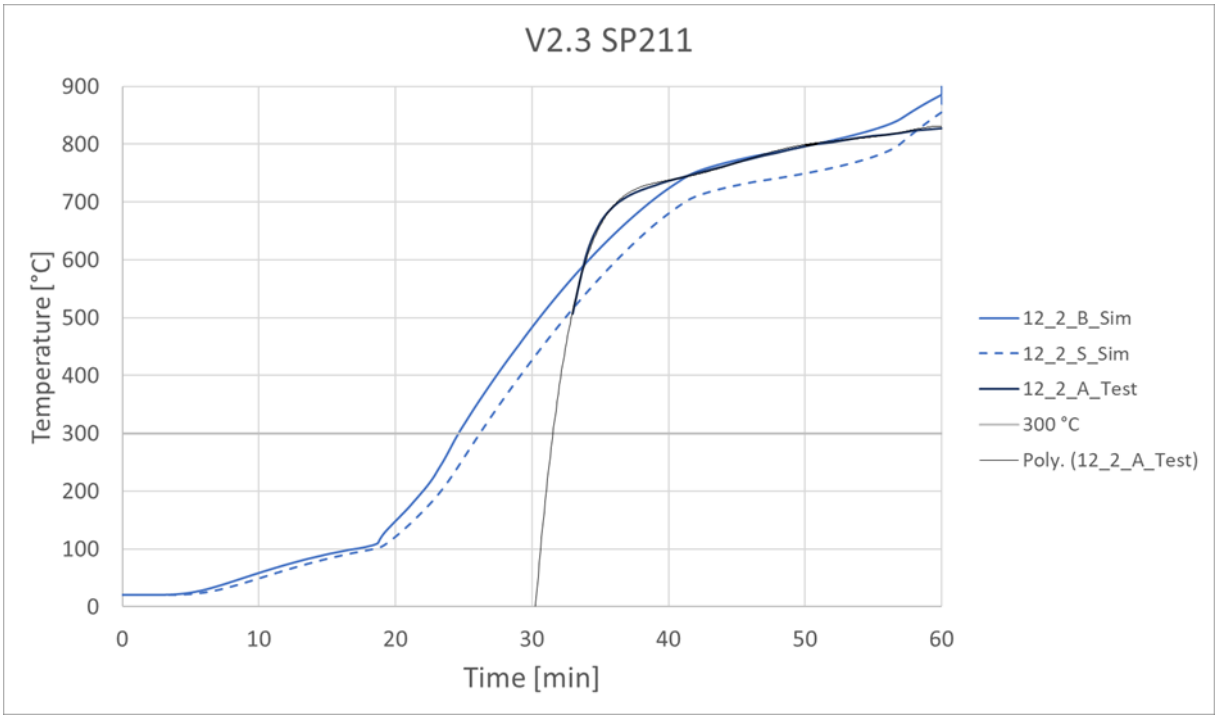

Figure 98: Comparison of temperature curves for measured and simulated results of specimen 211 and a 12 mm rod diameter with a glue line thickness of 1 mm

C Test series 4

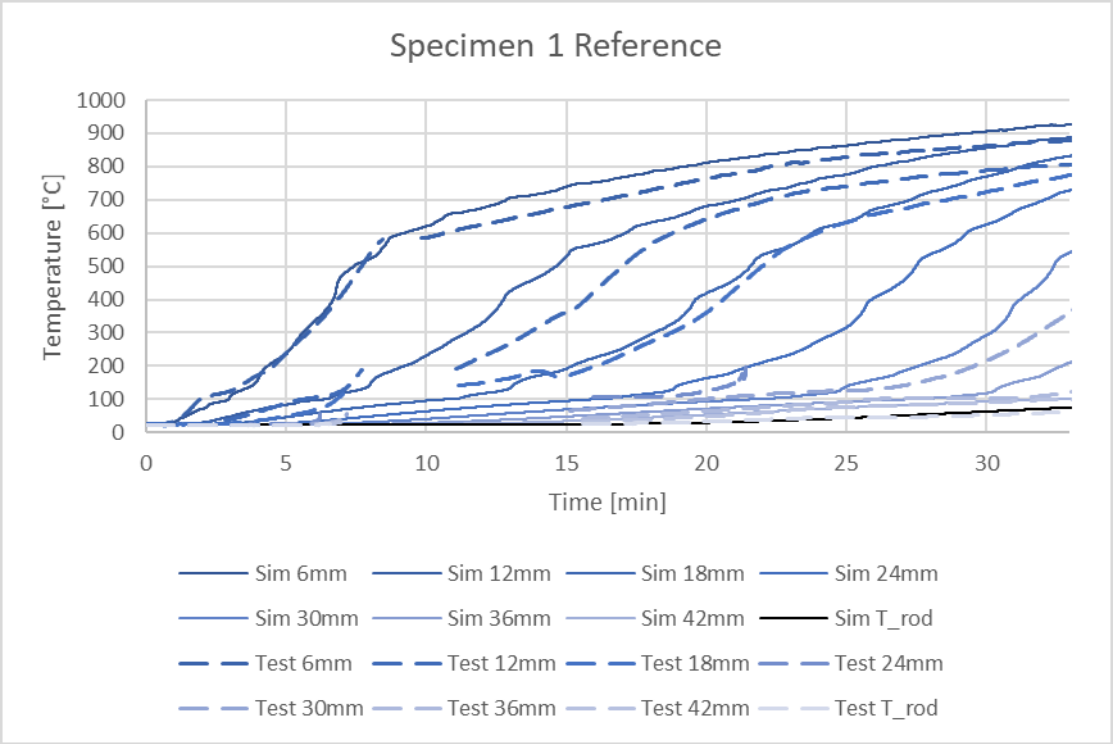

Figure 99: Comparison of temperature curves for measured and simulated results of reference specimen 1

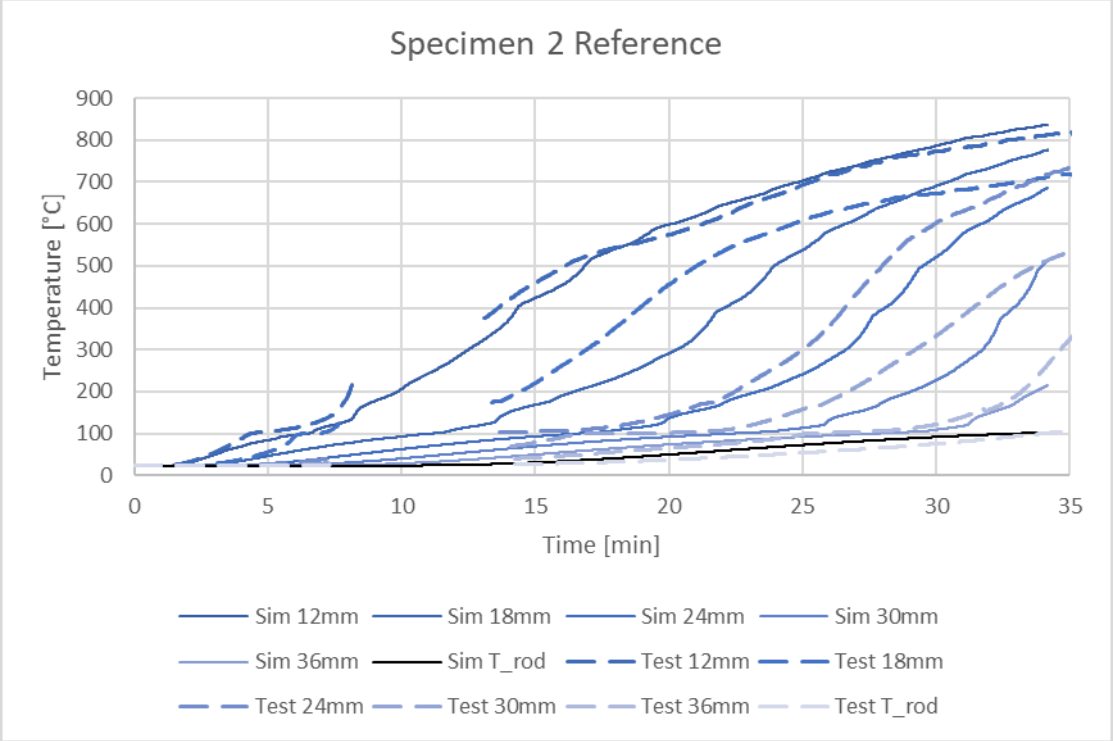

Figure 100: Comparison of temperature curves for measured and simulated results of reference specimen 2

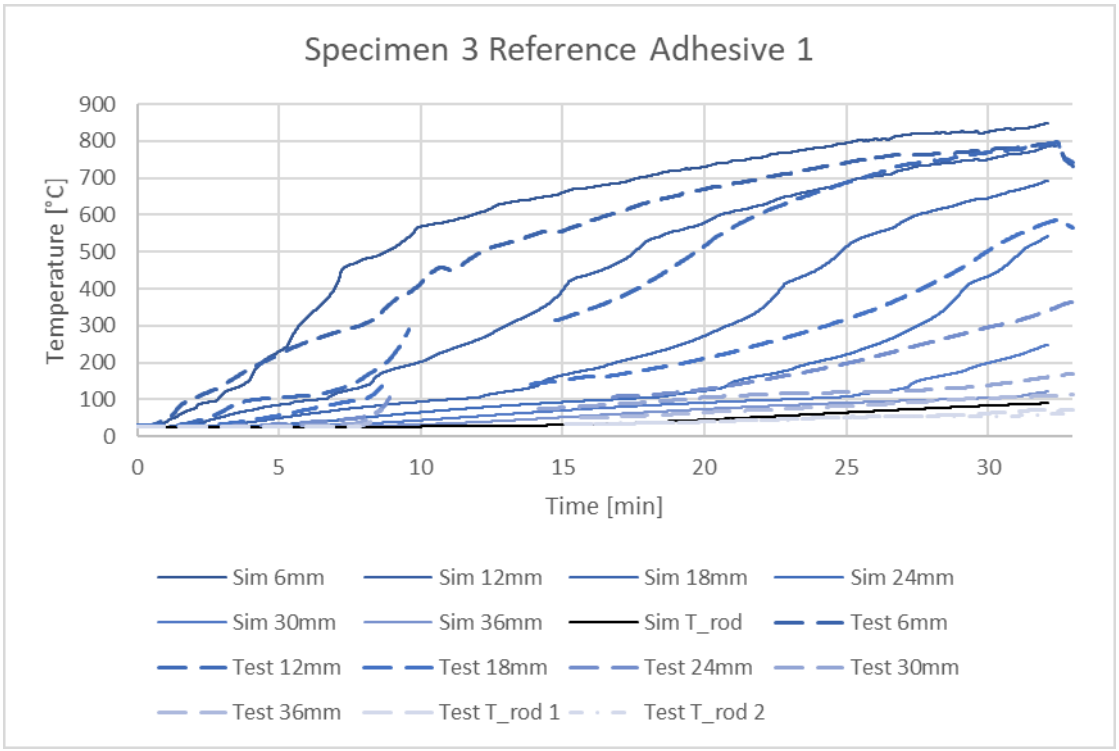

Figure 101: Comparison of temperature curves for measured and simulated results of reference specimen 3 with Adhesive 1

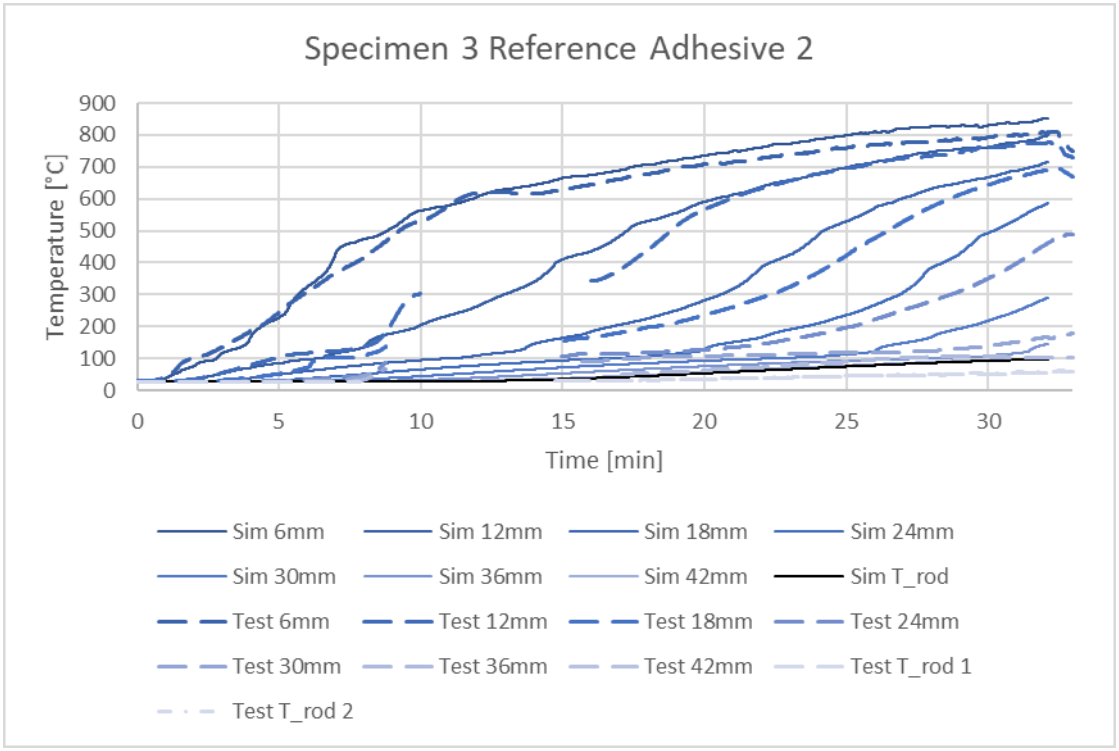

Figure 102: Comparison of temperature curves for measured and simulated results of reference specimen 3 with Adhesive 2

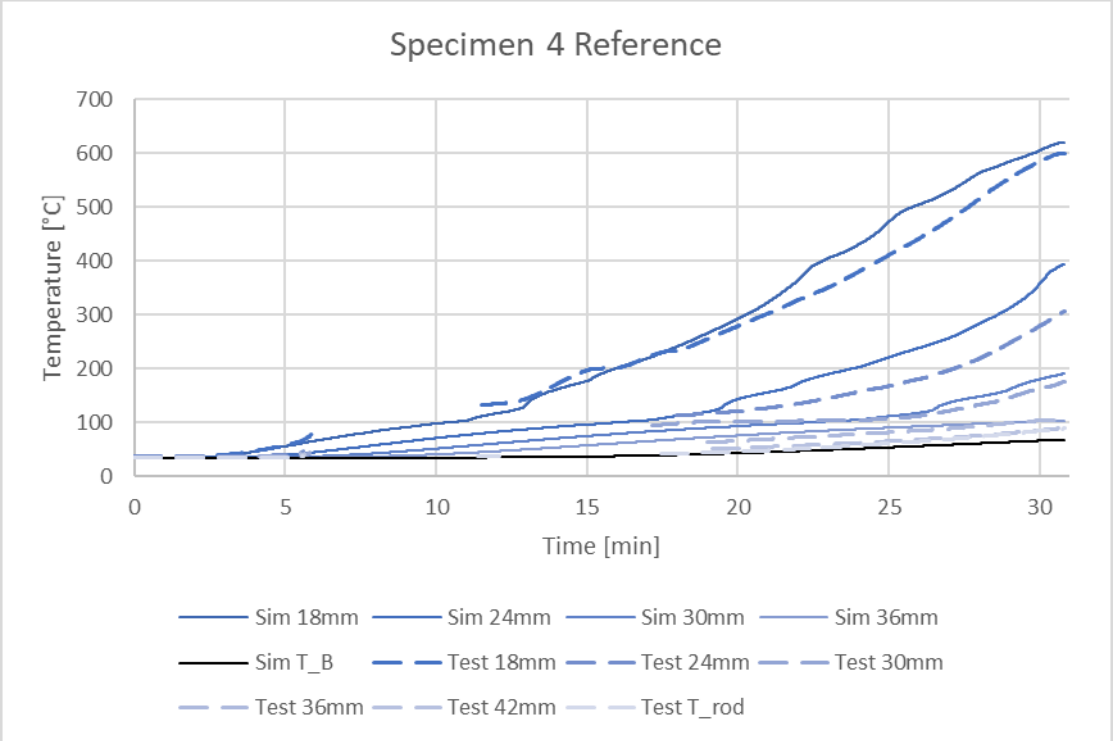

Figure 103: Comparison of temperature curves for measured and simulated results of reference specimen 4